

## **INFORMATION TO USERS**

This manuscript has been reproduced from the microfilm master. UMI films the text directly from the original or copy submitted. Thus, some thesis and dissertation copies are in typewriter face, while others may be from any type of computer printer.

**The quality of this reproduction is dependent upon the quality of the copy submitted.** Broken or indistinct print, colored or poor quality illustrations and photographs, print bleedthrough, substandard margins, and improper alignment can adversely affect reproduction.

In the unlikely event that the author did not send UMI a complete manuscript and there are missing pages, these will be noted. Also, if unauthorized copyright material had to be removed, a note will indicate the deletion.

Oversize materials (e.g., maps, drawings, charts) are reproduced by sectioning the original, beginning at the upper left-hand corner and continuing from left to right in equal sections with small overlaps. Each original is also photographed in one exposure and is included in reduced form at the back of the book.

Photographs included in the original manuscript have been reproduced xerographically in this copy. Higher quality 6" x 9" black and white photographic prints are available for any photographs or illustrations appearing in this copy for an additional charge. Contact UMI directly to order.

# **UMI**

A Bell & Howell Information Company  
300 North Zeeb Road, Ann Arbor MI 48106-1346 USA  
313/761-4700 800/521-0600



AN INVESTIGATION OF  
PULSED ELECTROCHEMICAL MACHINING  
OF H-13 TOOL STEEL

DISSERTATION

Presented in Partial Fulfillment of the Requirements for  
the Degree Doctor of Philosophy in the Graduate  
School of The Ohio State University

By

Blaine W. Lilly, Jr., M. S.

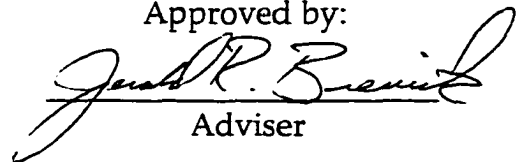
\* \* \* \* \*

The Ohio State University  
1998

Dissertation Committee:

Professor Jerald Brevick, Adviser  
Professor R. Allen Miller  
Professor Glyn Meyrick  
Professor Clark Mount-Campbell

Approved by:

  
Adviser

Graduate Program  
Industrial and  
Systems Engineering

**UMI Number: 9822340**

---

**UMI Microform 9822340**  
**Copyright 1998, by UMI Company. All rights reserved.**

**This microform edition is protected against unauthorized  
copying under Title 17, United States Code.**

---

**UMI**  
**300 North Zeeb Road**  
**Ann Arbor, MI 48103**

## ABSTRACT

Electro-discharge machining (EDM) is universally used in the die and mold making industry because of its ability to machine hardened steel into intricate shapes. However, the EDM process also creates a hard, brittle recast layer on the die surface, which must be removed by manual methods before the die can be put into service.

Recently pulsed electrochemical machining (PECM) has been proposed as a means of automating the removal of the EDM recast layer. Electrolytic methods such as PECM are known to create stress-free surfaces, but the control of these processes has proved to be difficult in the past. Because the power supply in PECM is pulsed, it offers more control to the user than has conventional ECM.

This dissertation presents a model for optimizing the die making process, with particular emphasis on optimizing the PECM pulse parameters to provide an optimum die surface in minimal time. The model is applied to a COTAC-51 PECM machine, and the results show significant improvement in the surface finish of the H-13 steel surface, and in the mechanical fatigue life of specimens machined from hardened premium grade H-13 tool steel.

Dedicated to the memory of my first and best teachers, my parents

## ACKNOWLEDGMENTS

I would like to thank the members of my committee, especially my adviser, Professor Jerry Brevick, and the Chairman of IWSE, Professor Allen Miller, for their unflagging support, encouragement, and friendship.

I am very grateful to Mr. Junzo Suzuki of Shizuoka Seiki Co., Ltd. and to Professor Taylan Altan for providing me with the machine on which this research was performed, and with the opportunity to use it.

I would like to thank Mr. Qi Shi for his many long hours preparing and running fatigue tests, and Mr. Jeff Sanders for the excellent SEM photography. Thanks also to Mr. Kevin Chen and Mr. Andrew Kaley for their hard work during the early portions of this research. I also thank Mr. Vincent Vohnout and Mr. Jerry Kingzett for many spirited discussions and helpful suggestions during the course of this work.

My deepest thanks go to Ms. Mary Hartzler and Mr. Cedric Sze, both the Department of Industrial, Welding, and Systems Engineering. Both of them were always willing to do whatever was necessary to assist me in finishing this work, and I cannot adequately express my gratitude for all their help.

Finally, and most especially, I want to thank my entire family for all the love and support they've provided me over the years, and to my best and closest friend, Agi Riskó, without whose love and encouragement none of this would have happened.

## VITA

July 20, 1949	Born - St. Albans, WV, USA
1971	B. A., English The Ohio State University
1983	B. S., Mechanical Engineering The Ohio State University
1986	M. S., Mechanical Engineering The Ohio State University
1986–1989	Staff Engineer ERC for Net Shape Manufacturing The Ohio State University
1989–1990	Research Associate Institute for Plastic Metalforming RWTH, Aachen, Germany
1994–present	Lecturer The Ohio State University

## PUBLICATIONS

### Research Publications

1. Lilly, B., J. Brevick, and C.-S. Chen, "The Effect of Pulsed Electro-Chemical Machining on the Fatigue Life of H-13 Steel", *Transactions of NAMRI/SME*, Vol. XXV, May, 1997.
2. Altan, T., C. Rodriguez, P. Fallböhmer, B. Lilly, "Machining Basics for Moldmaking", *Tooling and Production*, Vol. 61, No.11, February 1996, pp. 48–52.

3. Altan, T., and B. Lilly, "CAD/CAM/CAE of Dies and Molds", in *The CAD/CAM Handbook*, C. Machover, ed., New York, McGraw-Hill, 1995, pp. 383-401.
4. Ziehm, R., B. Lilly, J. Brevick, T. Altan, *Effect of Geometry on Electro-Chemical Polishing of Die Steels*, ERC for Net Shape Manufacturing, The Ohio State University, Columbus, Ohio Report No. ERC/NSM-D-95-33, July, 1995.
5. Geiger, A., B. Lilly, J. Brevick, J., T. Altan, *Parameter Optimization for an Electrochemical Polishing Machine*, ERC for Net Shape Manufacturing, The Ohio State University, Columbus, Report No. ERC/NSM-94-6, March, 1994.
6. Altan, T., Lilly, B.W., Kruth, J.P., König, W., Tönshoff, H.K., van Luttervelt, C.A., "Advanced Techniques for Die and Mold Manufacturing", *Annals of the CIRP*, Vol. 42/1, 1993.
7. Lilly, B.W., Bailey, R., Altan, T., "Automated Finishing of Dies and Molds: A State of the Art Review", in *Computer-Aided Design and Manufacture of Dies and Molds*, ASME PED- Vol. 32, Chicago, 1988, pp. 75-90.
8. Shivpuri, R., Tietmann, A., Kropp, E., and Lilly, B., "Investigation of a New Upset Test to Study the Formability of Steels for Cold Forging", *Transactions of the Society of Manufacturing Engineers, NAMRI/SME*, Vol. XVI, pp. 99-106, 1988.
9. Altan, T., and Lilly, B.W., "CAD/CAM/CAE of Dies and Other Complex Surfaces", in *The C4 Handbook: CAD, CAM, CIE, CIM*, Tab Books, 1988.
10. Lilly, B.W., et al., "Art to Part: CATIA to Injection Molding in an Educational Environment", *Proc. of the Sixth National Conf. on University Programs in Computer-Aided Engineering, Design, and Manufacturing, (UPCAEDM: 88)* Georgia Institute of Technology, Atlanta, 1988, pp. 182-186.
11. Lilly, B.W., *Preliminary Studies in Automated Finishing of Dies and Molds*, Engineering Research Center for Net Shape Manufacturing, The Ohio State University, Columbus, Report No. ERC/NSM-87-10, August, 1987.

## FIELDS OF STUDY

Major Field:       Industrial and Systems Engineering

## TABLE OF CONTENTS

	<u>Page</u>
Abstract	ii
Dedication	iii
Acknowledgments	iv
Vita	v
List of Tables	x
List of Figures	xii
<b>Chapters:</b>	
1. Introduction .....	1
1.1 The die finishing problem .....	1
1.2 A new die manufacturing paradigm .....	5
1.3 Scope and contents of the dissertation .....	10
2. Theoretical background and literature review .....	12
2.1 Introduction .....	12
2.2 Electro-discharge machining .....	14
2.2.1 Material removal .....	14
2.2.2 Effect of machining parameters .....	23
2.2.3 Surface integrity and microstructure .....	29
2.3 Pulsed electrochemical machining .....	46
2.3.1 Electrolytic metal removal .....	46
2.3.2 Passivation phenomena .....	60
2.3.3 Pulsed current machining .....	71
2.3.4 Effect of machining parameters .....	82
2.4 Effects of electromachining on die surfaces .....	85
2.4.1 General effects .....	85

2.4.2	Mechanical fatigue.....	87
3.	Optimization model: pulsed electrochemical machining.....	91
3.1	Objectives.....	91
3.2	General optimization model.....	93
3.3	An optimization model for diemaking.....	94
3.4	Optimizing PECM for die and mold finishing.....	99
3.4.1	PECM as a component of the larger system.....	99
3.4.2	Specifics of the problem.....	104
4.	Experimental background for the model.....	109
4.1	Objectives.....	109
4.2	Determination of the metal removal rate.....	111
4.2.1	Integrating PECM and EDM data.....	111
4.2.2	Removal rate calculation.....	116
4.3	Optimization of the surface polishing process.....	128
4.3.1	The role of the parameters in polishing.....	128
4.3.2	Design of the initial screening experiments.....	130
4.3.3	Design of the "second order" experiments.....	147
4.3.4	Determination of the smoothing rate.....	154
4.4	Concluding remarks.....	157
5.	Validation of PECM as a die finishing method.....	159
5.1	Objectives.....	159
5.2	Experimental procedure.....	160
5.2.1	Testing equipment.....	160
5.2.2	Selection of steel and heat treatment.....	162
5.2.3	Initial fatigue specimen design.....	163
5.2.4	Second fatigue specimen design.....	165
5.3	Results of the mechanical fatigue experiments.....	170
5.3.1	High-energy EDM treatment.....	170
5.3.2	Multiple-level EDM treatment.....	174
5.3.3	PECM and surface grinding treatments.....	182
6.	Conclusions and future work.....	198
6.1	Conclusions.....	198
6.2	Future work.....	200
	Bibliography.....	204

## LIST OF TABLES

<u>Table</u>		<u>Page</u>
2.1	Atomic weight, valence, and theoretical removal rates assuming a current of 1000A .....	54
2.2	Constituent elements of premium grade AISI H-13 tool steel, with percentages by weight and chemical equivalents .....	57
2.3	Four possible values of the chemical equivalent for H-13.....	58
2.4	Pulse parameters used in PECM research.....	84
2.5	Current densities, applied potentials, and workpiece materials used in PECM research .....	84
4.1	Chemical equivalents for H-13, assuming $Mo^{3+}$ , $V^{2+}$ .....	118
4.2	Theoretical removal rates for H-13 at 400 A.....	118
4.3	Initial parameter levels for screening experiment .....	131
4.4	Experimental design for initial screening experiment .....	133
4.5	Statistical profile of unpolished specimen surfaces.....	135
4.6	Pulse parameters and surface finish measurements for screening experiments .....	136
4.7	Parameter settings for second experimental series.....	149
4.8	Results of the second experimental series.....	150

5.1	EDM pulse levels for initial fatigue tests .....	171
5.2	EDM pulse levels for multiple level tests.....	175
5.3	Fatigue test results, multiple level tests.....	176
5.4	Fatigue test results, stress-relieved and non-stress-relieved multiple level specimens.....	178
5.5	Fatigue data, stress-relieved and non-stress-relieved specimens after high energy EDM treatment.....	185
5.6	EDM machining levels for 4.0 $\mu\text{m}$ $R_a$ surfaces .....	186
5.7	PECM machining parameters, 350 C/cm <sup>2</sup> .....	186

## LIST OF FIGURES

2.1	Typical EDM voltage and current pulses .....	16
2.2	EDM discharge and bubble .....	19
2.3	Idealization of voltage and current pulse forms.....	24
2.4	Comparison of EDM craters eroded at varying pulse parameters .....	28
2.5	SEM photo of EDM'd H-13 surface, 4.0 $\mu\text{m}$ $R_a$ .....	31
2.6	Three dimensional profilometer trace of EDM surface.....	32
2.7	EDM single discharge craters on several metals.....	34
2.8	Layers of surface damage due to EDM .....	35
2.9	SEM Photographs of Recast Layers of three tool steels .....	41
2.10	Cracking behavior of O-1 and D-6 steels.....	44
2.11	Schematic of ECM machining cell.....	50
2.12	Polarization curves in ECM.....	62
2.13	Dissolution in the active regime .....	63
2.14	Ideal current pulses in PECM.....	73
2.15	Schematic of duplex diffusion model.....	78
3.1	The die making process .....	96
4.1	SEM photograph of EDM recast layer— 4.0 $\mu\text{m}$ $R_a$ surface.....	113

4.2	Surfaces following EDM (left) and PECM (right).....	115
4.3	“Percentage by weight” prediction of mass removed.....	119
4.4	“Superposition” prediction of mass removed.....	119
4.5	Roughness and waviness profiles of polished and unpolished areas .....	121
4.6	Comparison of predicted and measured polishing depths.....	124
4.7	Comparison of predicted and measured mass removed.....	125
4.8	Valence of H-13 as a function of peak current density.....	128
4.9	Mean values for $R_a$ , $R_{max}$ , and $R_z$ —screening experiments .....	137
4.10	Variation of $R_a$ , $R_{max}$ , and $R_z$ with number of pulses.....	138
4.11	Main effects plot for $R_a$ .....	140
4.12	Main effects plot for $R_{max}$ .....	140
4.13	Composite interaction effects for $R_a$ .....	141
4.14	Interaction between pulse time and current density, $R_a$ .....	143
4.15	Interaction between pulse time and current density, $R_{max}$ .....	143
4.16	First order plot, $R_a$ as a function of current density and pulse time .....	145
4.17	First order plot, $R_a$ as a function of duty factor and pulse time .....	146
4.18	Experimental design for second series.....	148
4.19	Response surface for $R_a$ .....	151
4.20	Response surface for $W_t$ .....	152
4.21	Smoothing rate for three initial surface roughnesses.....	156
5.1	Design of the original fatigue specimen.....	164
5.2	FEM analysis of the first specimen design.....	167

5.3	Design of the second fatigue specimen.....	168
5.4	FEM analysis of the second fatigue specimen.....	169
5.5	S–N curve of specimens receiving high–energy–level EDM treatment.....	172
5.6	S–N curve of specimens receiving multiple–energy–level EDM treatment.....	178
5.7	S–N curves comparing multiple–energy–level and surface grinding treatments.....	181
5.8	Comparison of stress relieved and non–stress–relieved specimens after high energy EDM treatment.....	184
5.9	Fatigue specimens showing cleaning effect of long pulses.....	189
5.10	S–N diagrams of specimens polished using non–optimal (PECM–I) and optimal (PECM–II) machining parameters.....	190
5.11	S–N diagrams of EDM’d, PECM’d and surface ground specimens.....	191
5.12	Fractured surface showing crack initiation at corner.....	193
5.13	Fractured surface showing crack initiation at specimen surface.....	193
5.14	H–13 surface polished to 0.2 $\mu\text{m}$ Ra finish.....	195
5.15	H–13 surface showing grain boundary erosion.....	196
5.16	Extreme close–up view of grain boundary erosion.....	197

## CHAPTER 1

### INTRODUCTION

#### **1.1 The die finishing problem**

American industry at the beginning of a new century finds itself in a state of continuous transformation. For many manufacturing firms, what was traditionally a stable domestic market dominated by a few very large concerns has been transformed in the past few decades into a fiercely competitive global marketplace. Some American industries, such as consumer electronics, steel, and machine tools, have almost disappeared under the onslaught of Asian competition. In other, largely high technology markets American firms dominate the world market. In general, those firms that have survived and prospered in the new global arena have been those most willing to embrace both new technologies and new ideas for organizing the workplace.

The introduction of the lean manufacturing paradigm, based largely on the ideas of Toyoda, Ohno, and Shingo [1] [2] [3], has turned the traditional methods of American mass production upside down. No longer is it enough merely to achieve

economies of scale, if the huge production volumes needed to attain those economies result in increased waste, bloated payrolls, and hidden costs, with an attendant decrease in quality and value to the consumer. The lean manufacturing ethic demands that everyone involved focus on the needs of the customer, with the ultimate goal of producing essentially custom ordered parts at mass production volumes.

Along with the rapid dismantling of the mass production system has come an unprecedented increase in productivity brought about by the introduction of microprocessors into every aspect of manufacturing. From numerically-controlled machining centers on the shop floor to sophisticated software for creating component designs, simulating manufacturing processes, and controlling the flow of material through the plant, computers and microprocessors have dramatically impacted almost every aspect of manufacturing.

One economic segment that is often overlooked because it is invisible to the consumer is the twenty billion dollar industry devoted to building the tools, molds, and dies used by the piece part producers. While the die and mold making industry has been both an impetus for and a beneficiary of constant change since mid-century—one thinks immediately of the development of electro-discharge machining, numerically controlled machining, and tungsten carbide cutting tools—the past two decades in

particular have been a time of constant upheaval in the die and mold making trades, due largely to advances in computing technology.

It would be difficult to find an industry that has been more profoundly affected by the revolution in digital technology than the metalworking trade. Not only are machine tools capable of much greater precision with more degrees of freedom as a result of advanced hardware, but the very methods by which dies and molds are designed have been totally rethought as a result of CAD/CAM software and process simulation tools.

Design and fabrication of tooling has always been a major cost driver in bringing a new product design to market. Not only do these new tools cut these costs significantly, they can also drastically reduce the time required to bring a new product to fruition. Each new generation of software gives the product and tooling designers better tools for designing, testing and re-designing die and molds before they are ever cut into tool steel. Industry is rapidly moving to the point at which complex dies and molds exist only as data files until the moment when the programs are downloaded to the shop floor, and the tool steel is machined into final shape.

In the midst of all this change, one aspect of the die making process has remained largely immune to the advances in digital technology. In the final stages of production, after the die or mold been machined very close to its final shape by electro-discharge machining (EDM), the process reverts to the

time-honored methods of benchwork, in which the dies are finished by skilled hands with air grinders, abrasive stones, and polishing cloth.

In some cases, for example sheet metal forming dies, this process is unavoidable, due to current limits on our ability to predict the behavior of sheet metal during forming. Extensive tryout and rework cycles continue to be necessary because we are still not able to correctly design a complex sheet metal die correctly. The intervention of the die maker and his air grinder continues to be a necessary part of the process.

In other net shape processes, however, it is not a lack of understanding of the process that necessitates manual die finishing, but the lack of any other method for bringing the surface to a high finish, while removing the damaged layers left behind EDM. To put it simply, die and mold finishing is so complex a task that we are so far unable to duplicate it in hardware.

In 1988 this author conducted a survey for the ERC for Net Shape Manufacturing of die and mold finishing methods, both manual and automated. That report concluded that while several methods of automating the die finishing process were under development, none had really reached the stage where they could be introduced into production [4]. In the ten years since then, no significant progress in this field seems to have occurred. Instead, in response to concerns about the integrity and service life of surfaces produced by EDM, the producers of electro discharge machines have developed more sophisticated controllers that result in less damage to the

surface. And while some progress has been made in the development of hybrid machines that combine EDM with other techniques such as ECM, ultrasonic polishing, and abrasive slurries [5], little of this technology has found its way onto the shop floor. At the present time it is safe to say that die and mold finishing remains a manual operation in the overwhelming number of cases.

## **1.2 A new die manufacturing paradigm**

Why are improvements in die and mold finishing technology important? It is well established that the die surface plays a critical role in prolonged die life, in reduced friction and ejection forces, and in improved quality of the piece part. In net shape processes such as injection molding, where any minute flaw in the surface will be faithfully reproduced in the molded part, the surface quality is obviously of first importance. In other processes where surface finish is not a primary consideration, such as hot forging, the directionality of the finishing marks can have a pronounced effect on the flow of metal in the die.

Further, it is well established that the die finishing process consumes a relatively large percentage (up to 40%) of the total die or mold building cycle [6], [4]. Die and mold finishing is not only slow, it is expensive as well, since it requires relatively skilled workers to perform the task.

In addition, the lean manufacturing revolution brings new reasons for improving die and mold finishing techniques. High volume manufacturing today is operating under a new set of constraints. Chief among these are a continual reduction in time to market, a total commitment to quality, and the ability to produce wide variation in product offerings while using only a limited number of product assembly lines.

This changed environment for original equipment manufacturers is in turn leading to equally profound changes for their suppliers, including those companies who build dies and molds for the OEMs. First, and most obviously, the ability to offer a wider variation in product offerings means that more tooling is needed to produce these variations.

Secondly, reducing the time needed to introduce a new product to the marketplace means reducing the amount of time needed to turn a part drawing or CAD file into tooling. It is estimated that by the time the tooling for a product is designed and sent out for bids, approximately 90% of the final cost of the product is committed. The necessity of designing and building tooling quickly and correctly has become paramount.

When one considers what the role of tooling in the manufacturing environment really is, it is apparent that at a slightly more abstract level, the mold or die is both an information storage and retrieval device. In a typical net shape process, the material is brought to the die or mold either in a formless condition (injection molding and die casting) or in a very simple

form (sheet and billet forming). In any case, the role of the die or mold is to transform the raw material into an object having a distinct, often highly precise, geometry.

The die or mold itself contains a very large percentage of the information that will be encoded in the part itself, with the remainder of the information residing in the machine operating parameters. Not only is the information regarding the shape of the final piece part encoded in the die, but also the end results of process simulations and years of the die maker's experience also find their way into the die or mold, very often in those parts of the die that will not form part of the piece part itself, but which control the flow of material within the tool.

At this point it is important to distinguish between those processes in which our knowledge is sufficient to allow the die *designer* to determine the final shape of the die or mold, e.g., injection molding, die casting, and some forging operations, and those processes in which the final design of the die remains in the hands of the die *maker*, e.g., complex sheet metal dies. This is an important point because in the first case, we are now able to essentially define the die or mold as a data file residing in a computer, while in the second case, we cannot.

Sheet metal dies at this time are simply beyond our analytical abilities, and thus the information needed to reliably produce an acceptable part remains in the die itself, and nowhere else. Even if we reverse engineer a

sheetmetal die on a CMM, for example, and reproduce it using a CNC machining center, it is a certainty that the resulting die will not function as well as the original, without the further intervention of a skilled diemaker.

On the other hand, in the case of injection molding, die casting, and billet forming, simulation software has reached a level of sophistication sufficient to allow the designer to accurately predict thermal conditions in the die during a production cycle, as well as the flow of material within the die and material orientation (in the case of injection molding) and shrinkage. Given this information, it is now at least theoretically possible for the die designer to create a workable die or mold in the computer, which can then be duplicated on CNC machining centers to a high degree of precision.

Where does this lead? For many forward-thinking engineers, it leads to the conclusion that “the die is in the database” [7], [8]. If one accepts this idea, then along with the idea that the highest quality parts come from new dies comes the conclusion that when a die or mold is worn to the point at which it requires extensive repair, the best course of action is not to rebuild the die (or die section), but to discard it and build a new one.

This conclusion dovetails exactly with the basic need of the lean manufacturing enterprise to rapidly change tooling while keeping part quality consistently high. How does this idea impact die finishing? If the trend in die and mold making is toward replacement of an entire die or a die section, then obviously those finishing methods which reliably and repeatedly lead to:

- the closest possible approximation of the ideal die geometry;
- the highest possible surface integrity; and
- identical or nearly identical dies or die sections

will possess inherent advantages over any other die finishing method.

Given these goals, then the best finishing method is one in which the final surface geometry can be repeatedly created to within very close tolerances, with a die surface of high integrity. This implies that multiple die sections or mold cavities would be created by a *single* tool in a process that leads to little, or ideally *no* tool wear. By finishing the die surfaces with a single tool, we can eliminate a major source of variation between multiple copies of a die section.

This is not to say that by using a single, non-wearing polishing tool we are guaranteed identical piece parts, however. The polishing parameters will also play a large part in determining the shape and surface finish of the polished cavity, and must also be carefully controlled. In addition, even if identical cavities are created, the parameters of the actual production process will also have a direct effect on the geometry and quality of the final product. But being able to create multiple cavities from a single finishing tool would no doubt remove a large source of variation in the part geometries.

This dissertation is an investigation and evaluation of one such candidate process, pulsed electro-chemical machining (PECM). This process, developed in the last decade [9] [10], shows some promise as a potential means

of reliably reproducing multiple die or mold surfaces to exact dimensions. Because the process is electrolytic, the forming tool, typically a graphite or copper electrode, shows zero wear. In addition, the process is at least theoretically capable of working to tolerances on the order of tens of microns, while creating stress-free, highly polished surfaces. Thus it would seem to meet the criteria outlined above for an ideal polishing process.

### **1.3 Scope and contents of the dissertation**

This dissertation has four primary goals. The first is to present a model for optimizing the die or mold making process. The model should be able to account for variations in practice and technology from shop to shop, and it should also include the twin imperatives of reducing cost while improving the quality of the final product.

The second goal is to use pulsed electrochemical machining as a candidate process, and to show how it might be optimized in light of the larger model. A key point here is the integration of the PECM process into the already existing die making cycle with minimal upheaval and cost.

Third, the dissertation is intended to present results of research into the PECM process, how it is affected by variation in the principal parameters available to the user, and what kind and quality of surface might be achieved.

Finally, if PECM is to play a role in die making, it must add something of real value to the customer, in this case the user of the die or mold. In this

dissertation, mechanical fatigue life is the metric by which the process is to be judged, because almost every piece of net shape tooling is subjected to cyclic loading during its lifetime.

The dissertation is structured in the following way. Chapter Two provides the theoretical background necessary for understanding both the EDM process and its deleterious effect on die and mold surfaces, and the PECM process.

Chapter Three presents the general optimization model for the diemaking trade, and shows how the model might be applied to PECM in particular.

Chapter Four presents the results of research performed on an industrial PECM machine, the Shizuoka Seiki COTAC-51. The metal removal rate, surface finish, and surface quality are all examined in detail. This chapter concludes with a discussion of how the data presented fits into the optimization model of Chapter Three.

Chapter Five is devoted to the extensive set of mechanical fatigue tests on specimens prepared by EDM at multiple levels of surface damage, and by PECM following EDM. In this dissertation, the widely used tool steel AISI H-13 is used as the workpiece material.

Chapter Six summarizes the work of the dissertation, and presents several ideas for further research into pulsed electrochemical machining.

## CHAPTER 2

### THEORETICAL BACKGROUND AND LITERATURE REVIEW

#### **2.1 Introduction**

Die and mold finishing is only one step in a complex process that begins with the initial conceptual design of the piece part and ends with the release of the die or mold to production. The set of steps that a die component goes through depends both on the specific function of the component, and on the particular net shape process itself. The net shape processes in general all require complex molds and dies to transform raw material into useful parts.

The components undergo several discrete steps during the die making process, as the rough blanks are gradually turned into an extremely precise, complex machine. The particular set of processes any given die component is subjected to depend on the particular process for which the die or mold is intended, the type of steel, the degree of hardness desired, and so on. Typically a die begins with a drawing or CAD file of the part to be produced, and ends with the die being released to production.

For the purposes of the present work, the focus is on the last few stages of the process, during which the components are brought to their net or near net shape by electro-discharge machining, followed by a final polishing process intended to remove the damage caused by EDM and bring the die surface to a suitably fine finish.

Electro-discharge machining in die making can actually be seen as two distinct processes: a roughing process in which very high energy pulses are used to quickly remove die material and bring the surface close to its final shape, and a finishing process during which progressively lower levels of pulse energy are used, with the goal of producing a surface very close to the ideal geometry, with a relatively fine surface finish.

In some cases the rough machining is performed by milling operations and the EDM process, because it is much slower, is reserved only for the final metal removal following heat treating. In other cases, the entire die block is brought to final shape by EDM. And in still other cases, high speed milling is being used in combination with ceramic cutting tools to replace EDM altogether.

This chapter provides the theoretical background for understanding both the electro-discharge machining and pulsed electrochemical machining processes. The material on EDM is included in order that the process by which the die surface is initially degraded may be better understood, and also in order to be able to compare the two methods in terms of die finishing.

## 2.2 Electro–discharge machining

**2.2.1 Material removal** The EDM process was developed by the Soviet physicist Boris Lazarenko during the early years of the Second World War. Lazarenko was investigating the wear of electrical relays due to arcing, and noticed that the wear rate increased significantly when the contacts were immersed in a dielectric fluid. Noting that the wear rate was not affected by the hardness of the contacts themselves, he was quick to realize that this phenomenon could be used as a process for machining hard metals. By the end of the war, EDM was being used as a production machining process throughout the Soviet Union [11].

Interest in this new machining technology developed quickly in the West in the years immediately following the War. By the early sixties, researchers in the Soviet Union, Great Britain, Germany, and the United States were hard at work developing competing theories to explain the EDM phenomenon [12], [13], [14-17].

The physics of the EDM process is today well understood, although a few points of contention remain. The theory known as the *thermoelectric model* has been adopted by researchers in the field as the best explanation of the process. Electro–discharge machining is initiated when a charged electrode, usually copper or graphite, is brought within a few thousandths of an inch of the workpiece. Both the tool and workpiece are immersed in dielectric fluid,

which is most often hydrocarbon-based, although de-ionized water has also been used. When the potential gradient across the machining gap reaches a threshold value, the initial step in the discharge process begins.

The threshold potential is a function of many factors, including the resistivity of the dielectric, the geometry of the tool and workpiece, and the degree of debris present in the dielectric from previous discharges. In any event, at some point the resistance across the gap will be at a minimum. At this location the field will be strongest, and conductive particles created from previous discharges that have not been flushed from the gap will begin to concentrate here.

As the voltage pulse approaches its peak level (typically 50–200 V), the strength of the local field reaches a level at which electrons are stripped away from nuclei and begin to migrate toward the anode, leaving ionized particles behind. Because the mass of the electrons is several orders of magnitude less than that of the positively charged ions, they accelerate much more rapidly, so that in the initial stages almost all movement in the ionized channel is confined to the electrons. As the electrons migrate, they collide with other atoms, jarring loose more electrons in what is known as “impact ionization”. These electrons collide with yet more atoms, continuing the process and eventually causing an “avalanche breakdown”, a common failure mechanism for electrical capacitors [18].

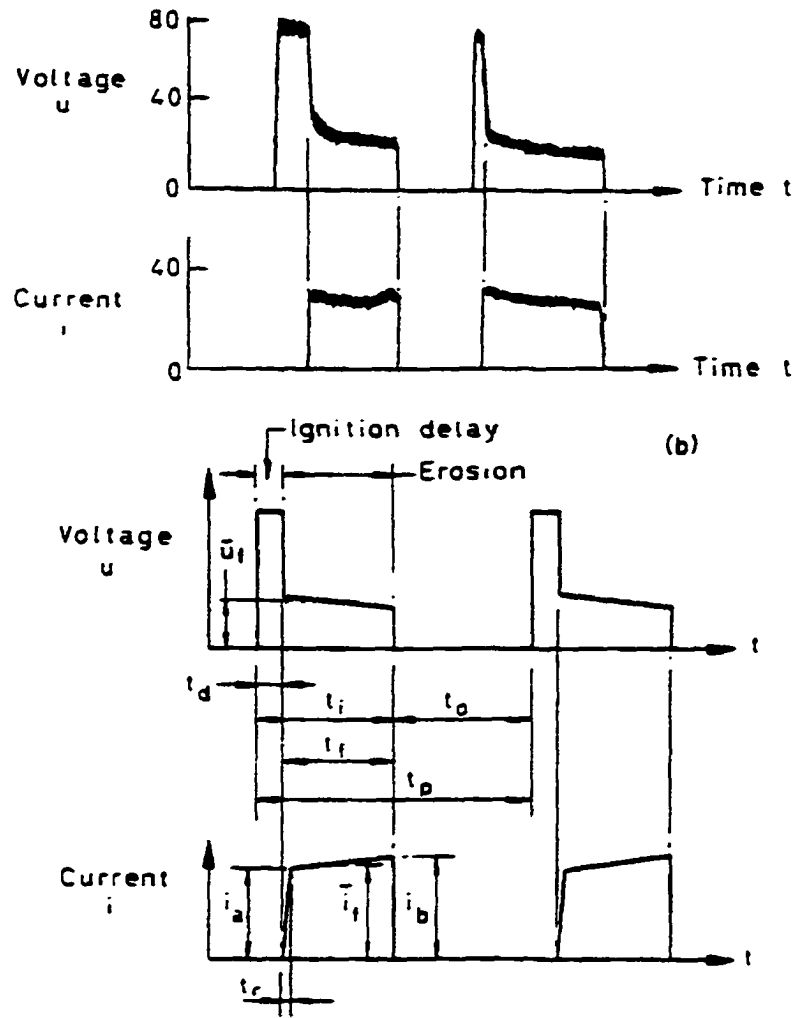


Figure 2.1: Typical EDM voltage and current pulses

As the avalanche of electrons begins to impact the anode (Crookall estimates the current density at the anode to be approximately  $10^6$  A/mm<sup>2</sup>), the positively charged ions begin to drift toward the cathode, a plasma channel forms across the gap, and current begins to flow. At this point, the voltage level drops off to roughly half of the peak value. It remains at the arc voltage level until the pulse is terminated by the machine control. Figure 2.1, taken from [19] , shows a typical voltage pulse during EDM.

The period between initiation of the voltage pulse and the onset of current flow is known as the “ignition delay”. Because it is affected by local conditions in the dielectric itself, ignition delay is a random phenomenon. If the machine controller regulates the time of the voltage pulse, then the ignition delay can play a major role in determining the metal removal rate, since the extent of the ignition delay reduces the length of the current pulse. Since the removal rate is a function of the current pulse, not the voltage pulse, longer ignition delays result in lower metal removal rates.

Ignition instability is a major source of poor surface quality in EDM, and in recent years much work has gone into controlling this aspect of the EDM process. One area that has received attention in the past decade is the application of controllers based on fuzzy logic principles to better control instabilities in ignition [20], [21].

At this point in the process, a plasma channel has formed, both tool and workpiece are impacted by either ions or electrons, and a bubble of vaporized

metal, tool material, and dielectric fluid begins to form around the channel. The role played by this bubble is crucial to understanding the thermoelectric model. Lazarenko noted in 1940 that discharges in a fluid greatly accelerate the rate of electrode wear. Zolotykh was apparently the first to apply high speed photography to the study of single discharges, and it was his observation that material was ejected at the very end of the discharge pulse. He attributed this phenomenon to the simultaneous collapse of the gas bubble surrounding the plasma channel[22].

Other researchers [Palatnik, 57], [Hockenberry, 65], confirmed Zolotykh's assertion that the inertia of the dielectric fluid is crucial to the process. The discharge bubble appears very soon after the establishment of the plasma channel itself. As the discharge progresses, this bubble expands (see Figure 2.2), as dielectric fluid and material from the electrode surfaces continue to evaporate. However, the inertia of the dielectric fluid in the remainder of the gap prevents the bubble from expanding rapidly enough to prevent the pressure in the bubble from reaching high levels.

Precise estimates of the extremes of temperature and pressure reached during a single EDM discharge have not yet been determined, to the best of the author's knowledge. Zolotykh, in his influential early paper, estimated that the pressure in the bubble in the very early stages of a discharge exceeded ten atmospheres [22]. At roughly the same time, Palatnik and Liulichev estimated temperatures in the channel as high as 6000° C [24]. More exact

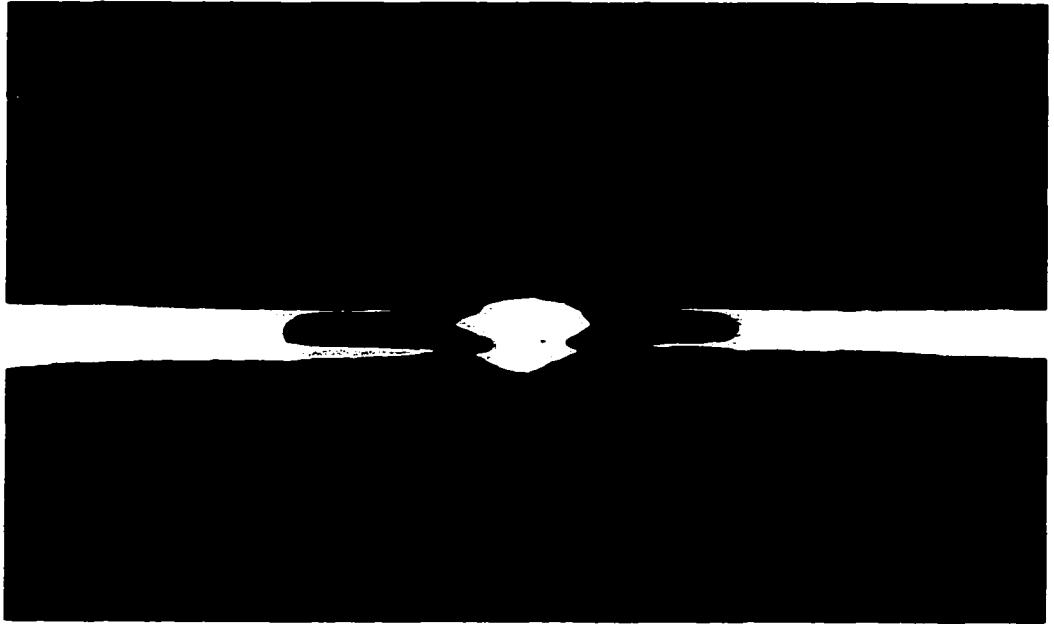


Figure 2.2 EDM discharge and bubble (from [23] )

approximations of these parameters remain elusive, but in any event, the temperature at the workpiece surface is known to reach levels well beyond the boiling point of the metal at atmospheric pressure. While the high pressure inside the discharge bubble prevents most of the material from boiling, at least some of the workpiece and tool material is assumed to evaporate during the discharge. [25].

It is important to note that the relative amounts of melting at the anode and cathode surfaces are largely a function of the pulse duration. For very short pulses, the electron flow predominates, and the anode will show a larger degree of melting than the cathode. For longer pulse times, however, cathode wear greatly exceeds anode wear, because the ions impacting the cathode surface are much more massive than the electrons at the anode. In fact, given a long enough pulse, the anode surface will actually begin to re-freeze, due to the spreading of the electron stream at the surface and the resultant decrease in current density.

For optimal tool/workpiece wear ratios, at relatively long pulse on-times the tool is usually configured as the anode, and for very short pulses as the cathode in conventional EDM [26]. In travelling wire EDM, on the other hand, where very little tool wear can be tolerated due to wire breakage, the standard polarity is reversed (i.e., the workpiece is the anode) and very short pulse times are used.

At the end of each voltage pulse, the expanding bubble surrounding the plasma channel quickly collapses. This sudden decrease in pressure causes the molten material at the surface of the workpiece to erupt into the gap. One point of contention that remains in the thermoelectric model concerns the issue of material removal. Some researchers contend that it is only during the very early stages of the current pulse that workpiece material is actually vaporized and removed from the surface. According to this model, longer pulses lead to more melting of the workpiece material, but the molten material is asserted to freeze on the workpiece surface after the discharge and remain there. It is the contention of these researchers that longer pulses result only in a heavier layer of recast material on the surface, not in an increase in material removal [27].

Other researchers [26], following Zolotykh, contend that it is at the end of the pulse that most of the material is ejected from the surface, with the collapse of the high pressure bubble surrounding the plasma channel. When the voltage pulse ends, the rapid drop in pressure within the bubble causes the metal that has been heated above the boiling temperature at atmospheric pressure to erupt into the gap. Lee, Lim, and their colleagues at the University of Singapore, assert that fully 85% of the molten material returns to the surface of the work, and freezes there [28]. Other researchers hold that the figure is much lower [27].

Given the difficulty in measuring such a quantity under realistic conditions, it is unlikely that a definitive answer will be forthcoming, and in fact the point is largely irrelevant to our purposes. Nevertheless, it is generally accepted that a substantial portion of the workpiece material that either melts or vaporizes during a discharge eventually freezes there, creating the recast or “white” layer. The rest of the material either remains in vapor form and escapes as gas bubbles through the dielectric to the atmosphere, or else solidifies into small droplets in the dielectric, and is carried out of the gap by the flow of dielectric fluid.

At this point, the single discharge is complete, and another discharge begins. For many years it was accepted that the next discharge would occur at random somewhere else in the gap where the local separation of tool and workpiece was a minimum. In fact, as noted above, the next discharge will occur where the local gap resistance is lowest. This may occur at the point of the smallest gap, but other factors, such as accumulated debris from previous discharges, also affect the location of the next discharge.

Kunieda and Kojima [29], [30] conducted a series of experiments that showed that contrary to previous theory, the plasma channel actually travels along the tool and workpiece surfaces during a single discharge. More importantly, they also proved that a series of discharges will tend to occur in close proximity to one another, and that the “discharge patch” will travel more or less at random in the gap. This work strongly suggests that previous

discharges will have an effect on subsequent ones, presumably due to the reduction in local resistivity due to the presence of debris and ionized particles in the fluid.

### **2.2.2 Effect of machining parameters**

State-of-the-art CNC EDM machines provide the user with a wide variety of machining options, including the use of multiple tools, orbital tool motion, and fuzzy logic to optimize machining stability. Not only is the user able to control the fundamental pulse parameters, such as on-time, peak current level, and duty factor; CNC controls allow the user to program complex three-dimensional tool paths to optimize cavity erosion and debris flushing as well. However, since these options do not directly affect the condition of the EDM'd surface, they will not be dealt with here.

Material removal in EDM is a function of the pulse energy and the pulse frequency. Modern EDM machines almost all employ solid state power supplies capable of producing uniform pulses at rates up to 250 megahertz. The user typically selects the peak voltage and peak current levels, as well as the pulse on-time and pulse duty factor. The duty factor is defined as the ratio of on-time to the total time required for a single pulse, and is more often employed as a user-defined input than is pulse off-time.

If metal removal rate were the only important process criterion, it would be an easy task to optimize the EDM process. In that case, each pulse would be

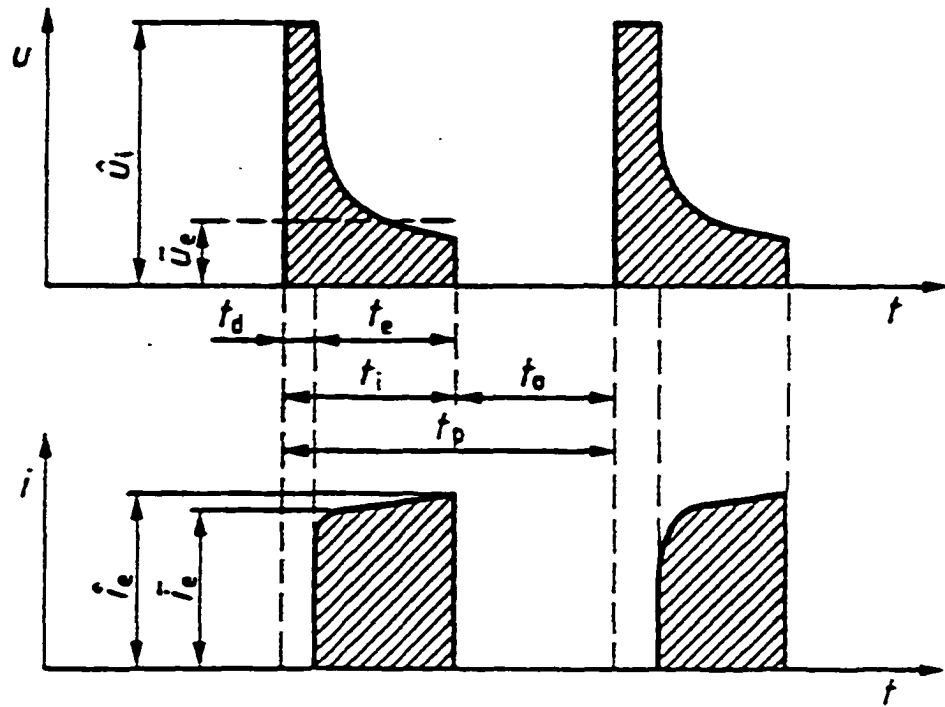


Figure 2.3: Idealization of voltage and current pulse forms (from [31] )

set for maximum possible energy level, and the duty factor would be set at the highest possible level that would permit adequate gap flushing. However, the set of parameters that maximize removal rate also lead to maximum surface damage and tool wear.

It has been well established that the amount of metal removed by a single discharge is directly proportional to the pulse energy. An idealization of the actual voltage and current pulses of Figure 2.1, shown in Figure 2.3, is taken from [31]. The energy of a single discharge is given by

$$W_e = U_e * i_e * t_e$$

where

$W_e$  = discharge energy

$U_e$  = average discharge voltage

$i_e$  = average discharge current

$t_e$  = discharge time

The power in a single pulse is then

$$P_e = W_e * f_e$$

where

$f_e$  = discharge frequency =  $1 / t_p$

While it might seem that any combination of voltage, current, and on-time giving an equivalent pulse energy would have a roughly identical effect on the workpiece surface, in fact that is not the case. The three parameters

play different roles in the process, both separately and in combination with the others.

The role played by the pulse voltage is perhaps the easiest to comprehend. Ignition of the discharge occurs when the potential across the machining gap reaches a threshold value. From this fact it is clear that the voltage level selected will directly impact the size of the machining gap: the larger the pulse voltage, the larger the gap the spark will be able to bridge. However, the voltage level selected also interacts with the other two parameters to affect surface finish, which will be described below.

The other two parameters, pulse current and on-time, play a much more direct role in defining both metal removal and resulting surface finish. For a given voltage, the values of current and pulse on-time selected will have a marked effect on the size and shape of the resulting surface crater. Figure 2.4, taken from [27], shows profilometer traces of two craters created from the same tool/workpiece combination, but with varying current levels and pulse times. Note that even though the total single pulse energy for the crater on right is over four times greater than the crater on the left, the resulting crater is much more shallow, and spread over a wider area.

In general, high current levels at high frequencies lead to narrow, deep craters, and low current levels at relatively lower frequencies lead to craters with a much wider, shallower configuration. Craters of this type lead to less surface damage to the workpiece. In addition, if relatively higher voltage

levels are used, resulting in a wider gap, the surface damage is decreased even further due to a decrease in heat penetration into the workpiece surface.

In practical terms, this means that the user can set the machine parameters to create aggressive cutting conditions during the roughing phase, when the object is to remove as much material as possible, and then use a different set of parameters to remove the surface damage caused by the initial erosion cycle. In fact, modern EDM machines allow the user to define an entire series of erosion cycles, each one slightly less aggressive than the previous one, in order to bring the eroded surface progressively closer to the net surface, all the while minimizing damage to the workpiece itself.

It should be noted at this point that the machining parameters also directly influence the amount of tool wear that occurs relative to the amount of metal removed. Tool wear in EDM is most strongly a function of the particular tool geometry: sharp radii and small features are quickly worn away during the erosion process. This is due both to the fact that discharges tend to concentrate in these areas, and also to the reduced heat conduction possible from small features. However, given that situation, the *relative* wear between tool and workpiece is most strongly affected by the pulse on-time, in conjunction with the chosen polarity.

As noted above, during the initiation of the discharge, electrons in the dielectric are very rapidly accelerated in the direction of the anode. An electron avalanche occurs which results in melting and vaporization of the

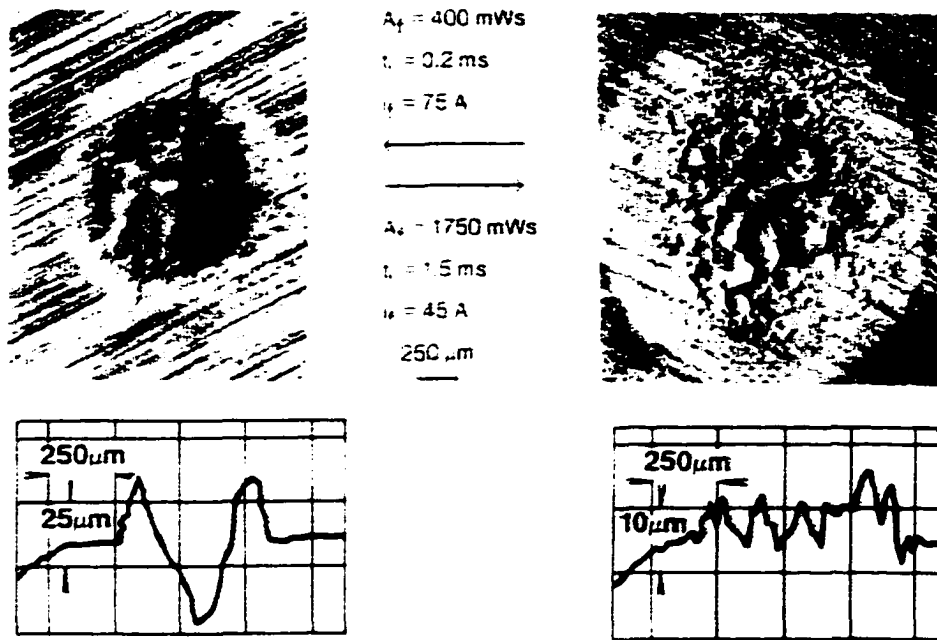


Figure 2.4: Comparison of EDM craters eroded at varying pulse parameters

(from [27])

anodic surface. However, as the pulse continues, the electron stream tends to widen with the expansion of the high pressure bubble, which leads to a decrease in the current density at the tool surface. This can lead to the anode surface cooling sufficiently during a single discharge for local freezing to occur.

At the same time, a longer pulse means that more ions impact the cathodic surface. Because the ions are much more massive than the electrons, for a longer pulse a relatively greater amount of melting will occur at the cathode. In the case of a very high current density over a short period of time, the erosion crater will be relatively narrow, but deep, as shown in Figure 2.4.

If the EDM machine is in so-called "standard polarity", the tool is the anode and the workpiece the cathode. Thus, for short pulse times, the tool surface will wear relatively more than the workpiece, whereas the reverse occurs for longer pulse times. For most erosion regimes, the preferable setup is obviously standard polarity, relatively modest current and voltage levels, and long pulse times. However, for finishing, it is often the case that reverse polarity is applied, with very short pulse times and high voltages, to achieve a high quality surface finish.

### **2.2.3 Surface integrity and microstructure**

The detailed explanation of the thermoelectric model given above is necessary for a basic understanding of how a typical EDM surface is created,

and why it has the unique characteristics that it does. EDM surfaces in general are unlike any other machined surface, in that they have no “lay” or overall pattern. The scanning electron microscope photograph of Figure 2.5 shows H-13 steel after being machined by EDM to a surface finish of approximately  $R_a = 4 \mu\text{m}$ .

Figure 2.6, taken from [32], shows a three dimensional profilometer trace of a typical EDM'd surface. Quite obviously, the surface shows no directionality of machining at all. To the naked eye, the surface presents a matte or shot-blasted finish. Examined microscopically, an EDM'd surface appears heavily cratered, showing evidence of melting and remelting; steel that has been EDM'd at high energy levels very often shows extensive surface cracking as well [28], [33].

Extensive single discharge studies on a number of different materials have shown a wide variation in the size, structure, and shape of individual craters [34], [35]. It has been established for some time that different materials react differently to the EDM process, and that the *combination* of tool and workpiece material plays a crucial role in determining the nature of the surface created [35], [36]. Individual craters generally vary in size from 20 to 50  $\mu\text{m}$  in diameter and 10 to 15  $\mu\text{m}$  in depth, though this is to some extent a function of the material as well [37]. Figure 2.7, taken from [27], shows single discharge craters created on a number of different materials.

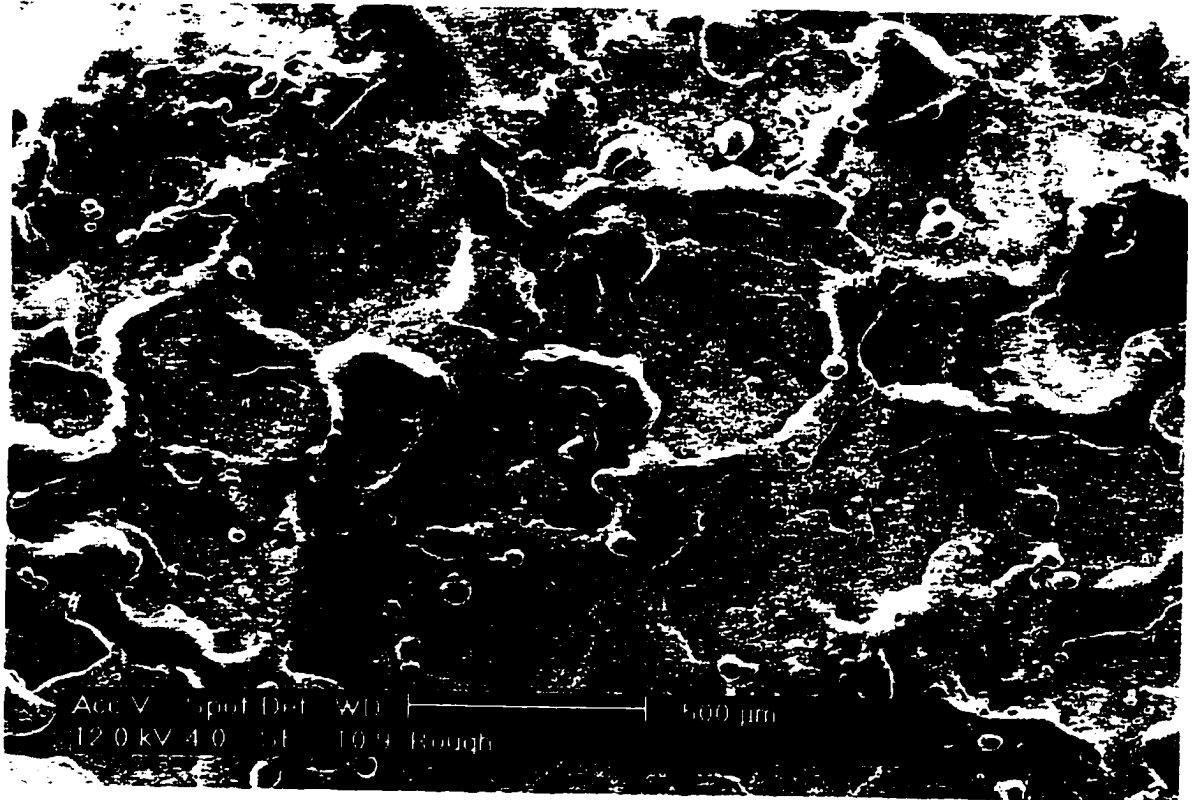


Figure 2.5 SEM photo of EDM'd H-13 surface,  $R_a = 4.0 \mu\text{m}$

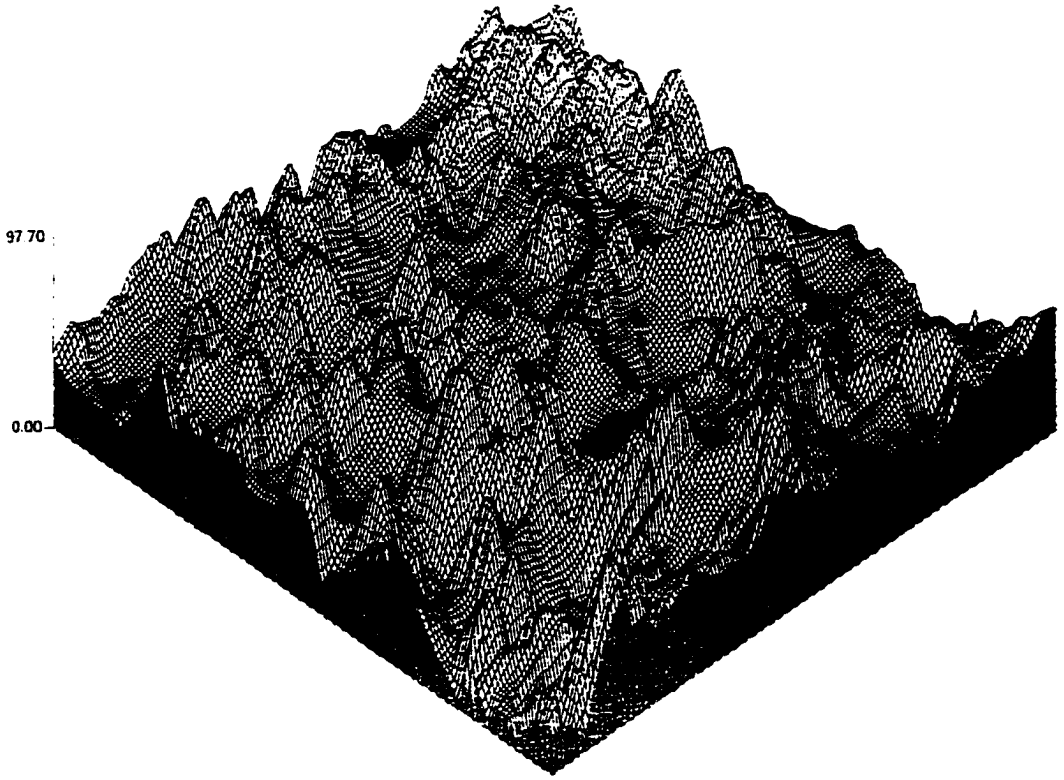


Figure 2.6: Three dimensional profilometer trace of EDM surface (from [32])

While much is known about the structure of EDM'd surfaces, it should be noted that after fifty years of research, there still exists some confusion regarding the terminology applied to surfaces eroded by EDM. While some researchers refer to the "heat affected zone" as the entire damaged layer, others use the same term to apply only to the layer beneath the outermost surface layer, which is variously known as the "white layer" or "recast layer".

In any event, it is generally agreed that EDM'd surfaces typically consist of at least two, and sometimes three, distinct layers, as shown in Figure 2.8. The topmost recast layer is also called the *white layer* because of its resistance to etching in standard metallographic reagents. Until very recently, almost nothing was known of the structure of this layer [37], which can vary from less than 5  $\mu\text{m}$  to more than 50  $\mu\text{m}$  in thickness. It is typically much harder than the parent metal, and is known to contain high amounts of carbon [39]. In those cases in which copper, rather than graphite, is used as the tool material, significant amounts of copper in addition to carbon are also found in the recast layer [40]. The presence of carbon in this case is attributed to dissolution by-products of the dielectric fluid, which is typically a hydrocarbon.

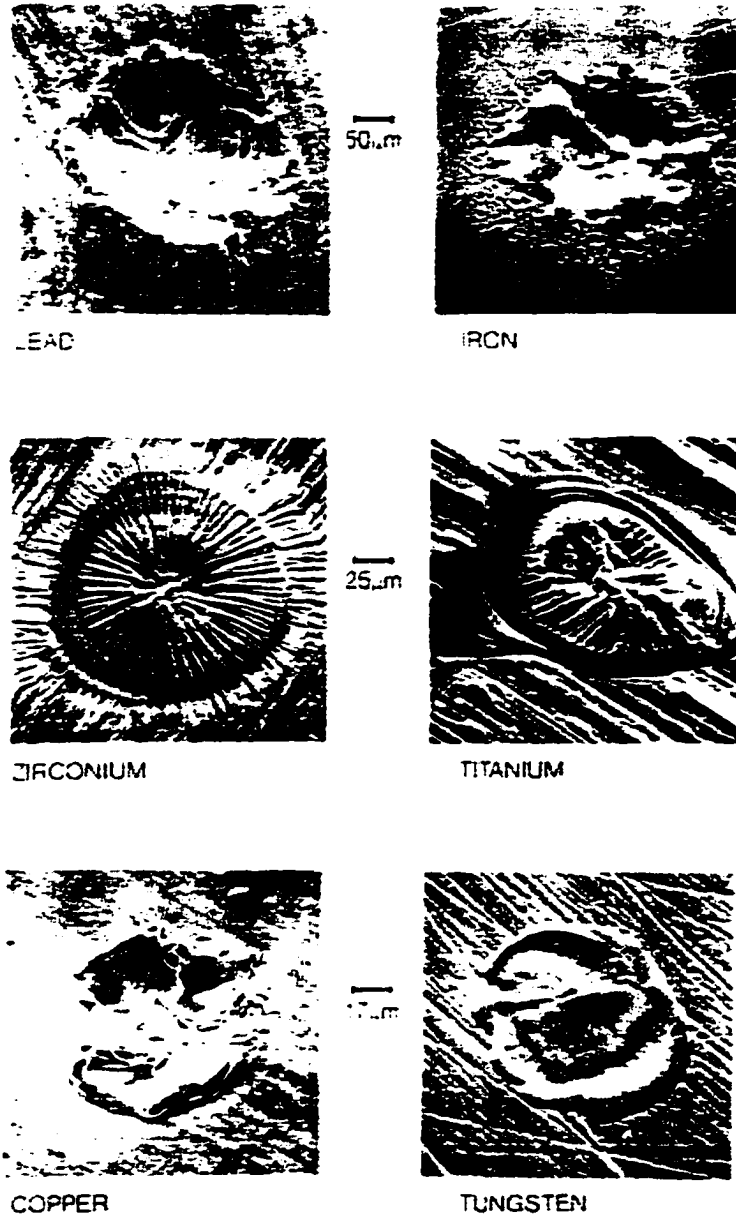


Figure 2.7: EDM single discharge craters on several metals, (from [27])

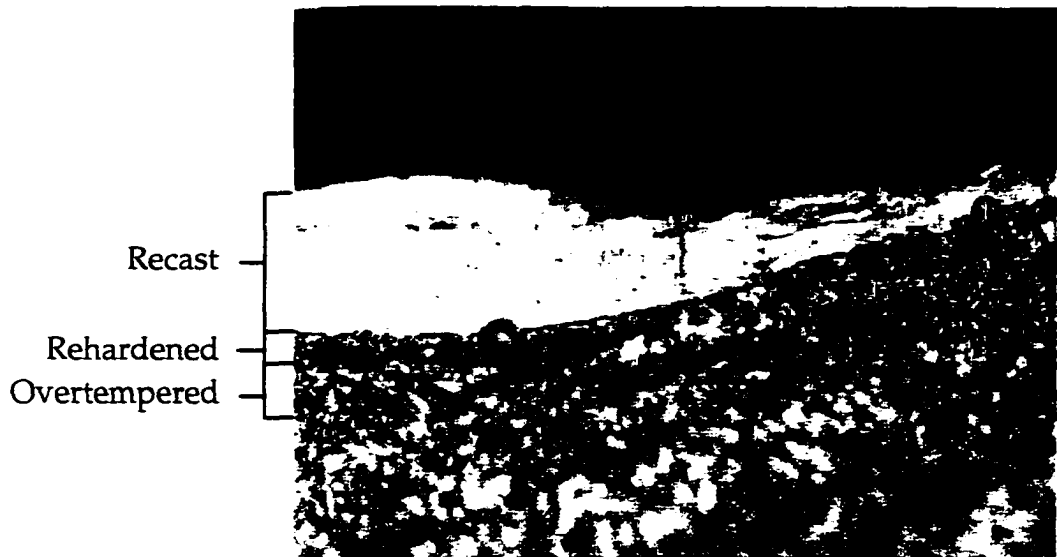


Figure 2.8: Layers of surface damage due to EDM (from [38]).

Beneath this layer one finds a thicker layer, softer than the parent material, known as the *overtempered zone*. This layer is assumed to be unaffected by changes in composition; the lower hardness is a result of annealing by the high surface temperatures reached during the EDM process. Some studies have shown that the thickness of this layer is not significantly affected by a reduction in average discharge energy, as one might expect. This finding is significant in terms of thermal fatigue, as the overtempered layer is thought to contribute to this failure mode [41].

Between the two layers one sometimes also finds a third layer, sometimes called the *re-hardened layer*. This structure is typically found only in surfaces that have been EDM'd at high energy levels, and for this reason is often overlooked. This layer also shows elevated carbon content as well as tool

material contamination, and is comparable in hardness to the recast layer [42]. The microstructure of this layer differs from that of the recast layer, however, because it has not been melted and rapidly cooled.

*Composition* It was recognized very early in the history of the EDM process that it produced surfaces of extreme hardness, and some of the earliest work was concerned with finding methods of using EDM as a surface hardening treatment. N. I. Lazarenko was perhaps the first to note that high levels of carbon could be found at or near the eroded surface. Much of the early research in the Soviet Union was concerned with finding viable methods of using the process to produce stable, hardened surfaces on steels [43].

The origin of the elevated carbon in EDM'd surfaces remained a source of controversy for some time. Barash attributed the saturation of carbon to diffusion of carbon from the parent material [44]. A more likely culprit was the pyrolysis by-products of the hydrocarbon dielectric, which was the source identified by Lloyd and Warren in their seminal paper published in 1964 [34]. It is now accepted that this is the source for most of the elevated carbon in the uppermost layers [39] although material from graphite electrodes also plays some role.

Several researchers have established that some of the contaminants trapped in the workpiece surface after freezing also come from the tool material. Roethel and his colleagues, among others, have confirmed the presence of copper in the recast layer, when copper electrodes were used [40].

Finally, Thomson noted that the difference in tool material can also play a role in the nature of the surface itself. He notes that when copper tools are used, many more small globules are present on the free surface, than are present with graphite tool electrodes [45]

*Microstructure* The most extensive research completed to date on the microstructure of the EDM surface layers is due to Lim, Lee, and their colleagues at the University of Singapore. They were the first to succeed in etching the recast layer, and thus were able to give more definitive answers concerning its microstructure. The material in this section is largely taken from their paper of 1991 [37], one of a series of papers they have written detailing the microstructure of the recast layer [28, 33, 42, 46, 47].

Lim and his colleagues looked at five different tool steels: AISI O1, A2, D2, D6, and M2. They EDM'd the samples at three different power levels (low, medium, and high energy) in a hydrocarbon dielectric and then attempted to etch them using a variety of chemical compounds. They were successful in etching all but the thinnest white layers on all the materials tested, using either Nital or an alkaline etchant consisting of chromic acid and sodium hydroxide.

They found that three general structural types are typically found in the recast layer. The first type has a multilayer structure, is typically from 20 to 50  $\mu\text{m}$  thick, and is apparently made up of layers of similar structure that were

deposited one after the other. The second type, which is composed of a single layer, has a thickness of about 10 to 20  $\mu\text{m}$ . This layer closely resembles the individual layers of the first type, and is dendritic and columnar in structure. The third type has a thickness of less than 10  $\mu\text{m}$ , and proved to be extremely resistant to etching, either by Nital or by boiling chromic acid–sodium hydroxide. This layer type is assumed to be structurally homogenous.

Lim *et al.* looked at the incidence of these three layer types as a function of discharge energy, and came up with a somewhat surprising result. First, they noted that the overall distribution of the three layer types was a function of the discharge energy. For example, for high energy discharges, the thick multi-layer type covered approximately 70% of the surface, the intermediate single layer 20%, and the thin layer 10%. For low energy discharges, the thin layer covered 90% of the surface, and the thick layer 10%. However, it should be kept in mind that for any given energy level, the thickness of the recast layer varied over a wide range.

The surprising fact is that the layer *type* depended not on the discharge energy, but on the *thickness* of the layer. To quote directly from the paper:

The present observations have shown that, although the spark energy affects the average thickness of the recast layer produced by EDM on tool steels, no direct relationships can be concluded between the types of recast layer microstructure and the discharge energy used. The results show that the microstructure of the recast layer produced by EDM is largely determined by its local thickness. In other words, the discharge energy used controls the average thickness of recast layer produced, and it is the thickness variations which in turn

determine the distribution of different recast layer types produced by the discharge condition. [37]

One possible explanation for the variation in thickness of the layers may lie in the fact that the typical EDM'd surface has been subjected to repeated discharges. It is self-evident that once the initial virgin surface is eroded, the material that is being removed and to some extent recast on the surface has already been through the process at least once. In other words, the material that is being removed from the surface is recast layer created by previous discharges. The repetitious nature of the EDM process may well account not only for the multiple layers present, but also for the very high carbon content (up to 30%) found by some researchers.

Having developed this classification of the recast layer, Lim *et al.* went on to look at the different tool steels in detail. Figure 2.9, taken from this paper, show scanning electron microscope photographs of three of these steels. Several interesting facts were observed from these experiments. First, they noted that for A2, D2, and D6, the ratio of the thickness of the uppermost layer to the innermost varied from 1.5 to 3 times as much. In contrast, the topmost layer in O1 (not shown) is thin, and is also much thinner than the innermost layer.

The other noticeable difference was the presence of a thick intermediate layer in the O1 and D6 steels, when compared to the A2 and D2. This layer was formed of interlocking dendrites extending in both directions from the

center of the layer. This contrasted to the intermediate layers in the A2 and D2, which were thin and showed little discernable structure.

They explained these differences in microstructure as follows. First, they note that at the end of each discharge, the molten metal can cool by two routes: quenching in the dielectric, and conductive heat transfer through the base material. They assert that the differences in relative thickness of the layers (inner and outer) is a function of the relative conductive heat transfer coefficients. For A2 and D2, which have lower thermal conductivity than O1, a proportionately larger flow of heat through the dielectric will result in a thicker band in the outermost layer, as the molten material freezes from the interface inward. In contrast, O1 with higher conductivity will show a thicker layer next to the base material. They also note that this would explain the columnar base layer in O1, as opposed to the dendritic layers in the air hardening steels.

The similarity in structure (i.e., a relatively thick, dendritic middle layer) between the O1 and D6 steels is attributed to the relatively high amount of tungsten in both of these steels. They note that since tungsten is known to lower the liquidus in the Fe-C system, it may increase the degree of undercooling in the melt, thus promoting solidification from within the melt and bi-directional dendritic growth in this intermediate layer. If this theory is



(a)



(b)



(c)

Figure 2.9: SEM Photographs of Recast Layers of Three Tool Steels:

(a) AISI A-2, (b) AISI D-6, AISI D-2 (from [37])

correct, similar behavior should also be observed in other hot working die steels, such as H-21, given their high levels of tungsten.

*Residual Stresses and Microcracks* One other aspect of the EDM'd surface may prove to be relevant to the current research, and should be noted here.

Microcracking is important simply because it is one of the predominant negative effects of EDM, as regards die and mold making. It is commonly accepted that these cracks occur when the molten metal cools very rapidly, giving rise to stresses at or near the surface that exceed the UTS of the material. These cracks are generally confined to the recast layer, but it is not unusual to find cracks that have penetrated through the recast into the overtempered zone.

The best work to date on this aspect of EDM is again due to Lee, Lim, and their colleagues at the University of Singapore [Lee, 92a], [Lee, 92b]. To summarize their work briefly, they looked at the cracking behavior of several materials, including pure copper and iron, low and medium carbon steel, and four of the tool steels reported on above. In general, they found the following: propensity to cracking is a strong function of thermal conductivity and material hardness. Metals with a high value of thermal conductivity, such as copper and iron, showed little or no cracking when EDM'd. Tool steels, on the other hand, show a strong tendency to crack, with the material having the

lowest conductivity, D-6, also showing the most tendency to crack, as shown in Figure 2.10.

Lee *et al* also relate cracking behavior to the three types of microstructures reported on in [37]. There is a pronounced tendency for cracking to occur in the multi-layered microstructure, but one must ask if this is a cause and effect relationship, or is it due to the fact that both phenomena occur at high spark energy levels. This is perhaps a moot point, since it seems to be impossible to create one without the other.

Because they function as sites for fatigue crack initiation, microcracks are known to severely reduce the useful life of dies and molds subjected to cyclic mechanical and thermal fatigue. For this reason, their presence on the die surface poses a major problem to both the forging and die casting industries [48]. To effectively alleviate the threat of premature die failure through thermal and mechanical fatigue, it would appear to be advisable to remove both the recast and overtempered layers.

Microcracks occur when the surface stresses created by EDM exceed the ultimate tensile strength of the metal. The formation of these cracks does not completely relieve these stresses, however. Residual stresses created by EDM have been a subject of research for many years.

Barash [44] was apparently the first researcher in the West to seriously investigate residual stresses in EDM, while similar work was carried out in the Soviet Union by Aleksandrov [49] and Aleksandrov and Zolotykh [50].

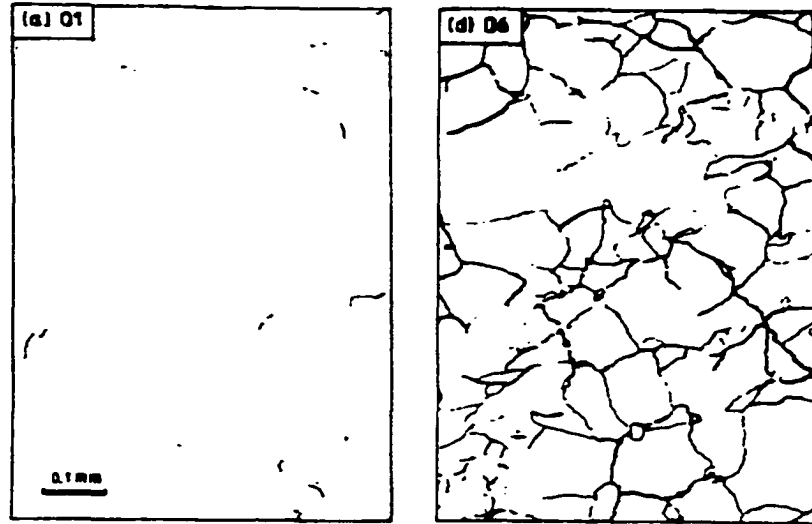


Figure 2.10: Cracking Behavior of O-1 and D-6 Steels, from [Lee, 92]

Barash removed discrete layers of metal from previously EDM'd specimens and estimated the residual stresses by the bending deflection method. He estimated stresses as high as 75,000 psi in carbon steel with a hardness of  $R_c$  50, and 150,000 psi in high speed steel of  $R_c$  64.

At roughly the same time, Lloyd and Warren [34] performed similar experiments on low carbon steels, and reported residual stresses that approached the ultimate tensile strength of the material. They also employed the bending deflection method and removed the EDM surface in layers 0.0002 inches thick. They found that tensile residual stresses were highest at the surface of the metal, very rapidly decreased to zero, and then were replaced by small residual compressive stresses in the core of the metal. These findings were in basic agreement with Barash and Aleksandrov.

The next important contribution is due to Crookall and Khor, whose paper from 1972 remains probably the most important work in this area [51]. In contrast to the earlier work, they performed tests using EDM machines employing the older relaxation-circuits, which were common from the earliest times to the Sixties, but also employed a newer machine that used a solid state control to generate pulses.

They tested copper, mild steel, and a hot work tool steel of composition similar to H-13. Confirming the earlier work, they found very high residual stresses resulted from EDM, with the stresses due to the relaxation circuit machine reaching a peak at the surface. However, they also discovered that

the location of the peak stresses varied with the type of pulse generating circuitry. In contrast to relaxation-circuit machines, the pulse-generator machine created the highest level of residual stresses slightly below the surface. The exact location of the peak stress varied with pulse energy, but varied from 20 to 50 microns below the surface. The phenomenon was observed in all tests conducted with this machine, and was assumed to be genuine. Again, they found the maximum stress level to be correlated with the pulse energy, with the peak stress approaching the UTS of the material.

Finally, Merdan and Arnell essentially repeated the work of Crookall and Khor, using AISI H-13 steel, and found essentially the same results [52]. Their work confirms that the maximum residual stress lies at a depth of approximately 20–40  $\mu\text{m}$  below the surface.

## **2.3 Pulsed electrochemical machining**

### **2.3.1 Electrolytic metal removal**

Because pulsed electrochemical machining (PECM) is a recent adaptation of the conventional ECM process, it makes sense to begin our analysis with the older method. In contrast to EDM, the theoretical basis for ECM has been known for many years. Michael Faraday was responsible for the initial research in electrolysis, and in 1832 was the first to show that the amount of material dissolved at an electrode in an electrolytic cell is directly proportional to the amount of current passed through it. The Faraday

constant is simply a measure of the amount of atoms removed from a metal per coulomb of charge passed, and Faraday's Law remains the fundamental equation used in ECM to calculate metal removal rate.

At first glance, there appear to be some similarities between EDM and ECM. In both processes, the shaped tool and the workpiece are brought into close proximity while immersed in a fluid. Because both processes use electric current to remove material, both require that the tool and the workpiece are electrically conductive. And theoretically, at least, in both cases the negative image of the tool is formed in the workpiece, though achieving an exact replica of the ECM tool can be very difficult.

In all other important respects, the processes are completely dissimilar. While EDM is a thermal process, ECM is not: although the heat generated in the machining gap in ECM can have a direct effect on the efficiency of the process, it is negligible when compared to the temperature inside the EDM plasma channel. Also, the fluid in which the EDM workpiece and tool are immersed is necessarily a dielectric, most often a hydrocarbon; ECM on the other hand requires an electrolyte, typically a concentrated solution of sodium chloride or sodium nitrate. Finally, while EDM currents are relatively small, on the order of 1 to 50 amperes, ECM requires extremely high current densities, often on the order of 100 amperes per square centimeter, to function effectively.

The basic electrochemical dissolution process is rather simple, and can be described with a few equations. A complete and detailed description of the ECM process, on the other hand, is extremely complex, requiring not only knowledge of the basic equations of electrochemistry (which also include secondary reactions occurring in the bulk of the electrolyte), but also a detailed description of the fluid flow and local electrical fields in the machining gap, as well as a detailed analysis of the physical and chemical changes occurring at the interface .

As an aid in understanding the pulsed ECM process, an overview of the conventional, steady-state DC ECM will be presented first. There are important differences between the two processes, however. Flow effects are minimized in pulsed ECM due to the fact that dissolution only occurs in bursts of a few milliseconds, which allows one to model the electrolyte as being essentially static. For the same reason, heating of the electrolyte in the machining gap can also be minimized by correctly choosing the pulse parameters.

On the other hand those aspects of the process that directly affect the surface of the workpiece do not differ appreciably between the two processes, and will be discussed in detail. Most of the information in this section is taken from Wilson [53] and McGeough [54]. It should be noted that only electrolysis in neutral salt solutions is described here. Electro-polishing in concentrated acids is not relevant to ECM, and will not be discussed.

Figure 2.11 shows the three basic elements of an electrochemical cell: the cathode, anode, and electrolyte. In ECM, the tool is always configured as the cathode, and the workpiece as the anode. In contrast to EDM, there is no option of reversing the polarity in ECM: *all* metal dissolution takes place at the anode. Only hydrogen is generated at the cathode, leading to one of the major advantages of ECM: zero tool wear. Thus the same tool can, in theory, be used in ECM to machine an unlimited number of workpieces.

When the tool is brought into close proximity with the workpiece, and a potential difference appears across the gap, electrolytic dissolution begins. The width of the machining gap is similar to that used in EDM (~ 0.1 mm), which allows the same tool/workpiece pair to be used in both processes.

The driving force for the reaction is the potential gradient between the two electrodes. With such a small machining gap, and a potential of only a few volts, very high gradients are created. In conventional ECM a typical machining gap might be 0.05 cm, with an applied voltage of 20V, which would give a gradient of almost 400 V/cm. In pulsed ECM, the gap size is considerably smaller, but the applied voltage is in the same range. These high potential gradients lead to very high current densities, on the order of 100 V/cm<sup>2</sup>.

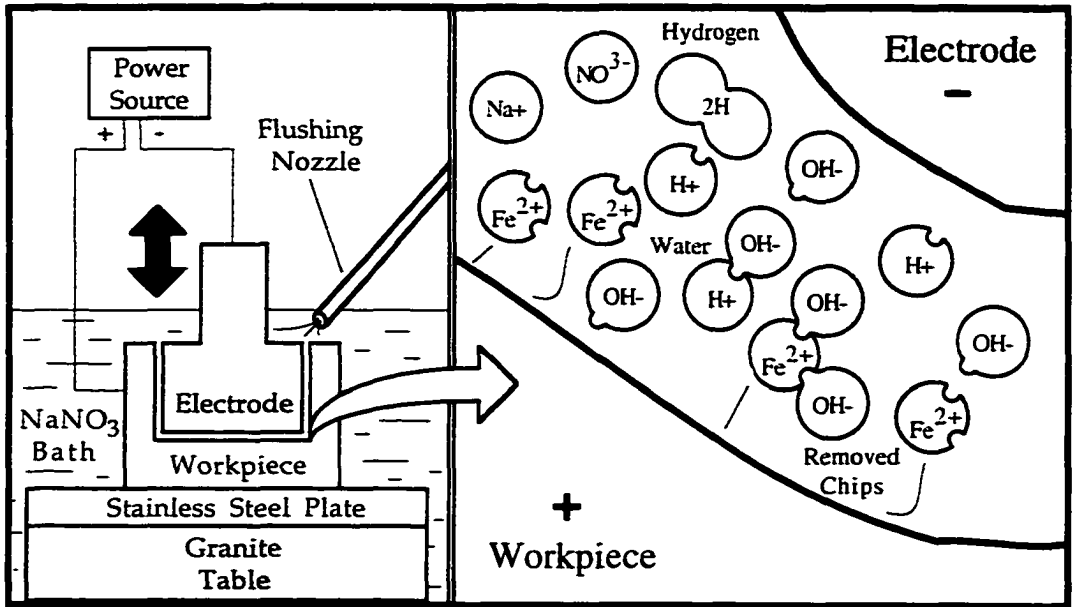
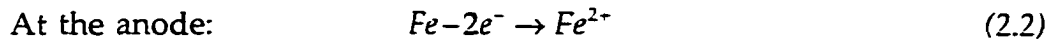
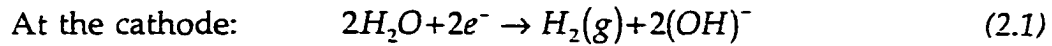
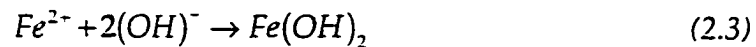


Figure 2.11 Schematic of ECM Machining Cell

The basic equations governing the reaction of a ferrous alloy in an electrolyte consisting of a basic salt and water are given by:



However, the iron ions do not remain in solution, but quickly combine with the hydroxyl ions created by the dissolution of water at the cathode:



In a simple electrochemical cell, in which the atomic weight and valence of the metal ions are known, the mass of metal dissolved is given by Faraday's Law:

$$m = \frac{A I t}{z F} \quad (2.4)$$

where  $A$  is the atomic weight,  $I$  is the current,  $t$  is the machining time,  $z$  is the valency of the dissolving ion, and  $F$  is Faraday's constant,  $F = 96,500$  coulombs/mol. The machining rate is then given by:

$$\dot{m} = \frac{AI}{zF} \quad (2.5)$$

and the volumetric removal rate is

$$\dot{v} = \frac{AI}{\rho_a F} \quad (2.6)$$

where  $\rho_a$  is the density of the metal in question.

The equations shown here give the *theoretical* removal rates for pure metals whose valencies are known. The efficiency,  $\Theta$ , of any electrochemical removal process for which the total current is known can then be calculated by:

$$\Theta = \frac{\text{actual mass removed}}{\text{theoretical mass removed}} \quad (2.7)$$

In actual practice, however, calculating the efficiency of the process is complicated by two factors. First, the valence for any given metal can change during actual operating conditions. For example, iron can ionize as either  $Fe^{2+}$ ,  $Fe^{3+}$ , or both, depending on the local potential, pH, and current density. Likewise, chromium can assume both  $Cr^{3+}$  and  $Cr^{6+}$  forms. Generally, most metals under actual ECM conditions, i.e., very high potential gradients, will

assume multiple valencies. Table 2.1, adapted from [54], shows typical valencies for several different metals under conditions typically encountered in ECM.

The problem of precisely determining the material removal rate and process efficiency becomes more difficult when machining tool steels, due to the relatively large number of alloying elements present. The two methods generally used for calculating removal rates for alloys are the “percentage by weight” method and the “superposition of charge” method. These both require calculating the chemical equivalent for the alloy.

By definition, the chemical equivalent for an element is simply the atomic weight of the element divided by the valence. For an alloy, the chemical equivalent is a bit more complex, as it entails knowing the percentage of each element present in the alloy, as well as its valence. For the “percentage by weight” method, the chemical equivalent is given by

$$\left[ \frac{A}{z} \right]_{\text{alloy}} = \frac{1}{100} \left[ X_A \frac{A_A}{z_A} + X_B \frac{A_B}{z_B} + X_C \frac{A_C}{z_C} + \dots \right] \quad (2.8)$$

where  $X_A$  is the percentage by weight of element A, and  $z_A$  is the valence of element A.

The mass removal rate is then given by

$$\dot{m} = \left[ \frac{A}{z} \right]_{\text{alloy}} \frac{I}{F} \quad (2.9)$$

Metal	Atomic Wt.	Valency	Density (g/cm <sup>3</sup> )	Removal rate	
				(g/s)	10 <sup>-6</sup> m <sup>3</sup> /s
<i>Aluminum</i>	26.97	3	2.67	0.093	0.035
<i>Chromium</i>		2		0.269	0.038
		3		0.180	
		6		0.090	
<i>Cobalt</i>	58.93	2	8.85	0.306	0.035
		3		0.204	
<i>Copper</i>	63.57	1	8.96	0.660	0.074
		2		0.329	
<i>Iron</i>	55.85	2	7.86	0.289	0.037
		3		0.193	
		2		0.126	
<i>Magnesium</i>	24.31	2	1.74	0.126	0.072
<i>Manganese</i>	54.94	2	7.43	0.285	0.038
		4		0.142	
		6		0.095	
		7		0.081	
<i>Molybdenum</i>	95.94	3	10.22	0.331	0.032
		4		0.248	
		6		0.166	
<i>Nickel</i>	58.71	2	8.90	0.304	0.034
		3		0.203	
<i>Silicon</i>	28.09	4	2.33	0.073	0.031
<i>Tin</i>	118.69	2	7.30	0.615	0.084
		4		0.307	
<i>Titanium</i>	47.9	3	4.51	0.165	0.037
		4		0.124	
<i>Tungsten</i>	183.85	6	19.3	0.317	0.016
		8		0.238	
<i>Vanadium</i>	50.94	2	5.8	0.264	0.046

Table 2.1: Atomic weight, valence, and theoretical removal rates assuming a current of 1000 A for several metals.

The "superposition of charge" method uses Faraday's law to calculate the amount of electrical charge that is needed to dissolve the mass contribution of each alloying element to a given mass (one gram) of the alloy. For element A, the charge required to dissolve its mass contribution ( $X_A/100$ ) g to one gram of the alloy is

$$\frac{X_A}{100} \frac{z_A}{A_A} F \text{ coulomb,} \quad (2.10)$$

and similarly for every other alloying element. The electrical charge to dissolve 1 gram of the alloy is then

$$\frac{z}{A}_{\text{alloy}} F \text{ coulomb} \quad (2.11)$$

Equating the sum of the charge for the alloying elements to the charge for the alloy,

$$\left[ \frac{z}{A} \right]_{\text{alloy}} F = \frac{F}{100} \left[ X_A \frac{z_A}{A_A} + X_B \frac{z_B}{A_B} + X_C \frac{z_C}{A_C} + \dots \right] \quad (2.12)$$

which leads to

$$\frac{A}{z}_{\text{alloy}} = 100 \div \left[ \frac{X_A}{A_A} + \frac{X_B}{A_B} + \frac{X_C}{A_C} + \dots \right] \quad (2.13)$$

These equations can be used to estimate the machining rates and efficiencies for alloys, but it must be remembered that their accuracy depends upon a knowledge of the actual valence of each of the alloying elements at operating conditions. In practice, this knowledge is impossible to attain, because the valence can change depending on local conditions in the machining gap. It should also be noted that these formulae only apply to metals. Several other elements that are commonly present in steels, such as carbon, silicon, and sulfur, are regarded as inert elements in these calculations.

This dissertation research concentrated exclusively on one tool steel, Premium Grade AISI H-13, which is widely used in the forging and die casting industries. The chemical composition of this steel is closely controlled, and has been developed expressly for applications in which hardness at high temperatures is required.

Table 2.2 shows the chemical composition of the steel, along with the percentage by weight of the alloying elements and their chemical equivalents, calculated for the four possible combinations of  $Fe^{2+}$ ,  $Fe^{3+}$ ,  $Cr^{3+}$  and  $Cr^{6+}$ .

Element (Valence)	Fe (2)	Fe (3)	Cr (3)	Cr (6)	Si (4)	Mo (3)	V (2)
Percentage Weight, (X)	90.8	90.8	5.2	5.2	1.0	1.3	0.95
Mole Fraction	1.63	1.63	0.1	0.1	0.036	0.014	0.019
Chem. Equiv. (A/z)	27.93	18.61	17.33	8.67	7.02	31.98	25.47
Product $X(A/z) \times 10^{-2}$	25.36	16.90	0.90	0.45	0.07	0.42	0.24
Quotient $X/(A/z)$	3.25	4.88	0.30	0.60	0.14	0.041	0.037

Table 2.2: Constituent elements of AISI H-13 tool steel, with percentages by weight and chemical equivalents

Table 2.3 shows the mass and volumetric removal rates for H-13 calculated according to both methods for the four possible combinations of valences of iron and chromium. Although molybdenum also can assume multiple valences, its contribution to the alloy chemical equivalent is so small that it is not considered here. These values will be compared to actual experimental data in Chapter 4.

Method	Fe <sup>2+</sup> Cr <sup>3+</sup>	Fe <sup>2+</sup> Cr <sup>6+</sup>	Fe <sup>3+</sup> Cr <sup>3+</sup>	Fe <sup>3+</sup> Cr <sup>6+</sup>
Percentage by Weight	27.1	26.6	18.6	18.2
Superposition of Charge	26.45	24.5	18.48	17.51

Table 2.3: Four possible values of the chemical equivalent for H-13

If the two electrodes remain stationary in static electrolyte, the reactions described above will occur for a few seconds, but then will quickly drop off, as two phenomena occur. First, the anode surface recedes from the cathode, as metal ions are dissolved, which causes the potential gradient to decrease. At the same time, the resistance in the gap increases (due to waste products, heating of the electrolyte, and formation of hydrogen bubbles at the cathode). These two events result in a rapid decrease in the current density.

Electrolysis as a viable machining method requires two additional factors. First, the tool must be continuously moved toward the workpiece, at a rate equal to the rate of metal removal, in order to maintain a constant gap

between cathode and anode, and thus a constant potential gradient. An exhaustive summary of machine controls in conventional ECM is given in [55] and in [56]. An equally thorough survey of control algorithms for PECM is presented in [10].

Secondly, the electrolyte in the working gap must be removed at a rate sufficient to remove the by-products of the reaction (gas bubbles, and metal salts) that would otherwise accumulate. In addition, the very high current density levels heat the electrolyte to boiling temperatures quickly if the heat is not removed from the gap. Boiling of the electrolyte leads to arcing between tool and workpiece, with serious damage to both surfaces. Even in those cases where the heating is not enough to boil the electrolyte, the conductivity decreases very rapidly with heating, leading to variations in removal rate along the direction of the electrolyte flow, and consequent imprecision in duplicating the tool shape.

In conventional ECM, with its high current density and metal removal rate, the electrolyte is typically forced into the gap at high velocity (100–200 ft/sec), which requires correspondingly high pressures (80–400 psi). These high pressures tend to force the electrodes apart, which results in the massive structures of most production ECM systems. When servo control of the tool and an efficient flushing system are added to the basic electrolytic process, an ECM machining cell is created. The metal removal rates in conventional

ECM are on the order of 0.010 to 0.100 in./min, considerably higher than those attained by EDM.

As noted above, however, it is difficult to machine the negative image of the ECM electrode into the workpiece. This is due both to gradients in the temperature along the flow path, and the fact that the flow pattern of the electrolyte causes local distortions in the conductivity, leading to distorted surfaces. In order to counteract this problem, much work has gone into predicting flow effects, and compensating for them in tool design. However, this problem remains complex, and is the primary reason why ECM has not been used more extensively in tool and die work. As we will see, however, this problem is largely eliminated in Pulsed ECM.

### **2.3.2 Passivation phenomena**

Some of the complexities inherent in ECM can be ignored in PECM. Fluid effects are for the most part non-existent, because the electrolyte is essentially static during the machining cycle. Electric field effects can also be ignored if we take the surfaces to be essentially planar as a first approximation. However, one aspect of ECM cannot be overlooked: the effects of the passivating films that rapidly coat the surface of the workpiece when the potential gradient exceeds a fairly low value.

The phenomenon of passivation has been a subject of intense interest for many years in the study of corrosion phenomena. (See, for example, [57]

and[58]).) The literature dealing with passivation is extensive, but thankfully we can concentrate on a small part of it here. An excellent survey of passivation in ECM and PECM is given by Datta [Datta, 93], and the summary presented here follows his presentation closely. The behavior of metal anodes in electrochemical cells can be broken down into three regimes: active, passive, and transpassive.

*Active Dissolution* Figure 2.12, taken from [Datta, 93] shows the three distinct anode polarization regimes quite clearly. The first region, which occurs at low potential levels, is known as the active region. In this region, current density increases quite rapidly with increasing potential. Current flow in this region is due to the direct dissolution of metal ions into the electrolyte.

Active dissolution results in the removal of atoms from energetically favorable kink sites on close packed atomic planes. Due to this dependence on the atomic structure, the metal removal rate depends on the orientation of the crystal planes at the interface. Because the metal grains at the interface are randomly oriented, differential dissolution will take place, giving rise to an etched surface. Figure 2.13, taken from [60] shows surfaces that have been machined in the active mode. Note the pronounced difference in dissolution that has occurred at the grain boundaries.

*Passivation* At slightly higher anode potentials, the current decreases to almost zero; this is the regime in which passivating layers form on the anode

surface. These layers, which are oxides of the metals composing the anode, prevent dissolution at high rates from occurring. Because the metal surface is

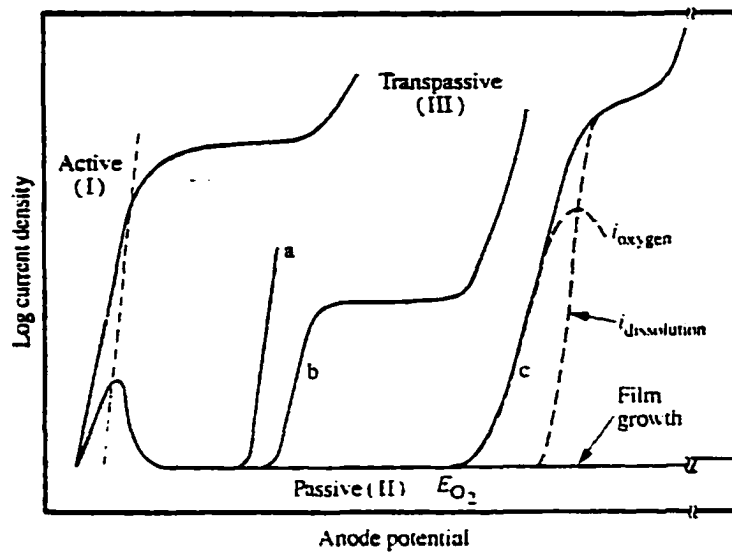


Figure 2.12: Polarization curves in ECM (from [59])

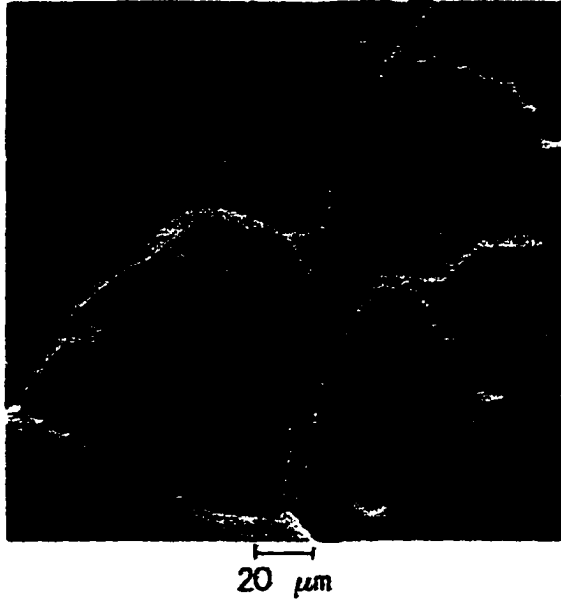


Figure 2.13: Dissolution in the active regime (from[60])

coated with a film; dissolution is controlled by the rate at which ions and electrons can diffuse through the film. To quote directly from Datta:

The dissolution current in the passive potential region is controlled by the rate of dissolution of the passive film, which in turn depends on the ionic conductivity of the film and its solubility in the electrolyte. In general, the passive current is of the order of  $\mu\text{A}/\text{cm}^2$  and is independent of applied potential in the passive potential range. The thickness, composition, and electrical properties of passive films depend on the metal involved, the solution, and the applied potential.

Passive films play an important role in ECM in controlling unwanted dissolution away from the machining gap, and in creating a polished surface. The passivation of metals is a complex phenomenon depending not only on the metal and the anode potential, but also on the type of electrolyte. In ECM, both passivating and non-passivating electrolytes are used. Passivating electrolytes include nitrates and chlorates, while non-passivating electrolytes contain aggressive ions, such as chlorine and bromine.

In general, passivating electrolytes allow for better surface finish and improved dimensional control. Surface finishes are improved in passivating electrolytes because dissolution is limited by ionic diffusion through the passivating layer. As opposed to the preferential dissolution seen in the active region, where the anode surface is directly exposed to the electrolyte, dissolution through the passive film occurs randomly at weak points in the film, which means that no particular grain orientation is preferred, resulting in a polished, rather than etched, surface.

Dimensional control is improved in passivating electrolytes because leakage currents outside the machining gap are typically not strong enough to destroy the passive layer. Instead, oxygen is evolved at the oxide layer/electrolyte interface, and the substrate is unaffected. It should be noted here that the COTAC PECM machine on which the work described here uses a 40% NaNO<sub>2</sub> solution as an electrolyte, which is strongly passivating.

*Transpassive Dissolution* Returning to Figure 2.12, as the anode potential continues to increase, the current density again begins to rise rapidly. This area is known as the transpassive potential region, and it is in this regime that electro-chemical machining occurs. Three major modes of anodic transpassive behavior are shown by the three curves in Figure 2.12 labelled *a*, *b*, and *c*, of which only curves *a* and *c* concern us here (curve *b* relates to electropolishing in concentrated acids).

In non-passivating electrolytes, such as NaCl, the aggressive chloride ions will penetrate the passivating film at its weak points, leading to the localized destruction of the layer. Once the passivating layer has been disrupted, active dissolution of the substrate at these locations quickly follows, and a pitted surface results. The potential level at which this occurs is called the *critical pitting potential*, shown as curve "*a*" in Figure 2.12.

At potential levels exceeding the critical pitting potential two reactions are possible: oxidation and dissolution, both of which are shown by curve *c*. Oxidation can take two forms: oxidation of the passive film into a soluble

species, or oxidation of the electrolyte solution itself. An example of the first oxidation mode is shown by the behavior of chromium in sulfuric acid: chromium is initially coated with a passive layer of trivalent chromium, which is transformed in the transpassive region into an oxide of hexavalent chromium, which is highly soluble and also quite unhealthy for humans. This reaction is noted here because hexavalent chromium poses the most serious health risk to humans using ECM to machine chromium-containing tool steels.

The other mode of oxidation is solution oxidation. To quote again from [59]:

On passive films that are relatively stable and exhibit electron conduction, oxygen evolution takes place by solution oxidation upon anodic polarization into the transpassive potential, namely  $2\text{H}_2\text{O} \rightarrow \text{O}_2 + 4\text{H}^+ + 4\text{e}^-$ . In these metal-electrolyte systems, transpassive metal dissolution sets in at potentials much higher than the potential for oxygen evolution. At still higher potentials, very high metal dissolution rates may be reached.

It is in this most extreme region of the polarization curve that ECM occurs. At these very high potential levels, the passivating film begins to disintegrate, exposing the base metal surface to the action of the electrolyte. Datta and Landolt, using short current pulses on nickel, showed that transpassive film breakdown was initiated at discrete sites on the film. The number of these sites increased with increasing current density. They further showed that these nucleation sites for film breakdown grew in distinct directions along

preferred crystallographic planes, as in the active dissolution region. By exposing a single crystal of nickel with a {111} orientation to the electrolyte, they were able to determine that the growth of the dissolution site proceeded in three directions 120° apart, consistent with growth along the {111} projections [61].

Datta references several studies which show that transpassive dissolution efficiency is independent of the thickness of the passivating film itself. He explains this by noting that two separate mechanisms co-exist during transpassive dissolution: the creation of pores and pits, accompanied by active dissolution, and the transfer of electrons through the film, resulting in oxygen evolution. He notes that high rate transpassive dissolution involves both de-passivation of the anode surface along with re-passivation, both of which determine to what extent the surface is coated with the passivating film, and thus the current efficiency of the process.

*Electrolyte Transport Mechanisms*      So far we have looked only at the processes occurring at or in the anode surface itself. However, dissolution of the surface depends on the ability of the electrolyte to carry the reaction products away from the interface. Since the concentration of metal ions at the surface is much higher than the concentration within the bulk electrolyte, and since this concentration has a direct effect on the efficiency of the process,

it is also necessary to look briefly at the processes occurring within the electrolyte as well.

The metal ions produced by the dissolution of the surface move into the bulk of the electrolyte by two transport mechanisms: convective diffusion and migration. Since the electrolyte anions will congregate at the electrolyte/anode interface, the movement of metal ions away from the surface is compensated by the movement of the anions toward the anode. The concentration of the ions at the surface depends on the current density, the dissolution efficiency of the metal or alloy, and the hydrodynamic conditions in the electrolyte. Previous work has shown that the limiting current density, defined as the current density at which salt precipitation begins, is a function of the electrolyte velocity relative to the metal surface. From this, one can conclude that the limiting current density is controlled by convective mass transport.

For an anodic reaction controlled by convective mass transport, the current is given by:

$$i = nFD \frac{C_s - C_b}{\delta} \quad (2.14)$$

where  $D$  is the effective diffusion coefficient,  $C_s$  is the concentration at the surface,  $C_b$  is the concentration in the bulk, and  $\delta$  is the diffusion layer thickness. The Nernst diffusion layer concept has been extensively used in

the ECM literature to obtain a simplified model of the mass transport mechanism. According to this model, a stagnant diffusion layer of thickness  $\delta$  is assumed to exist at the anode. Inside this layer a concentration gradient exists, and transport within the layer occurs solely by diffusion. Outside the layer, transport is assumed to occur exclusively by convection, and concentration is assumed constant. The thickness of this anodic diffusion layer is a function of hydrodynamic conditions and is given by

$$\delta = \frac{L}{Sh} \quad (2.15)$$

where  $L$  is a characteristic length, and  $Sh$  is the Sherwood number, which is a function of the Reynolds number ( $Re$ ) and the Schmidt number ( $Sc$ ),

$$Re = \frac{D_h v}{\nu} \quad \text{and} \quad Sc = \frac{\nu}{D}.$$

This anodic diffusion layer will play an important role in the analysis of pulsed ECM, as we will see in the following section. For the present, it is enough to note that the concentration of metal ions at the anode is a function of the current density. When the production of ions exceeds the saturation limit in the diffusion layer, metal salt will precipitate from the solution, and a thin salt film will form on the surface of the anode. At this point the

polarization curve will show a limiting current plateau, and this limiting current is given by

$$i_l = nFD \frac{C_{sat}}{\delta} \quad (2.16)$$

where  $C_{sat}$  is the saturation concentration of the salt at the anode surface. Since the electrolyte is assumed to contain a very small amount of metal,  $C_b$  is taken to be zero here.

The formation of the salt film is important because it plays an important role in the rate of dissolution during ECM and in the morphology of the resulting surface. To quote again from Datta:

At low current densities, surface etching is observed which, dependent on the metal–electrolyte combination, reveals crystallographic steps and etch pits, preferred grain boundary attack, or finely dispersed microstructure. Anodic dissolution under these conditions leads to extremely rough surfaces.... On the other hand, the formation of salt films at the surface suppresses the influence of crystallographic orientation and surface defects on the dissolution process, leading to microfinishing. The presence of salt films may increase the anode potential to such high values that dissolution reactions involving a higher oxidation state or the onset of oxygen evolution may become possible.

The intent of this section has been to introduce some aspects of the ECM process that seem most relevant in explaining how the process works, and how surfaces are affected. Several important areas of research in ECM, notably tool design and servo control of the machining gap, have not been explored

because they play little or no role in affecting the finished surface. In the next section, we will re-visit some of the topics discussed here, in order to explain how they differ once the current is pulsed periodically, rather than maintained at a steady state value.

### **2.3.3 Pulsed current electrochemical machining**

The analysis of the ECM process to this point has assumed a DC power source, in which the only variable has been the current density. While conventional ECM has become an important machining process in the aerospace industry, the limitations of ECM have prevented its widespread acceptance in other industries. This is due largely to the fact that removal of the reaction products from the machining gap necessitates pumping electrolyte through the gap in sufficient quantities to remove the reaction products. This leads in turn to massive machine structures and expensive pumping systems on the one hand, and to complex simulations to predict the ideal tool shape on the other.

These problems can be largely eliminated by using a pulsed, rather than DC, power supply. By applying a pulsed current to the gap, one can reap the benefits of a very high instantaneous current density without the undesirable side effects of electrolyte boiling and degradation of the process by waste products. Further, by using a pulsed current, one gains a larger degree of control over the process: instead of controlling only the current density, we

can now independently control current density, pulse on–time, and pulse off–time.

However, the metal removal rate is greatly decreased in PECM, to the point that it is really only useful either as a method for micromachining precision components, or for surface finishing applications. In this section the theory of pulsed ECM will be presented as a refinement of conventional ECM as presented in the last section. The two major issues in pulsed ECM, electrolyte heating and mass transport effects, will be dealt with separately. The development in this section is taken largely from [62].

*Physics of the PECM Process* While in principle either voltage or current pulses can be applied to the machining gap, it will be assumed here that rectangular current pulses are applied, in accord with the method employed by the control system of the COTAC–51 PECM machine [63], [64]. Figure 2.14 shows an idealized model of a current pulse, where  $i_p$  is the peak current density,  $t_p$  is the pulse on–time,  $t'_p$  is the pulse off–time,  $t_{pp}$  is the pulse period, and the duty cycle is defined as  $t_p/t_{pp}$ . For such a system, the average current density,  $i_a$ , is given by

$$i_a = \frac{i_p t_p}{t_{pp}} \quad (2.17)$$

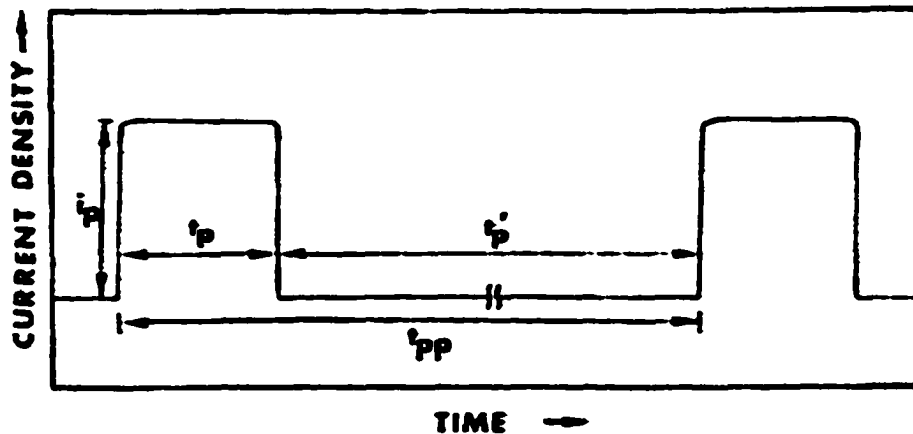


Figure 2.14: Ideal Current Pulses in PECM, from [62]

*Electrolyte Heating* Electrolyte heating and disposal of the waste products are the two primary issues, because they both have a negative effect on the dissolution process. Due to the cyclic nature of PECM, electrolyte heating can be broken down into instantaneous heating, occurring during a single cycle pulse, and average heating, corresponding to an increase in electrolyte temperature over a period of several pulses. Because electrolyte flow is much lower in PECM than in conventional ECM, the “residence time” of a given volume of fluid in the machining gap is typically much longer for PECM. Since the pulse times typically used in PECM are on the order of milliseconds, we can realistically model the electrolyte as being stationary during a single pulse. The *instantaneous* temperature rise,  $\Delta T_p$ , is then:

$$\Delta T_p = \frac{i_p^2 t_p}{\kappa \rho C_p}, \quad (t_p \ll L/u) \quad (2.18)$$

where  $\kappa$  is the specific conductivity,  $\rho$  is the density, and  $C_p$  is the specific heat of the electrolyte. If  $L$  and  $u$  are the gap length and the fluid velocity, respectively, then  $L/u$  defines an average residence time for a given volume of electrolyte.

If all of the fluid heated during a single pulse is to be removed from the gap between pulses, then the pulse off time,  $t'_p$ , must be greater than the ratio  $L/u$ . The average rise in electrolyte temperature is then given by

$$\Delta T_a = \frac{i_a^2 L}{\kappa \rho C_p u} = \frac{i_p^2 (t_p / t_{pp})^2 L}{\kappa \rho C_p u} \quad (2.19)$$

Average and instantaneous temperature rise do not have the same effects on the PECM process. Instantaneous rise in temperature can lead to electrolyte boiling, process instability, and even sparking across the machining gap, if the boiling exposes enough surface area of the tool and workpiece. Average temperature rise, because it leads to a temperature gradient in the direction of flow, can lead to a variation in the electrolyte conductivity, and hence to a loss of dimensional precision. The ratio of instantaneous to average heating is given by

$$R_T = \frac{\Delta T_p}{\Delta T_a} = \frac{(t_p u / L)}{(t_p / t_{pp})^2} \quad (2.20)$$

Note that the ratio is independent of the current density. It follows that by correctly choosing the pulse parameters, we can optimize  $R_T$  for a given set of hydrodynamic conditions. However, it should also be noted that the average machining rate is also a function of the average current, which as equation 17 shows is also directly affected by reducing the pulse on-time.

*Mass Transport* The other major advantage of using a pulsed current source is that it allows the electrolyte to recover during the periods of zero current flow. The metal dissolved from the anode surface is either carried away by the electrolyte, or returns to the anode surface as a metal salt precipitate. The formation of a salt film on the anode surface determines whether the surface will be etched or polished, and the salt film is itself a function of the current density.

From the development in the preceding section, we know that the current density for the steady state process is given by

$$i = nFD \frac{C_s - C_b}{\delta} \quad (2.14)$$

We can now introduce the current efficiency,  $\Theta_i$ , which is a function of the metal and electrolyte, as well as the current density, into the equation:

$$i = \frac{nFD}{\Theta_i} \frac{(C_s - C_b)}{\delta} \quad (2.21)$$

Here  $C_s$  is the metal ion concentration at the anode surface, and  $C_b$  is the concentration in the bulk. With increasing current density, all other conditions remaining constant, the electrolyte concentration,  $C_s$ , reaches saturation,  $C_{sat}$ , at which point the salt film precipitates from the electrolyte. We can then define the limiting current by

$$i_l = \frac{nFD}{\Theta_l} \frac{C_{sat}}{\delta} \quad (2.22)$$

where  $\Theta_l$  is the current efficiency at the limiting current condition. The limiting current is significant because the anode potential, the stoichiometry of the process, and the resulting surface finish can be quite different depending on whether the process occurs above or below the limiting current. Datta and Landolt have shown [65],[66] that surface brightening coincides with the formation of a salt layer, i.e., when the current exceeds the limiting current condition.

Datta and Landolt use a duplex diffusion layer model that was first proposed by Ibl [67] in analyzing pulsed electroplating. Basically, the model consists of a time dependent pulsating layer of thickness  $\delta_p$  adjacent to the anode surface, within which the concentration of metal ions varies periodically with time, and an outer layer of thickness  $\delta'_p = \delta - \delta_p$ , in which the concentration of ions is time-invariant. Figure 2.15 shows a schematic of this model, taken from [62]. Although this model is a simplification of the true state of the boundary layer, Ibl has shown that it gives results close to those obtained from more elaborate models.

To calculate the thickness of the inner layer,  $\delta_p$ , we use the mass balance of dissolved metal ions in the diffusion layer over time  $t_p$ . From Faraday's Law we know that the amount of metal dissolved per unit area during time  $t_p$  is

$$m = \frac{\Theta_p i_p t_p}{nF} \quad (2.23)$$

where  $i_p$  is the peak current density and  $\Theta_p$  is the corresponding current efficiency. The amount of metal lost through the outer layer during the same pulse time,  $t_p$ , is

$$m = \frac{\Theta_p i_a t_p}{nF} \quad (2.24)$$

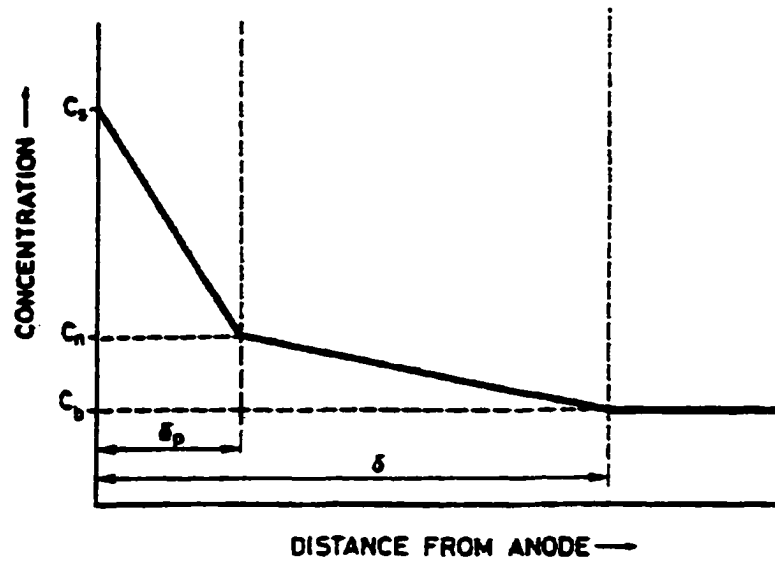


Figure 2.15: Schematic of Duplex Diffusion Model (from [62])

where  $i_a$  is the average current density. The difference between the two terms is the amount of metal ion accumulated in the pulsating layer. This is the amount of metal ion that will diffuse into the bulk solution during the pulse off-time.

If we assume a linear concentration profile in the pulsating layer, then the amount of accumulated ions is just

$$\frac{(c_s - c_n)\delta_p}{2} \quad (2.25)$$

which leads to the mass balance equation,

$$\frac{\Theta_p i_p t_p}{nF} \approx \frac{\Theta_p i_a t_p}{nF} + (c_s - c_n) \frac{\delta_p}{2} \quad (2.26)$$

where the peak current density,  $i_p$ , is given by

$$i_p = \frac{nFD}{\Theta_p} \frac{c_s - c_n}{\delta_p} \quad (2.27)$$

From (17), (26), and (27), we arrive at the thickness of the pulsating layer,  $\delta_p$ , at the end of a single pulse:

$$\delta_p = \sqrt{2Dt_p(1-t_p/t_{pp})} \quad (2.28)$$

which at low duty cycles can be approximated as

$$\delta_p = \sqrt{2Dt_p} \quad (2.29)$$

Thus for short current pulses, instantaneous current densities much higher than those used in steady state conditions can be applied without reaching the limiting current. If we define the limiting current density  $i_{pl}$  as the current density at which  $c_s = c_{sat}$  at the end of a pulse, then

$$i_{pl} = \frac{nFD}{\Theta_{pl}} \frac{c_{sat} - c_n}{\delta_p} \quad (2.30)$$

Applying equation (2. 22), and setting  $c_b = 0$ , we arrive at an equation for the ratio of the pulsed limiting current density to the steady state limiting current density,

$$\frac{i_{pl}}{i_p} = \frac{\Theta_l}{\Theta_{pl}} \frac{\delta}{\delta_p} \left( 1 - \frac{c_n}{c_{sat}} \right) \quad (2.31)$$

To find the ratio  $(c_n/c_{sat})$ , we set the amount of metal dissolved during the pulse on-time,  $t_p$ , equal to the amount diffusing through the outer diffusion layer,  $\delta - \delta_p$ , during the entire pulse period,  $t_{pp}$ :

$$\frac{\Theta_p i_p t_p}{nF} = D \frac{c_n - c_b}{\delta - \delta_p} t_{pp} \quad (2.32)$$

If we set  $c_b = 0$ , and using (2.27), we obtain:

$$\frac{c_n}{c_s} = \frac{(t_p/t_{pp})[(\delta/\delta_p) - 1]}{1 + (t_p/t_{pp})[(\delta/\delta_p) - 1]} \quad (2.33)$$

Finally, by setting  $c_s = c_{sat}$  at the limiting current density  $i_{pl}$ , we have

$$\frac{i_{pl}}{i_l} = \frac{\Theta_l}{\Theta_{pl}} \left[ \frac{\delta_p}{\delta} \left( 1 - \frac{t_p}{t_{pp}} \right) + \frac{t_p}{t_{pp}} \right]^{-1} \quad (2.34)$$

Thus for given hydrodynamic conditions, we can adjust the pulse parameters  $i_p$ ,  $t_p$ , and  $t_{pp}$  to work on either side of the limiting pulse current density.

### 2.3.4 Effect of machining parameters

One of the major advantages that PECM shows in comparison to direct current ECM is the much greater degree of process control afforded the user. While in conventional ECM the user can select the current density, the type and concentration of electrolyte, and perhaps the electrolyte flushing pressure and velocity, with PECM the user has a far greater degree of control over the dissolution mechanism itself.

The PECM user can select not only the current density, but also the pulse parameters: on-time, off-time, and thus the duty factor, and the number of pulses in a group for those machines which permit grouping of pulses. In addition, the user controls the initial gap size and of course the type and concentration of electrolyte used.

Two brief summaries of actual research conducted up to the early 1990's was compiled by Wei [56], and by Rajurkar et al. [10]. The very brief synopsis presented here is compiled from these two sources.

The two major parameters which can be used in PECM to affect the erosion process, in addition to the current density, are pulse on-time and off-time. However, it is much more common to specify pulse on-time and duty factor, which is defined as the ratio of on-time to the sum of on and off-times. Table 2.4 is a summary of pulse on-times, off-times, and duty factors used in PECM research to date. Table 2.5 contains similar information on applied potential, current density, and workpiece material.

Based on the discussion in the previous section, it should be clear that the effect of any given parameter can't be considered in isolation. For example, the effect of any given pulse on-time and duty factor combination will be strongly affected by the current density and the initial gap size, to some degree.

In general, it is true that shorter pulses tend to confine anodic dissolution to the region experiencing the highest current density, i.e., the machining gap. Hence stray dissolution is minimized, and desired metal dissolution is increased, with short pulse on-times. Shorter pulse times also give a better surface finish, in general. However, it is also clear that using a very short pulse time will increase the total machining time, and hence the cost of the operation. On the other hand, the maximum pulse on-time is limited by electrolyte boiling in the gap, which leads to arcing and damage to tool and workpiece.

Longer pulse off-times have been shown to allow a more complete recovery of the electrolyte in the gap, as heat and waste products are removed. However, as is the case with short on-times, long off-times lead to a decrease in the machining efficiency, and an increase in cost. Some PECM machines, such as the COTAC-51 manufactured by the Shizuoka Seiki Co., attempt to alleviate this problem by grouping short pulses together. This allows the user another possible parameter for optimizing the process. Between bursts of

t (on) (ms)	t(off) (ms)	Frequency (Hz)	Duty Cycle %	Workpiece
200	?	5	?	Mo
100	100	5	50	Mo
50	150	5	25	Mo
0.5	2.5	333	17	Ti
1.0	5	167	17	Ti
0.5	1	667	33	Steel
1.0	2	333	33	Steel
2.0	4	167	33	Steel
10	500	1.96	2	Ti

Table 2.4 Pulse parameters used in PECM research (after [10] )

Applied Potential (V)	Current Density (A/cm <sup>2</sup> )	Workpiece
2 – 4	30 – 48	Steel/Nickel
0.2 – 4 20 – 50	30 – 50	Molybdenum Steel, Titanium
12 – 16	160	Steel, Titanium
20 – 25	—	Titanium
5 – 10	200	Various
10 – 25	—	Titanium
10 – 31	15 – 115	TiC, ZrC TiB <sub>2</sub> , ZrB <sub>2</sub>
—	5 – 60	Mild Steel
6 – 13	15 – 45	Steel

Table 2.5 Current Densities, Applied Potentials, and Workpiece Materials Used in PECM Research (after [10] )

short pulses the tool retracts from the workpiece and the gap is thoroughly flushed, leading to better surface finish and increased machining efficiency.

In summary, it is fair to say at this point that little research has been done on optimizing the PECM process. The effects of the primary PECM parameters, alone and in combination with others, has yet to be determined.

## **2.4 Effects of electromachining on die surfaces**

### **2.4.1 General effects**

Dies and molds fail in service when they fail to produce a number of piece parts sufficient to adequately amortize the cost of producing the tooling. Premature die failure can have several root causes, but most die failures can be traced to some sort of surface phenomenon, whether heat checking, excessive wear, or mechanical fatigue, that is very often due to the methods used to manufacture the die.

Die failure mechanisms tend to fall into two groups: those that occur in a variety of industries and processes, and those that are specific to a very narrow range of operating parameters. In the first group are such phenomena as abrasive and adhesive wear of die surfaces, and sudden catastrophic failure of a die section. Wear is of course a mechanism that every die surface that comes into contact with the workpiece material faces to some degree. Catastrophic die failure on the other hand is typically the result of poor die

design or a flaw in the manufacture of the die itself, for example incorrect heat treating.

Mechanical fatigue failure is also a mechanism that belongs to this group, because it can occur in any process in which the die is subjected to a cyclic stress. Other than dies used in continuous processes such as extrusion or drawing, almost all dies and molds are subjected to a cyclic loading environment. Failure in mechanical fatigue differs from the first two processes, however, in that the surface gradually degrades over time to the point at which catastrophic failure occurs. In a sense, then it is a combination of the other two failure modes.

In the second category are such processes as thermal fatigue or “heat checking” that are specific to processes such as die casting and hot forging. In this case it is the thermal cycle itself that creates the stresses leading to die failure, though very often these thermal stresses are combined with and aggravated by mechanical stresses as well. While thermal fatigue is similar in some respects to mechanical fatigue, it rarely results in a sudden catastrophic failure of the die. Rather, the die surface degrades over time to the point at which it can no longer produce usable parts, and must be replaced.

Both thermal and mechanical fatigue are known to be strongly affected by the quality of the die surface. Both are also known to be negatively impacted by the electrodischarge machining process, due to the nature of the recast layer mentioned earlier. Much less is known about the effects of

electrochemical machining on thermal and mechanical fatigue, though it is generally assumed to be a much more benign process. In this section the literature on the effects of EDM and ECM on mechanical and thermal fatigue is surveyed, and some likely correlations between the two failure modes are also noted.

#### **2.4.2 Effects of electromachining on mechanical fatigue**

*Electro-Discharge Machining* It has long been recognized that EDM has a pronounced negative effect on the service life of machine elements subjected to mechanical fatigue loading. It is for this reason alone that EDM has always been viewed with extreme caution by the aerospace industry when it is proposed as a method for machining parts from "difficult" metals.

Much of the early work on fatigue was done by Aleksandrov in the Soviet Union, and Lloyd and Warren in Great Britain, as noted in the section on residual stresses. Aleksandrov examined the effects of varying EDM pulse lengths on the fatigue life of a heat-resistant nickel-base alloy, EI437B, and a steel designated EYaiT. Both metals were eroded at pulse lengths of 130, 480, and 1050  $\mu\text{sec}$ , and then subjected to mechanical fatigue loading.

He found that the fatigue life of the nickel-base alloy was severely degraded by the EDM process, and that the degree of reduction in fatigue life was a strong function of the pulse on-time, which he attributed to the depth of the microcracks. For pulses of 1050  $\mu\text{sec}$ , the fatigue strength at  $10^7$  cycles

decreased by 30% from specimens machined by mechanical methods.

Alexsandrov found that removing 0.1 mm of the EDM'd surface by grinding and polishing did little to restore the fatigue strength of the material, but after 0.2 mm of metal was removed, the fatigue strength was restored to the pre-EDM level. He asserted that this proved that the reduction in fatigue life was due solely to the presence of microcracks penetrating through the recast layer into the base metal [49].

Lloyd and Warren examined the effect of EDM on a 0.2% C mild steel, which was then subjected to fatigue testing by completely reversed bending. They noted a slight reduction (5%) in the fatigue strength of the steel after EDM, and also found a slight improvement in the fatigue life following stress relieving. They also took this as evidence that the major damage to steels from the EDM process is a result of the microcracks which result, rather than the residual stresses [34].

More recently Abu Zeid researched the effect of the EDM machining parameters on the fatigue life of AISI D6 tool steel [68], while Béjar et al. examined the effect of oxidation of the surface following EDM on the fatigue life of AISI D-3 tool steel [69]. While neither of these papers added significantly to our understanding of the process, both confirmed the widely held assumption that the microcracks resulting from the rapid cooling of the surface are the prime source of reduced fatigue strength in EDM'd metals.

*Electrochemical Machining* The effects of electrochemical machining on mechanical fatigue have been examined by several researchers over the past few decades. It is generally held that electrochemical machining results in a totally stress-free surface, thus the data generated on such surfaces reflect the true condition of the material. Whether or not this “true condition” is better or worse than that due to any given machining process or surface preparation depends on the residual stresses left by the method in question.

Cina, for example, found that the fatigue values generally reported for polished steel specimens are artificially high, due to the cold working of the specimen surface by the polishing method. He compared specimens of several stainless steels and a low alloy steel that were highly polished with emery to samples polished electrochemically, and concluded that the lower fatigue strength of the specimens finished electrochemically more accurately represented the true fatigue strength of the steels [70].

Similar results have been reported by Rowden [71], Morozov [72], and Rumyantsev and Davydov [73]. Rowden looked at specimens prepared by several “non-conventional” methods, including EDM, ECM, laser, electron beam, and plasma machining to determine the effects of the various processes on fatigue life. He found, in agreement with other work in the field, that surfaces prepared by ECM generally had a lower fatigue life than those prepared by conventional machining methods, since such methods typically leave a compressive residual stress on the surface, which of course acts to

impede crack growth. On the other hand, methods such as EDM that result in tensile residual stresses (along with significant amounts of microcracking) result in surfaces that are inferior to ECM'd surfaces.

To the best of this author's knowledge, all of the research reported to date on the effects of ECM on fatigue life has used conventional, i.e., steady-state ECM. No research has been found on the effects of pulsed ECM on fatigue life, but there is no reason to believe that the results would be significantly different from those reported, since the surfaces are essentially the same. If anything, the pulsed ECM process should result in an improvement in fatigue performance, because the surface finishes attainable by the process are generally better than those of steady-state ECM.

## CHAPTER 3

### OPTIMIZATION MODEL FOR PULSED ELECTROCHEMICAL MACHINING

#### 3.1 Objectives

This chapter has two primary objectives: to present an optimization model for a typical die making production cycle, and to show how this model might be used to optimize pulsed electrochemical machining for the specific task of finishing die and mold surfaces.

To briefly reiterate the argument presented in the first chapter, the optimization of the die making cycle entails more than simply minimizing the time required for producing a given tool. While the time required to produce dies and/or molds for a product line is certainly one of the major cost factors in initiating production, because tooling production is so unlike any other part of the modern manufacturing enterprise, the optimization of the process requires that much attention be paid to the unique constraints that appear at every step.

Dies and molds are essentially custom items, with production runs typically consisting of a single item or else a very small number of duplicates. In the automotive industry, sheet metal dies are typically fabricated in pairs for the left and right hand sides of the automobile. For production processes in which die wear is severe, e.g., die casting, it is common for a die to be built along with several extra sets of inserts, which can be replaced as heat checking occurs.

In any case, the overriding concern in die and mold making is always the quality of the final product. Since dies and molds transfer their geometry (and often their surface finish) to piece parts thousands or millions of times over their useful lifetimes, they must be as nearly perfect as possible, given the ever-present constraints of time and cost.

The perfect die or mold has never been built, but if it could be it would have a zero tolerance geometry, an absolutely perfect surface finish for the application, would show zero wear, and would never fail in service through mechanical or thermal fatigue, or catastrophic failure. Optimizing the die or mold production cycle, therefore, means producing the highest quality tool in the shortest possible time at the lowest possible cost.

Given the intensely competitive nature of the market, time and cost pressures on the die or mold maker are relentless, and in the past several years, have become even more so. Nevertheless, it remains a fact that the quality of the tool has to remain paramount, if even greater costs in time and

money are to be avoided downstream, when inferior tooling leads to losses in production time and unacceptably high scrap rates.

The model presented here combines production time and cost in a way that allows for variation from shop to shop, depending on the specific machine tools and processes present. The quality function of each process is then defined according to the unique demands of that process, and optimized individually. For some processes, such as rough machining die blanks into a near-net shape suitable for heat treating, well-developed mathematical models are applicable. For other processes, such as EDM and PECM, no such models exist, thus models based on empirical data must be used.

### 3.2 General optimization model

The mathematical model of an optimization problem has two major components: a statement of the function to be optimized, and a set of constraints. This model has been developed over a number of years; the specific formulation given here has been largely adapted from Stoecker [74].

The function to be optimized is termed the *objective function*, and in “real world” engineering problems is almost always a function of several independent variables. If we let  $y$  represent the objective function, then

$$y = y(x_1, x_2, \dots, x_n) \rightarrow \text{optimize} \quad (3.1)$$

In any actual physical problem certain constraints on the objective function will also be present. These constraints either take the form of equality constraints

$$\phi_1 = \phi_1(x_1, x_2, \dots, x_n) = 0 \tag{3.2}$$

.....

$$\phi_m = \phi_m(x_1, x_2, \dots, x_n) = 0$$

or inequality constraints

$$\psi_1 = \psi_1(x_1, x_2, \dots, x_n) \leq L_1 \tag{3.3}$$

.....

$$\psi_j = \psi_j(x_1, x_2, \dots, x_n) \leq L_j$$

depending on the nature of the problem. Further, the sense of the inequalities in the latter case is determined by the actual physical conditions of the system being optimized.

Two further points bear mentioning. First, if an additive constant appears in the objective function, it does not affect the values of the independent variables at which the optimum occurs. Thus if

$$y = a + Y(x_1, x_2, \dots, x_n)$$

then the minimum of  $y$  is

$$\min[a + Y(x_1, x_2, \dots, x_n)] = a + \min[Y(x_1, x_2, \dots, x_n)]$$

Finally, the maximum of a function occurs at the same point as the minimum of the negative of the function:

$$\max[y(x_1, x_2, \dots, x_n)] = -\min[-y(x_1, x_2, \dots, x_n)]$$

### 3.3 An optimization model for die making

A rather detailed flowchart of the die and mold making process, taken from [5], is shown in Figure 3.1. The process of turning a part design into a functioning tool is a complex task requiring several steps. One major cost of building tooling is converting the part model into a die or mold model that can then be fabricated. The part design must be altered to allow for such complicating factors as shrinkage and draft, in the case of casting processes, or springback and metal flow within the die in the case of the forming processes. To ensure that the die or mold that is built actually meets the tolerance requirements of the tool design, both the in-process workpiece and incidental tooling such as EDM electrodes must be inspected at several intermediate steps to ensure conformance to the tolerances specified by the designer.

In general, we can say that the cost of building a die or mold is the sum of the material cost, the overhead costs, and the costs of machine time and skilled labor. One possible formulation is shown below:

$$C_{total} = C_{material} + C_{overhead} + R_{CAD}(Time_{CAD}) + R_{RM}(Time_{RM}) + R_{HT}(Time_{HT}) + R_{EDM}(Time_{EDM}) + R_P(Time_P) + R_{Ins}(Time_{Ins}) + R_{Try}(Time_{Try}) \quad (3.4)$$

where  $R_{CAD}$ ,  $R_{RM}$ , etc. are any given shop's rates for the specific task, and  $Time_{CAD}$ , etc. is the amount of time devoted to that task.

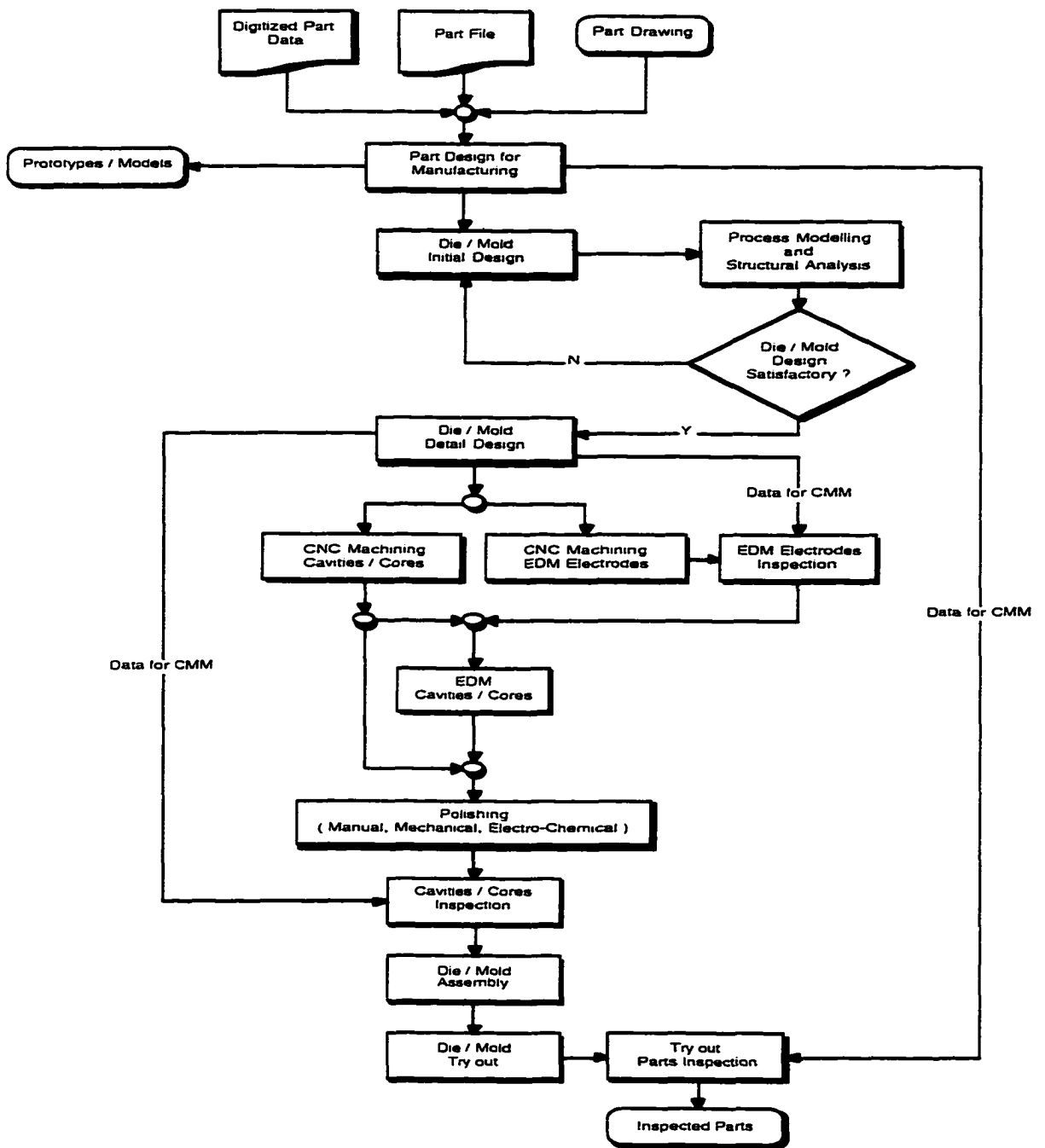


Figure 3.1: The diemaking process (from [5] )

Structuring the die manufacturing operation in this way has two advantages. First, it allows for individual variations among shops in terms of the rates charged for each operation. A shop that has invested heavily in high-speed machining centers and precision fixturing, for example, will presumably devote considerably less time to machining, but the rate charged per hour will be much higher than a shop using less sophisticated equipment.

Secondly, this structure makes clear that each specific process is optimized individually, according to the constraints unique to that process. As an example, a software package such as Optimill might be employed for the purpose of optimizing NC machining [75]. In this case, the objective function, which presumably would be total machining time, is a function of several independent variables, some of which that are easily measured, such as feed rate, number of cutting edges, and spindle speed, and some that are material and tool dependent.

The constraints on the machining stage of the process, however, would change along with the shape of the workpiece. In the early stages, when the primary objective is to rapidly remove large amounts of steel, the only true constraint on the speed at which the material removed is the strength of the cutting tool and the fixturing. At this stage, factors such as tool deflection and the accuracy of the machined surface are of relatively little interest.

At later stages of the process, however, either the forces on the cutting tool or the deviation of the generated surface from the ideal geometry would constrain the system. In either case, the physics of metal cutting is well

enough understood that mathematical formulations of the objective function and the constraints are possible.

For the heat treatment of the die block, on the other hand, the objective function is again the total time required to achieve the desired material properties, but in this case the constraints are maximum allowable grain size, minimum hardness, maximum allowable distortion, etc. In this case, constraints such as the grain size can be more or less accurately estimated by equations, while the distortion of the die component, because it is strongly influenced by the geometry of the workpiece, is very difficult to predict.

In summary, two points should be noted here. First, while the time devoted to each step of the overall process is the objective function to be minimized, each of the individual processes is governed by a set of constraints that are determined by the unique characteristics of that operation. The constraints for a single process, e.g., machining, can vary in time depending on the specific role that process plays in the production cycle at any given moment.

Secondly, in processes such as metalcutting the constraints are well-understood, and can be expressed to a high degree of precision as equations, which allow for the use of a set of well developed optimization techniques. For processes such as heat treating, EDM, and PECM, on the other hand, the constraints cannot be so precisely formulated.

In these cases, either our understanding of the chemistry and physics is not developed to the point of being able to use mathematical equations to

describe and optimize them, which is the case for PECM and to a lesser extent for EDM, or else the processes are so dependent on the geometry of the tool that no mathematical generalizations are possible, for example in estimating EDM tool wear or distortion in heat treating. For these processes, extensive experiments are necessary to generate data on which to base the optimization process.

Methods for optimizing multi-variable objective functions are many and varied. Techniques for optimizing processes that can be described mathematically include Lagrange multipliers, dynamic programming, linear programming, and geometric programming, to name only a few. For those processes that defy mathematical description, various search techniques have been developed. The basic method used here is to generate several values of the objective function for differing combinations of the independent variables, and then apply the search techniques to estimate the location in the state space of the optimal solution.

### **3.4 Optimizing PECM for die and mold finishing**

#### **3.4.1 PECM as a component of the larger system**

If one accepts the argument presented in Chapter One regarding the ideal die finishing process, then if PECM is to play a role as a viable finishing process it must:

- replicate the ideal die geometry to the closest possible tolerances

- create the best possible surface finish
- create multiple die cavities with identical geometries
- be easily integrated into the total die production process.

Given the current state of the art of diemaking, in which EDM plays a major role, it is very likely that any polishing process will follow the final EDM cycle, in which the die surface is brought to within a few thousandths of an inch of the ideal geometry. In this dissertation, it is assumed that PECM will only be applied to die sections that have been first been machined by EDM.

While the optimization of the EDM cycle itself is outside the scope of this work, it can't be ignored entirely, because EDM and PECM are linked together in several ways. First, and most obviously, the major role of PECM in diemaking is to completely and predictably remove any surface damage to the die caused by the EDM process itself.

This damage is very often thought of as being totally contained in the outermost recast or "white" layer, but this is by no means a fact. It is not uncommon, when examining EDM'd surfaces under the microscope, to find microcracks extending through the recast layer into the base material, especially on surfaces that have been subjected to aggressive, high-energy EDM pulses. It has also been suggested that the overtempered layer lying just beneath the recast layer may play a negative role in thermal fatigue of die casting dies [48].

In order to use the PECM process, or any automated process, to remove the damaged layer, we must be able to predict with some certainty how deep the damaged surface penetrates into the metal. Because the thickness of the recast layer varies considerably over the machined surface, statistical models must be developed to predict the damaged layer thickness as a function of the EDM parameters.

Secondly, the surface characteristics created by the EDM process play a role in the PECM cycle that follows. Experimental data presented in the following chapter will clearly show that the surface finish attainable by PECM for a given amount of charge per unit area is strongly affected by the initial roughness of the surface, which is a result of the EDM parameters used. In short, it is not useful to discuss optimizing the PECM process in isolation—it must be seen as an integral part of the system.

In terms of the requirements outlined above, how does PECM measure up as a potentially viable process? Given the current state of our knowledge of the process, it has to be admitted that many of the answers remain unknown. However, certain general assumptions about the process can be made at this point.

First, in terms of being able to replicate the “ideal” geometry of the surface, PECM looks very attractive. Because the process is electrolytic and removes metal from the surface one atom at a time, theoretically at least it’s possible to use the process to remove metal in layers a few microns thick. If such a level of precision can be attained in actual practice, then PECM would

look attractive not only for surface polishing, but also for micromachining applications as well. In fact, research in using PECM in this way is currently underway in the microelectronics industry [76].

The question of best possible surface finish remains an open question at this point. Again, due to the nature of the process it would seem to be theoretically possible, at least, to create a very smooth surface with PECM. However, as the discussion in Chapter Two shows, the tendency of electrolytic processes to attack each grain with a greater or lesser aggressivity seems to indicate that achieving extremely high surface finishes with PECM may be difficult.

Creating multiple die cavities with “identical” dimensions would seem to be ideally suited to PECM. Theoretically, the only reaction occurring at the cathode in an electrolytic cell is the generation of hydrogen, as was noted in Chapter Two. If the PECM tool actually does experience “zero wear” during machining, then this would constitute a major advantage for this process. Dies and molds with multiple identical cavities are very common in many processes, such as injection molding. A polishing tool capable of reproducing precisely the same cavity repeatedly would definitely be a boon to industry.

Finally, it would appear that PECM can be easily integrated into the die making process. As it is presently configured, the process is capable of using a finishing EDM electrode as the polishing tool, so it would appear ideally suited to integrating into the process after EDM. However, certain problems appear on closer inspection. First, state-of-the-art EDM machines and practice

extensively use orbital EDM to erode die cavities to near finish dimensions. This process has two major advantages: flushing in the cavity is enhanced by the orbital movement of the tool (in the X-Y plane), and very sharp interior corners and features can be machined while minimizing electrode wear on these features.

At present, PECM does not have orbital capabilities, nor is it likely to develop them soon. The details of the process are given below, but at present the machine requires an electrode machined in the exact shape and size of the cavity, minus a clearance gap of roughly 0.08 mm (0.004 inches). Machining a separate electrode for the PECM process would require the generation of a separate computer model and cutting paths, which while not an extremely expensive operation nevertheless introduces added cost and opportunity for error.

Secondly, EDM users in North America traditionally use graphite as the electrode material of choice. While copper is more extensively used in Japan and Europe, graphite accounts for roughly 85% of the electrodes made and used here. While copper offers certain advantages, there is no question that graphite, especially in the finer grades, is easier to cut into very intricate, fragile shapes.

The problem with using graphite in PECM is that the electrolyte, which is typically a salt solution such as sodium nitrate or sodium chloride, will soak into the pores in the tool, and when it crystallizes as it dries, expand and

break the electrodes from within. Given the expense of manufacturing the electrodes, this could also pose significant problems.

### 3.4.2 Specifics of the problem

Fitting the PECM process into the general optimization model of the preceding section entails developing the objective function, determining what constraints affect the system, and integrating the process into the larger picture.

From the general model for the die making cycle given by Equation 3.4, it's clear that for this model, processing *time* is the function to be optimized in every step of the die making process. For the PECM process, the time needed to polish a die surface can be defined as

$$Time_{PECM} = f(\text{Initial surface}, \text{Metal removal rate}) \quad 3.5$$

where

$$\text{Initial surface} = f(\text{EDM pulse parameters}, \text{Material properties}) \quad 3.6$$

and the metal removal rate, as defined by Faraday's Law, is

$$\text{Metal removal rate} = f(\text{Chemical equivalent}_{\text{alloy}}, \text{Current density}, \text{Time}) \quad 3.7$$

The constraints on the current density and pulse parameters are imposed by the conditions that the temperature of the electrolyte in the gap not exceed the boiling point, and that metal salts not precipitate. These constraints are governed by equations 2.19, 2.30, and 2.34:

$$\Delta T_a = \frac{i_a^2 L}{\kappa \rho C_p u} = \frac{i_p^2 (t_p / t_{pp})^2 L}{\kappa \rho C_p u} \quad (2.19)$$

$$i_{pl} = \frac{nFD}{\Theta_{pl}} \frac{c_{sat} - c_n}{\delta_p} \quad (2.30)$$

$$\frac{i_{pl}}{i_l} = \frac{\Theta_l}{\Theta_{pl}} \left[ \frac{\delta_p}{\delta} \left( 1 - \frac{t_p}{t_{pp}} \right) + \frac{t_p}{t_{pp}} \right]^{-i} \quad (2.34)$$

Because PECM must be integrated into the die making cycle after EDM, it is crucial that we have an idea of what the surface damage done by the EDM process is. Because developing a usable statistical model for the depth of the damaged layer was beyond the scope of this work, a slightly different approach was used. Based on personal experience in die making, I decided to choose a typical surface finish for a die section coming out of the EDM process, and use that as a starting point for the PECM cycle.

Accordingly, I chose to use a surface finish of 4.0  $R_a$  as a benchmark for an EDM surface. As will be explained in the next chapter, tests were then performed to determine the depth of the recast layer for H-13 steel at this level of surface finish. Finally, further tests were conducted to determine a level of charge that would reliably remove all trace of EDM damage from the steel. While this solution is not optimal in the sense that the two processes were not examined in tandem to determine the best possible combination of machining times and energy levels, it does represent a workable solution given the time constraints that were present.

Once this issue was determined, the research focused strictly on the PECM process itself. As in every step of the die making process, two separate issues must be considered with PECM: determining how the metal removal rate (MRR) of the process is affected by the process parameters, and equally importantly, developing a model to predict how the polished surface finish varies with the same set of parameters.

In theory, the metal removal rate can be predicted by Faraday's Law of Dissolution, which states that the mass of metal dissolved is given by the chemical equivalent of the metal, multiplied by the total charge, divided by a constant. In actuality, the MRR is considerably more difficult to predict, because of the complexity of the real situation. In fact, alloy steels are composites of several different metals, each of which is capable of ionizing at multiple valences. Rosset *et al.* found that the effective valence of a tool steel can vary widely depending on the level of current density used [77].

However, it is clear that the Faraday Law provides an accurate model for metal dissolution, once we are able to determine the value of the constants for the equation. Thus the task of predicting the amount of a given steel that will be dissolved for a given level of charge seems to be relatively straightforward. This was the second step to be taken.

The question of optimizing the surface finish is a much more difficult problem. Surface finish in general is difficult to characterize, as evidenced by the somewhat bewildering array of surface measurements that have been developed over the years by DIN, ASTM, ISO, and others. Almost no work

has been published in the general area of surface finish and ECM, let alone PECM. Because conventional ECM was used almost solely for aerospace applications, rather than tooling production, surface finish was usually not a primary consideration.

In PECM the problem is compounded by the fact that the surface finish is strongly affected not only by the pulse parameters themselves, but also by the unique combination of metal and electrolyte [59, 76, 77]. In addition, the initial condition of the surface also plays a role in determining the initial rate of smoothing. Finally, the pulse parameters: on-time, duty factor, and current density must also be included in an optimization algorithm.

In this dissertation the response surface methodology was used to gain an understanding the functional relationship between surface finish in PECM and the most important process parameters. The approach generally follows the method outlined by Box, Hunter, and Hunter [78], which consists of several stages. The first stage is a factorial screening experiment, designed to determine the overall "lay" of the response surface. These first experiments are used to fit a first-order polynomial to the data. From this planar model of the surface, the "direction of steepest ascent" is used to determine the best location for a second series of experiments, which are intended to develop a second order model of the surface. Depending on the shape of this second-order surface, canonical analysis may be useful in determining the underlying physical relationships that are revealed by the data.

Applying this method to the problem of optimizing surface finish in PECM, the experimental method consisted of an initial full factorial design using two levels of five factors: pulse on-time, duty factor, peak current density, number of pulses in a pulse group, and initial gap dimension. Based on the results of this work, a second series of experiments were performed to more accurately depict the shape of the response surface in a much smaller region.

To summarize the approach taken here: the thrust of this work is to optimize the surface finish obtainable by applying PECM after an initial EDM treatment. No attempt is made to minimize the total time required for either process or for the combination of the two processes. However, once an effective valence is calculated for H-13 in  $\text{NaNO}_3$  electrolyte, the application of the Faraday Law is straightforward. The details of the experiments performed to determine the effective valence and to optimize the surface finish of the steel subject to the constraints outlined above are provided in the following chapter.

## CHAPTER 4

### EXPERIMENTAL BACKGROUND FOR THE MODEL

#### 4.1 Objectives

This chapter has three primary objectives: to describe in detail the experimental designs that were used; to present data on the metal removal rate, smoothing rate, attainable surface finish, and the nature of the surface; and finally to explain how the results of the experiments can be used in connection with the model proposed in Chapter Three to begin to optimize the PECM process in die and mold making.

The structure of this chapter generally follows the strategy outlined in section 3.4.2. The first step was to determine from microscopic examination of surfaces prepared by EDM how the thickness of the recast layer varied with applied energy. Although by nature the recast layer shows wide variance in thickness, the goal here was to determine a maximum layer thickness that could be used as a minimum removal depth for the PECM process.

The second step involved a series of tests to determine as closely as possible the actual metal removal depth in PECM. Because the removal rate is known to vary with applied current density, tests were conducted at several levels of current density. Two different methods of determining the removed depth were used in the experiments, with varying results. The experimental results were also used to calculate an effective valence for the H-13 tool steel used here.

Having determined the removal rate of the PECM process within reasonable limits, the next task was to try to optimize the surface finish of the steel. Following the method of Box, Hunter, and Hunter, design of experiments techniques were used in two stages here to develop a response surface for surface finish as a function of the relevant machining parameters.

In the initial screening stage essentially all the PECM parameters that can be adjusted by the user were included in the experimental design. Based on the results of this set of experiments, the parameter list was narrowed, and a second set of experiments was performed to establish the shape of the response surface in a very limited region of the parameter space.

Optimizing the PECM process for die and mold making requires a knowledge not only of metal removal rate and surface finish, but also how the two aspects are combined. Thus the issue of the smoothing rate is dealt with after the description of the surface finish.

Finally, the chapter concludes with a brief examination of the surface of the H-13 steel resulting from the PECM process, and a brief discussion of some possible techniques for use in future work.

## **4.2 Determination of the metal removal rate**

### **4.2.1 Integrating PECM and EDM**

In order to truly optimize the entire die and mold making cycle, it's essential that each component be integrated as much as possible into the total process. One of the key factors in this integration process is knowing at what point the workpiece should move from one stage to the next. For example, how close to the net shape should the block be machined before going to heat treat? If the rough machining is too close, the distortion resulting from heat treating may render the die section useless; if too much metal is left, then the excess must be removed by EDM at a much slower pace and at greater cost.

The question with regard to integrating PECM into the process is one of determining how much material must be removed from the EDM'd surface to ensure that the surface is restored to its pre-EDM state. From the material presented in Chapter Two, two facts should be clear. First, the thickness of the recast layer is a function not only of the spark energy, but of the particular levels of current and pulse time selected. Second, the thickness of the layer can vary greatly over a single surface eroded at precisely the same parameters.

Due to time limitations, it was not possible in this research project to develop a statistical model for the thickness of the recast layer as a function of the EDM pulse parameters. However, there is no practical obstacle to developing such a model, and it is one of the first steps that will be taken on concluding the present work. Instead I have taken the approach of eroding samples to what I consider to be a reasonable level of surface finish, and then applying PECM to them to a depth sufficient to remove all trace of the recast layer.

The specimens were cut out of the same blocks of H-13 that were used to fabricate the mechanical fatigue specimens described in the following chapter. The steel was heat treated to a Rockwell "C" condition of 46, which is typical of die casting dies, though slightly lower than the condition of hot forging dies [79].

Figure 4.1 is a photograph of a typical H-13 specimen after EDM. The two surfaces shown were both taken from the same sample. It was eroded on the AGIE 2U EDM machine to a surface roughness of  $R_a=4.0$ , sectioned with the Sodick wire EDM, and the sections were then mounted face to face (to minimize edge rounding) and metallographically polished, etched, and examined with the scanning electron microscope. (The black material in the center of the photograph is the mounting medium.)

From this photograph, it is clear that the thickness of the recast layer varies widely over even the small area shown here. The thinnest section is



Figure 4.1 SEM Photograph of EDM Recast Layer— 4.0  $R_a$  Surface

roughly 5  $\mu\text{m}$  in depth, while the large protrusion on the surface to the right is about five times as thick. However, even this section does not exceed 30  $\mu\text{m}$  in thickness. The slightly darker band lying under the recast layer shows the extent of the overtempered zone. On both sections shown here, the total thickness of the heat affected zone does not exceed 50  $\mu\text{m}$ .

Figure 4.2 shows a similar arrangement of two sections of H-13 prepared identically to those shown above, including an EDM treatment to a surface finish of 4.0  $R_a$ . In this case, the section to the right has been polished with PECM to a level of 300 Coulombs per square centimeter after EDM erosion. It is clear that all trace of the recast layer has been completely removed from the surface.

Several samples were prepared in this way and examined under the microscope, and it became clear that a polishing cycle of 300 C/cm<sup>2</sup> was more than enough to remove all trace of the recast layer. Unfortunately, time did not allow for a thorough investigation of the minimum polish necessary to remove the recast material. Thus the "optimization" described here is not truly optimal, because the polishing routine was allowed to run longer than was probably necessary. However, as will be explained in a later section, a minimum amount of charge is also needed to produce a surface at given finish, so it should be kept in mind that simply removing the recast layer does not in itself guarantee an optimal surface.

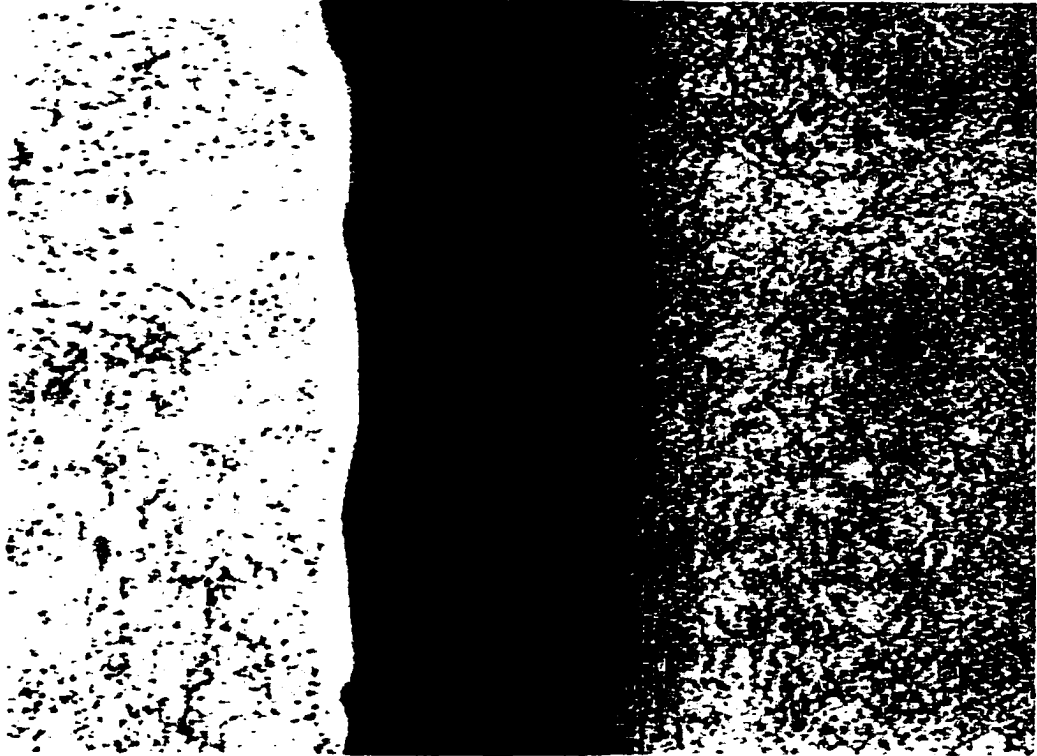


Figure 4.2: EDM'd H-13 on left, surface on right PECM'd at  $300\text{ C/cm}^2$   
(Surface etched 15 seconds in 2% Nital, 200X)

One logical question to ask at this point is, to what effect the initial surface roughness affects the polishing cycle. Particularly with a dissolution process, it would seem logical that a rougher surface, with a greater surface area exposed to the electrolyte, would dissolve more quickly than a smooth surface. Experiments were performed to determine the effect of surface roughness on smoothing rate, but the details will be deferred to a later section.

#### 4.2.2 Removal rate determination

Faraday's Law of Electrolysis is the basic governing equation for all electrolytic processes, whether electroplating, electropolishing in acids, or electrochemical machining. From Chapter Two, the mass of metal removed by an electrolytic process is given by

$$m = \frac{AIt}{zF} \quad (2.4)$$

where

$m$  = mass removed

$A$  = atomic weight of element in question

$z$  = valence of the element

$I$  = average current

$t$  = time of dissolution

$F$  = Faraday constant, 96,500 C.

From this fundamental equation, the mass and volumetric removal rates are easily derived:

$$\dot{m} = \frac{AI}{zF} \quad (2.5)$$

and

$$\dot{v} = \frac{AI}{\rho_a F} \quad (2.6)$$

From the development in Chapter Two, we know that the behavior of an alloy undergoing electrochemical machining is quite complex. Leaving the passivation phenomenon out of the picture for the time being, it is still quite difficult to predict the removal rate of an alloy, due to the fact that two atoms of the same metal can dissolve at different valences, depending on the local pH, and the local field strength [54].

Several theoretical removal rates for premium grade H-13 steel were calculated and listed in Table 2.2. Based on the assumption that iron dissolves both as  $\text{Fe}^{2+}$  and  $\text{Fe}^{3+}$ , and chromium as  $\text{Cr}^{3+}$  and  $\text{Cr}^{6+}$ , both the "percentage by weight" and the "superposition of charge" methods were used to calculate four possible alloy chemical equivalents for H-13, which are shown in Table 4.1. Applying these values to Faraday's Law results in the estimated removal rates shown in Table 4.2 for a total current of 400A. The volumetric removal rate is calculated by dividing the mass removal rate by the density of H-13, which was found by experiment to be  $7.63 \text{ g/cm}^3$ .

Method	Fe <sup>2+</sup> Cr <sup>3+</sup>	Fe <sup>2+</sup> Cr <sup>6+</sup>	Fe <sup>3+</sup> Cr <sup>3+</sup>	Fe <sup>3+</sup> Cr <sup>6+</sup>
Percentage by Weight	27.1	26.6	18.6	18.2
Superposition of Charge	26.45	24.5	18.48	17.51

Table 4.1 Chemical Equivalents for H-13 Steel, Assuming Mo<sup>3+</sup>, V<sup>2+</sup>

Figures 4.3 and 4.4 show the mass of H-13 removed as a function of time as calculated by the two methods. Figure 4.3 shows the results of the "percentage by weight" method, and Figure 4.4 the "superposition of charge" method. From these figures, it is clear that the valence of iron is the dominant factor, as one would expect.

Method	Fe <sup>2+</sup> Cr <sup>3+</sup>		Fe <sup>2+</sup> Cr <sup>6+</sup>		Fe <sup>3+</sup> Cr <sup>3+</sup>		Fe <sup>3+</sup> Cr <sup>6+</sup>	
	Mass g/s	Vol. cm <sup>3</sup> /s						
Percentage by Weight	0.112	0.015	0.110	0.014	0.077	0.010	0.075	0.070
Superposition of Charge	0.109	0.014	0.101	0.013	0.077	0.010	0.073	0.009

Table 4.2 Theoretical removal rates for H-13 steel at 400 A

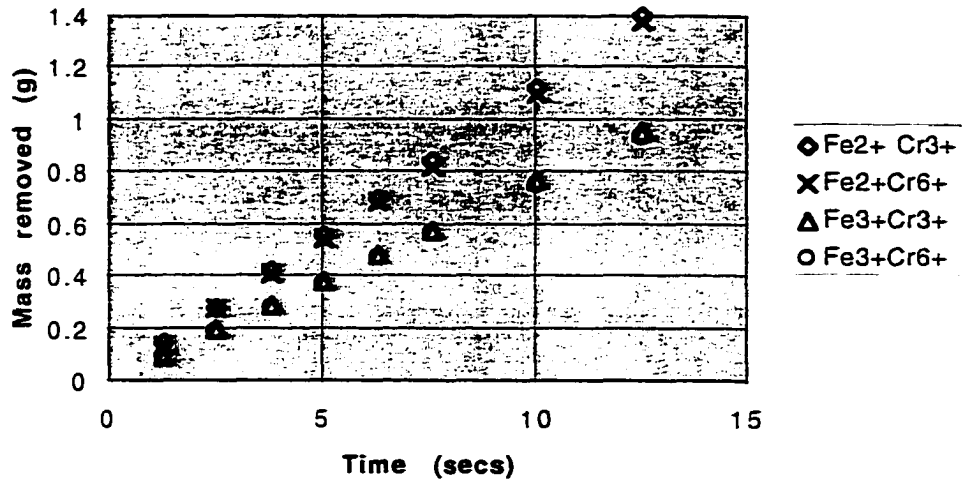


Figure 4.3: "Percentage by weight" prediction, H-13, 400A

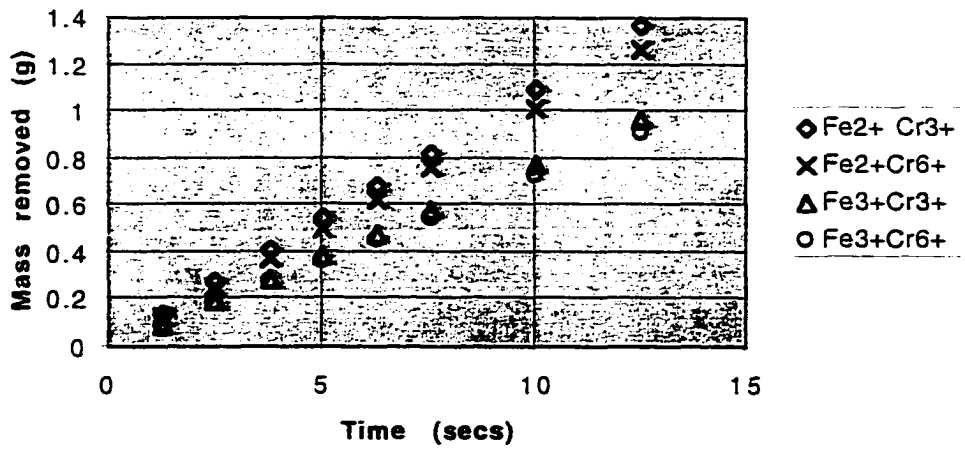


Figure 4.4: "Superposition" prediction, H-13, 400A

In order to determine how closely H-13 under PECM conditions approached the theoretical removal rates, it was necessary to find a method that could measure either the volumetric removal rate or the mass removal rate precisely enough to be useful. The first method that was tried employed the Federal 4000 profilometer. This device, which traverses a diamond stylus across the measured surface, is capable of measuring surface roughness, and also the waviness of the surface by filtering out the high frequency signal.

Several specimens were prepared from heat treated H-13, and then polished with a square copper electrode of area  $10 \text{ cm}^2$ . A current density of  $40 \text{ A/cm}^2$  was applied, with a pulse on-time of 5 ms, an off-time of 255 ms, and an initial machining gap of  $80 \text{ }\mu\text{m}$ . At every 500 Coulombs, the process was halted and the specimen taken out of the machine, cleaned with distilled water followed by acetone, and a series of profilometer traces taken.

Because the samples were slightly larger than the electrode, an unpolished ridge remained along one side of each sample. By beginning the profilometer trace at this location and then traversing the stylus into the polished region, the instrument was able to measure the amount of metal removed from the virgin billet to within a few microns.

A representative profilometer trace is shown in Figure 4.5. The upper trace is the smoothed waviness profile, and the lower the unfiltered

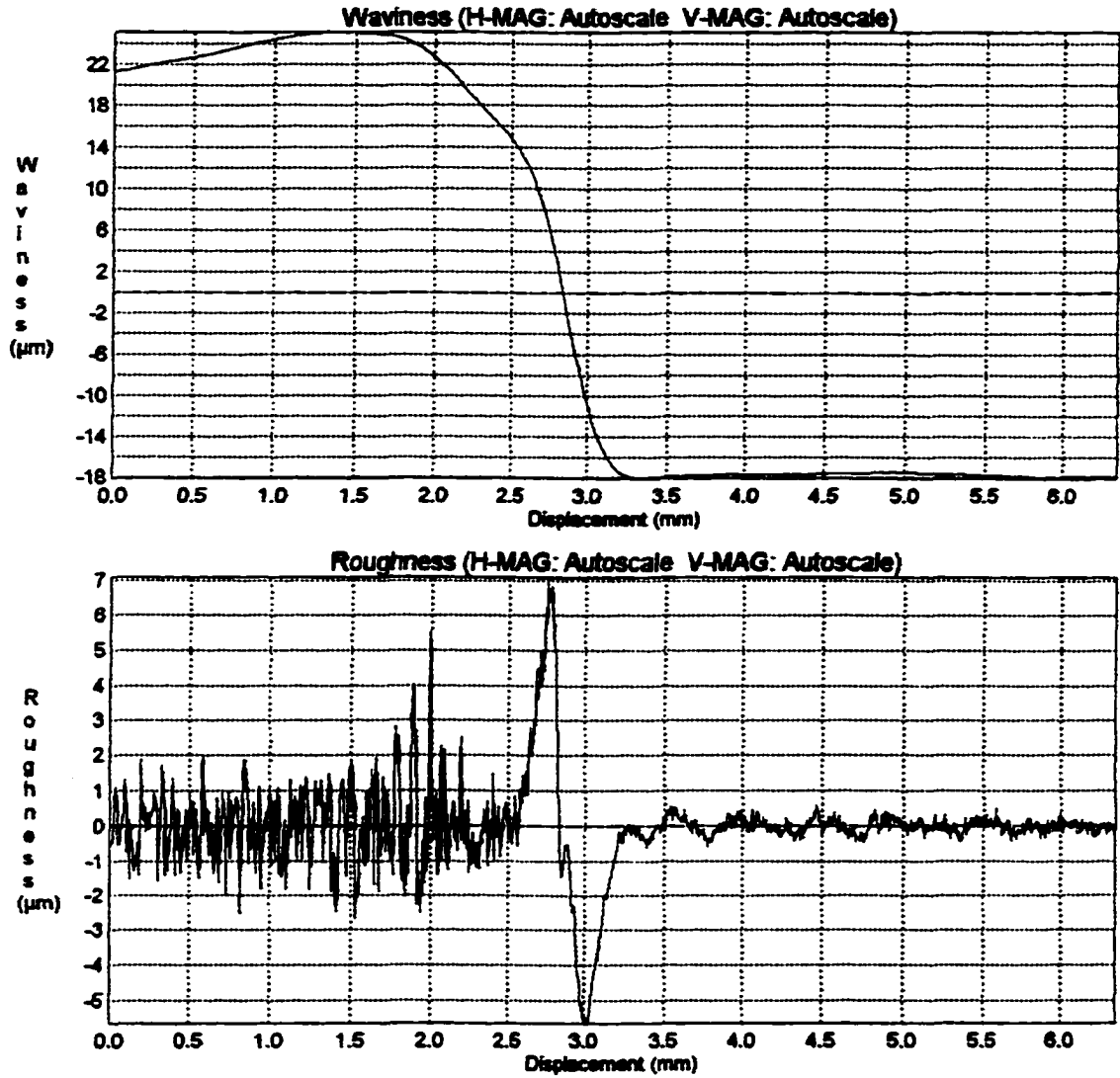


Figure 4.5: Traces showing roughness and waviness of the polished area

roughness profile. The area to the left in both profiles is the unpolished, as-EDM'd surface, with the PECM'd surface to the right. This particular surface was polished to  $R_a = 0.2 \mu\text{m}$  finish. The total charge applied at this point in the test was  $150 \text{ C/cm}^2$ .

The standard waviness parameter  $W_t$  was used to estimate the depth of metal removed during the process.  $W_t$  is defined by the standard DIN 4774 as the vertical distance between two parallel lines enclosing the waviness profile at the least separation distance. For each specimen, three different traces were taken and an average value computed, which was then taken to be the removal depth.

The results of these first experiments are given in Figure 4.6, plotted against the amounts predicted by the two methods shown in Figures 4.4 and 4.5. Data for two different specimens are shown. Each data point is the average of at least three  $W_t$  plotted against the polishing time. The agreement of the data with the predicted values was surprisingly good, and indicated a high efficiency for the process.

Although these results looked very promising, the method used to determine the removal depth led naturally to the question of how accurate the data actually was. This was due to the fact that the measured parameter,  $W_t$ , varied widely depending on the location of the surface measurement. It was noted on several samples that the polished surface showed a strong

contour, with the deepest section at the edge of the polished region, exactly where these measurements were taken.

At the time of these experiments, it was also not clear how to polish the surface without creating an oxide layer on the surface. The thickness of this layer varied from approximately 0.02 to 0.06 mm, depending on the pulse parameters used. Because it was necessary to avoid this layer while taking the measurements of  $W_v$ , and due to the fact that typically a large percentage of the surface was covered by the layer, a truly random measurement of the polished surface could not be made.

The presence of the oxide layer also prevented using simple weight measurements to determine the mass removed. However, when it became clear that a series of relatively long (20 ms) pulses interrupted by flushing cycles would efficiently remove all visible trace of the oxide layer, it became possible to rely on weight measurements to determine the mass removal.

Figure 4.7 shows the results of a series of experiments that were intended to obtain a better estimate of the true removal rate for H-13 steel undergoing PECM. Two sets of specimens, consisting of four specimens in each set, were eroded under identical conditions. The first set of specimens had been EDM'd to an initial surface roughness of  $2.0 R_a$ , and the second to an initial roughness of  $12 R_a$ . Thus a secondary goal of the experiment was to determine what effect if any initial surface roughness plays in the removal rate.

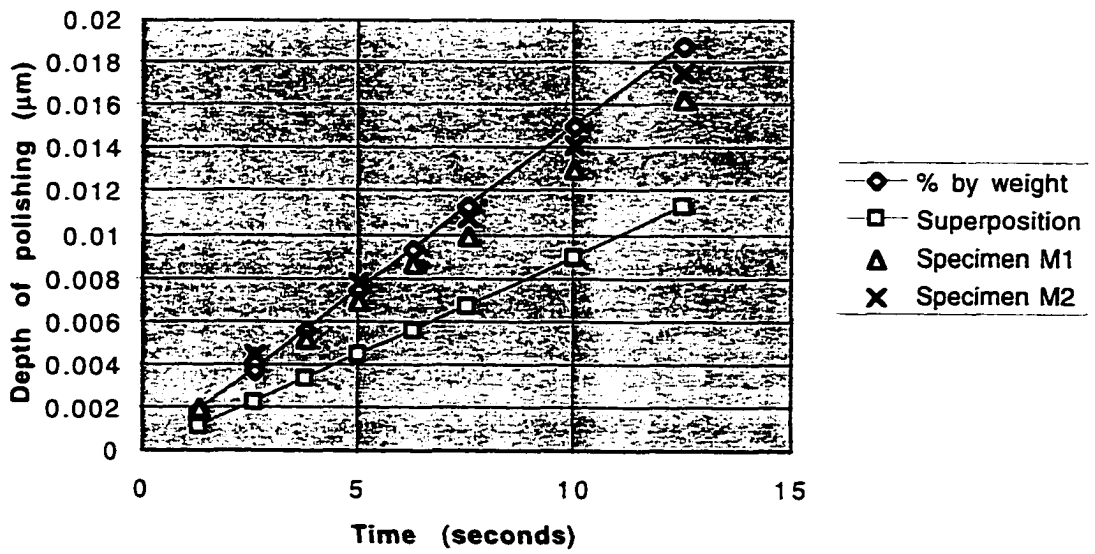


Figure 4.6: Comparison of measured and predicted polishing depths

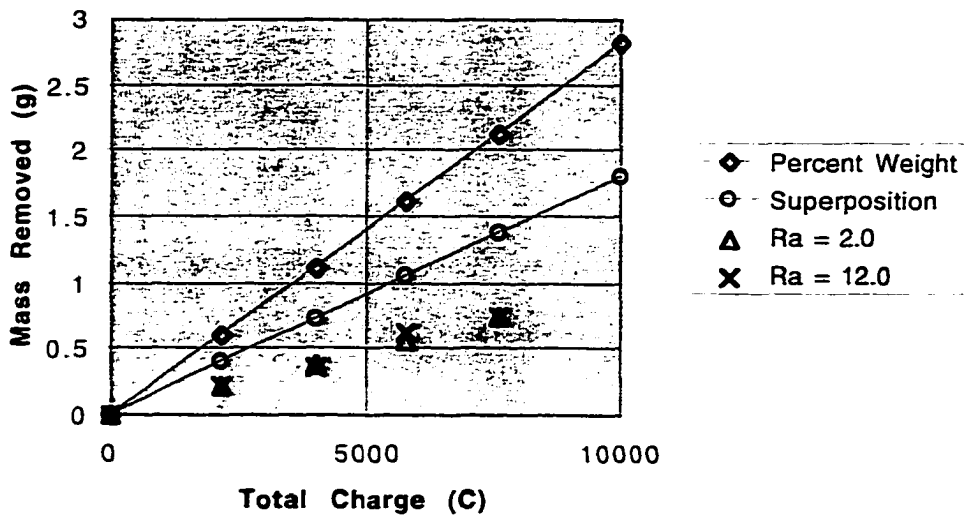


Figure 4.7: Comparison of predicted and actual mass removed

Four different levels were applied to the specimens, with one specimen in each set receiving either 2200, 4000, 5800, or 7600 Coulombs. The polishing routine, which will be described in more detail below, was a combination of 5 ms pulses and 20 ms pulses. The shorter pulses were used for the actual metal removal, and the longer pulses were used to clean the oxide layer from the surface.

Two facts quickly emerge from these experiments. First, initial surface finish seems to have no effect on the amount of metal dissolved. While the surface roughness may accelerate dissolution in the early stages, this effect is clearly not discernable after a very short time.

Secondly, a comparison of Figure 4.6 and 4.7 shows a wide discrepancy in the results of these experiments and the earlier tests using the Federal profilometer to measure mass removed. Clearly, the mass measurements, which are considerably more reliable than the profilometer traces, show that the PECM process as used here was not nearly as efficient as predicted by the Faraday Law.

From Chapter Two, efficiency in electrochemical dissolution is defined as

$$\Theta = \frac{\text{actual mass removed}}{\text{theoretical mass removed}} \quad (2.7)$$

Using the “percentage by weight” chemical equivalent, and assuming that dissolution primarily occurs with the valence condition  $\text{Fe}^{2+} \text{Cr}^{3+}$ , the efficiency of the process under these conditions is approximately 35% for all eight specimens.

Another useful method for gauging the efficiency of the process is to calculate the “effective valence” of the process. Rosset and his colleagues looked at effective valence of three tool steels in different electrolytes (1M and 6M  $\text{NaNO}_3$ , 4M  $\text{NaCl}$ ), and found that the valence varied from a peak of 10 at a current density of 30  $\text{A}/\text{cm}^2$  to a steady-state value of 3 at current densities above 60  $\text{A}/\text{cm}^2$  [77].

With the ability to accurately measure the mass removed during the process, the effective valence is again given by the Faraday Law:

$$z = \frac{M_{\text{alloy}} I t}{m F} \quad (4.1)$$

where  $M_{\text{alloy}}$  is the atomic weight of the alloy, defined as

$$M_{\text{alloy}} = \sum x_j M_j \quad (4.2)$$

$M_j$  = atomic weight of component  $j$ , and

$x_j$  = mole fraction of component  $j$ .

From the composition of H-13 given in Table 2.2, the atomic weight of premium grade H-13 was found to be approximately 93.8 gr/mol. Applying this value to equation 4.1, the effective valence of H-13 was found to vary between 5.18 at 100 A/cm<sup>2</sup> and 6.74 at 60 A/cm<sup>2</sup>. These results are in line with the values Rosset et al. found for a .4%C, 12%Cr tool steel, and are shown in Figure 4.8.

The decrease in valence with increasing peak current density makes sense in light of the passivation chart of Datta shown in Figure 2.13. At current densities above the passivation level but slightly below the transpassive region, significant oxygen evolution occurs at the anode. This effect translates to reduced metal removal, and an increase in the effective valence of the alloy.

The use of both short (5 ms) pulses and longer (20 ms) pulses will be explained in more detail below, but the basic idea is that the longer pulses are used to break up and remove the heavy oxide layer that typically forms on the surface during the "erosion" (short pulse) section of the polishing cycle. These longer pulses make up a major percentage of the total erosion time, but they

result in very little metal removal. The end result is reduced efficiency of the process, which can be seen as the higher effective valence for the alloy.

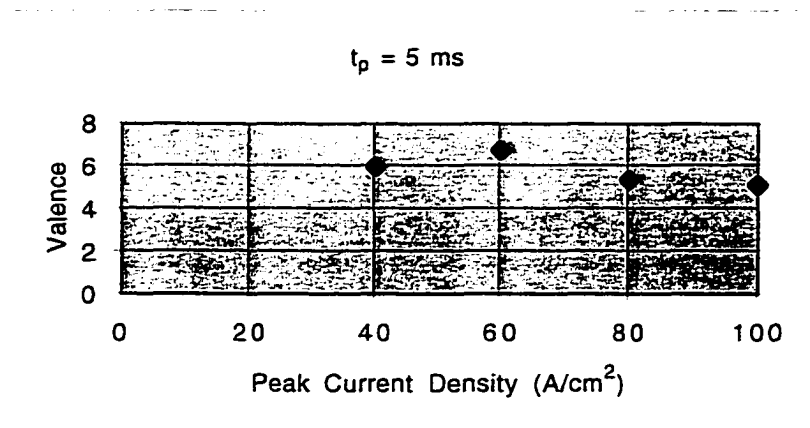


Figure 4.8: Valence of H-13 as a function of peak current density

### 4.3 Optimization of the surface polishing process

#### 4.3.1 The role of the parameters in polishing

In section 2. 3.4, the machining parameters available to the PECM user were outlined. To recap briefly, they are: peak current density, in A/cm<sup>2</sup>, pulse on- and off-times, in milliseconds, number of individual pulses in a pulse group, and the overall number of pulse groups. The initial voltage is also input by the user, but this value will change as the machine controller attempts to maintain a constant peak current across the gap. Both the gap width, the state of the workpiece surface, the conductivity of the electrolyte,

and the degree to which the workpiece is grounded have a strong effect on the voltage required.

In addition, the user decides on an initial gap between the tool and workpiece; because the tool returns to the same location after flushing cycles, rather than maintaining a constant gap, the gap rapidly grows to several times the initial value. For many of the experiments described in this dissertation, the initial gap width was set at 80  $\mu\text{m}$ . However, after a few hundred Coulombs have passed across the gap, it has typically doubled or tripled in width.

Two other factors are generally regarded as playing an important role in the process: the pH and the temperature of the electrolyte. It has been my experience in conducting this research that the pH varied very little over time. It remained fairly constant at a value of 8.2 – 8.4 during the entire period of these experiments.

The bulk temperature of the electrolyte was another matter. Typically, at the beginning of an experimental run the temperature was approximately 25C, but at the end of the run it often had climbed 8 or 10 degrees Celsius. It is a fact that the conductivity of the electrolyte will increase significantly with a rise in temperature. During most of the experiments performed here, the conductivity of the solution ranged from 180 mS/cm to 200+ mS/cm (the conductivity meter was unable to measure conductivity above 200 mS/cm).

Temperature of the bulk electrolyte may indeed play a role in the process, but because there was no way to control this parameter, it was not included in the experimental design. While this might seem to be a large and obvious source of error, I would contend that because the current pulses typically occur in groups of at least five pulses separated by periods not longer than 250 milliseconds, the temperature in the machining gap very quickly reaches levels high above the bulk temperature of the electrolyte in any case.

#### 4.3.2 Design of the initial screening experiments

The experiments to determine the parameter set that would result in optimal surface finish occurred in two stages. The first stage, called the “screening” stage here, was intended to give an overall view of the parameter space in terms of surface finish. For this stage, the parameters to be varied were:

- Current density,  $J$ , A/cm<sup>2</sup>
- Pulse on-time,  $T_{on}$ , msec
- Duty factor,  $\gamma$
- Number of pulses in a pulse group
- Gap width

Following the procedures outlined in Box, Hunter, and Hunter, [78] a two level full factorial experimental plan was devised. Following Box’s recommendation that in the initial stages of an experimental design as much

of the parameter space as possible should be covered, the levels of each parameter were selected as shown in Table 4.3.

Level	Current Density (A/cm <sup>2</sup> )	Pulse On-time (msec)	Duty Factor %	Pulses/Group	Gap Width (μm)
0	30	5	1	5	60
1	50	10	3	10	100

Table 4.3: Initial parameter levels for screening experiment

These settings were designed to bracket that part of the parameter space used by the COTAC controller for its “default” settings. The COTAC-51 queries the user regarding the desired depth of removal and the initial surface roughness of the workpiece. Based on the user’s input, the machine then inserts a set of default values into the control algorithm. The user has the option of accepting these parameter levels or modifying them.

The flaw in this system is that the algorithm used by the controller to determine these initial levels is unavailable to the user. Further, use of the default values was not found to result in very desirable surfaces. Typically, the surfaces polished using the default parameters were heavily oxidized, and the surface finish adversely affected as a result [38].

The algorithm used by the COTAC controller to initialize the polishing cycle does not take into account the material to be eroded. This in itself is a

major flaw, because tool steels are known to react quite differently to the process, depending on the type and amount of the alloying elements. In any event, the default parameters were used as a guide for determining the initial levels of the parameters for this series of tests.

The experimental design for the first sixteen tests is shown in Table 4.4. Because initial gap width was considered likely to be the least significant parameter, it was held at a constant level for the first experimental run. The experiments were conducted in random order, and every attempt was made to conduct each of the experiments in an identical fashion.

Because the mass of material removed is theoretically a function only of the amount of charge passed across the gap during the process, the total charge was held constant at  $250 \text{ C/cm}^2$  for all of these experiments. In order to compensate for the two levels of current density (30 and  $50 \text{ A/cm}^2$ ), pulse time (5 and 15 ms), and number of pulses in a group (5 and 15) while holding the total charge constant, the total number of pulses varied between 333 pulses for 5 ms pulses in groups of 5 at  $30 \text{ A/cm}^2$  to only 7 pulse groups for 15 ms pulses in groups of 15 at  $50 \text{ A/cm}^2$ .

Before any of the tests were run 24 separate profilometer traces were made on 8 of the specimens to determine their mean surface roughness. In order to more accurately categorize the surface and the process, three surface parameters were used:  $R_a$ , which is defined by ISO Standard 4287/1 as "the arithmetical average of all departures of the profile from the mean line

Specimen Number	Run Order	Current Density	$T_{on}$	Duty ( $T_{off}$ )	Pulses (Total)	Gap
1	1	30	5	1% (495)	5 (333)	60
2	5	50	5	1% (495)	5 (200)	60
3	2	30	10	1% (990)	5 (167)	60
4	6	50	10	1% (990)	5 (100)	60
5	3	30	5	3% (162)	5 (333)	60
6	7	50	5	3% (162)	5 (200)	60
7	4	30	10	3% (333)	5 (167)	60
8	8	50	10	3% (333)	5 (100)	60
9	9	30	5	1% (495)	15 (111)	60
10	11	50	5	1% (495)	15 (67)	60
11	15	30	10	1% (990)	15 (56)	60
12	12	50	10	1% (990)	15 (7)	60
13	10	30	5	3% (162)	15 (111)	60
14	14	50	5	3% (162)	15 (67)	60
15	16	30	10	3% (333)	15 (56)	60
16	13	50	10	3% (333)	15 (7)	60

Table 4.4: Experimental design for initial screening experiments

throughout the sampling length”,  $R_{\max}$ , which is defined by the DIN standard 4768 as “the largest single peak-to-valley height ( $Z_1$ ) within five adjoining sample lengths, and  $R_z$ , defined by DIN 4768/1 as “the average of the single peak-to-valley heights of five adjoining sampling lengths  $l_s$ ” [80].

All three of these surface measurements were used in order to give a better idea of how the PECM process attacks the metal surface. Given the nature of the process, it would seem logical that the largest irregularities in the surface, to which the parameters  $R_{\max}$  and  $R_z$  would be most sensitive, would be the first attacked by the dissolution process. Not only would they have a large surface exposed to the electrolyte, but the local field would be concentrated at them as well.  $R_a$ , because it is the average deviation of the surface from the mean line, should give a better representation of the overall texture of the surface, but will tend to minimize the effect of single large deviations in the surface.

Table 4.5 shows the basic statistical profile of the three parameters. As expected, both the mean and the standard deviations for  $R_{\max}$  and  $R_z$  were an order of magnitude larger than those for  $R_a$ . This is also a reflection of the nature of the EDM'd surface. As evidenced by Figure 2.6, a surface that has undergone EDM even at a relatively low power level will nevertheless show a wide variation in the depth and texture of the recast layer.

	$R_a$	$R_{max}$	$R_z$
Mean	3.7	26.4	21.9
Std. Deviation	0.3	3.4	2.0

Table 4.5: Statistical profile of unpolished specimen surfaces

Following the first set of 16 experiments, each of the specimens was cleaned thoroughly in distilled water and acetone, and then re-measured on the profilometer. Three surface traces were made for each of the sixteen samples, and the mean and standard deviation of  $R_a$ ,  $R_{max}$  and  $R_z$  were calculated for each specimen. The mean values for the three surface finish parameters are plotted for each specimen in Figure 4.9, and are tabulated along with the experimental levels for each sample in Table 4.6.

The figure shows the values for the  $R_a$  parameter on the left axis, and the scale for the  $R_{max}$  and  $R_z$  parameters on the right. The most striking aspect of this chart is the fact that all three parameters move as a group across all the specimens.  $R_{max}$  and  $R_z$  are generally an order of magnitude greater than  $R_a$ , but the trend for all three is the same. It is also clear that specimens 1 and 3 show a surface finish slightly better than the average, while the surface finish for specimens 12 and 16 is considerably worse than the other specimens.

Sample No.	Current Density (A/cm <sup>2</sup> )	On Time (msec)	Duty Factor (%)	Pulses/Group	R <sub>a</sub>	R <sub>max</sub>	R <sub>z</sub>
1	30	5	1	5	.33	2	1.5
2	50	5	1	5	.7	5	3.9
3	30	10	1	5	.33	1.9	1.2
4	50	10	1	5	.5	2.8	2.1
5	30	5	3	5	.73	3.9	2.9
6	50	5	3	5	.66	4	2.9
7	30	10	3	5	.6	4.1	3.3
8	50	10	3	5	.76	4.8	3.7
9	30	5	1	15	.96	6.3	4.9
10	50	5	1	15	.83	6	5
11	30	10	1	15	.73	6.1	4.4
12	50	10	1	15	2.4	17.7	15.6
13	30	5	3	15	.57	4.9	3.5
14	50	5	3	15	1.2	10.1	7.6
15	30	10	3	15	1.1	9.1	7.4
16	50	10	3	15	2.5	20.7	16.7

Table 4.6: Pulse and surface finish parameters for screening experiments

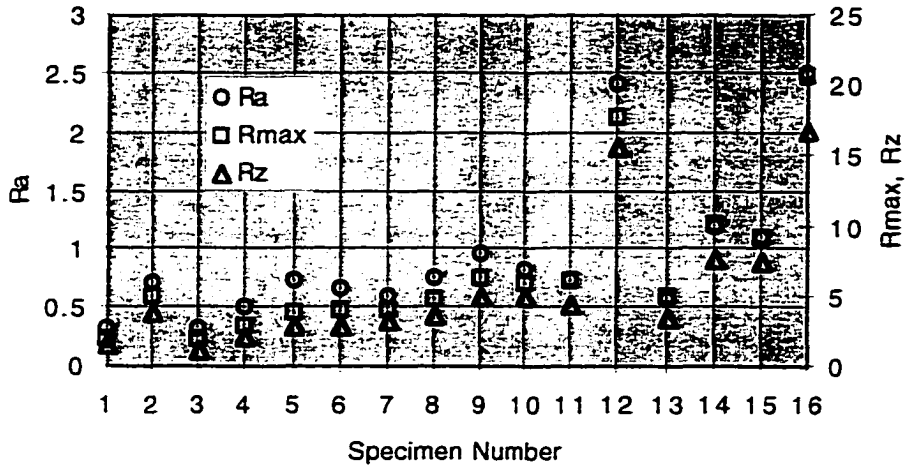


Figure 4.9: Mean values for  $R_a$ ,  $R_{max}$ ,  $R_z$  — screening experiments

Because the surface finish of these two specimens was so clearly inferior to that of the other fourteen, the calculations used to determine the pulse count were redone, and an error was discovered. In actuality, the two specimens should have each received thirty-three pulse groups of fifteen pulses, rather than the seven pulse groups they actually were given. Because the error was discovered after this set of experiments was completed, the data from these runs could not be duplicated, and so was disregarded in the analysis that follows.

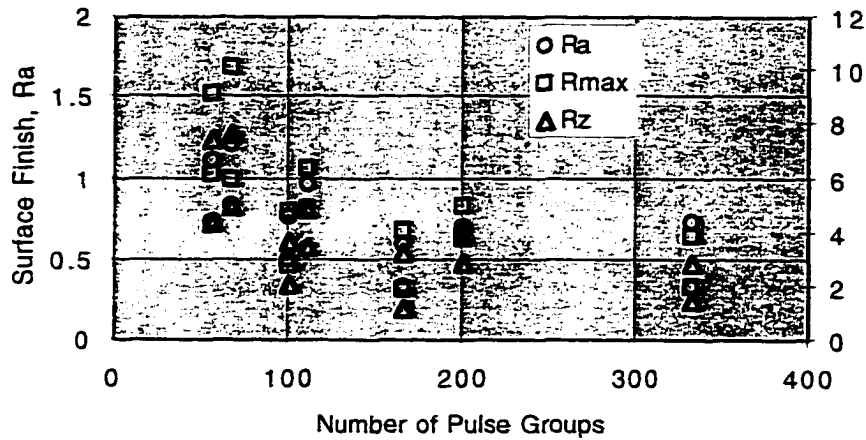


Figure 4.10:  $R_a$ ,  $R_{max}$ , and  $R_z$  as a function of number of pulse groups

In order to more clearly gauge the effect of the number of pulse groups on the surface finish, the data of Figure 4.9 were replotted as a function of the number of pulse groups, as shown in Figure 4.10. Graphing the data in this way seems to indicate a correlation between the number of pulse groups and the surface finish, at least for the two parameters,  $R_{max}$  and  $R_z$ , that measure the peak surface asperities. It would seem that these parameters decline quickly with increasing number of pulse groups, for the same total charge, while the averaged parameter,  $R_a$ , does not show as pronounced an effect.

In order to more accurately assess the effect of each pulse parameter on the surface finish, main effects plots based on the raw data were calculated for each of the three surface parameters using the Minitab statistical software

program. Figures 4.11 and 4.12, show the main effects of current density, pulse time, pulse duty factor, and number of pulses in a single group on  $R_a$  and  $R_{max}$ , respectively. Because the data for  $R_z$  closely follows  $R_{max}$ , it is not included here.

As expected from Figure 4.10, the main effects plots were similar for both surface parameters. They appear to show that increasing the current density, duty factor and number of pulses in a single group results in an inferior surface finish (i.e., an increase in  $R_a$  or  $R_{max}$ ) while increasing the pulse on-time leads to improved surface finish. However, Box [78] warns against placing too much weight on main effects plots when a strong interaction is suspected to exist among the factors under study.

For this reason, a series of interaction plots for the four factors being considered here were also created. The composite interaction plot is shown in Figure 4.13, for  $R_a$  only. (In the interests of brevity, and because all three of the surface parameters measured show similar behavior, only the  $R_a$  data will be presented from this point on.)

This chart shows that a significant amount of interaction probably exists between the pulse on-time and the current density level, to a lesser degree between pulse on-time and the duty factor, and to an even lesser

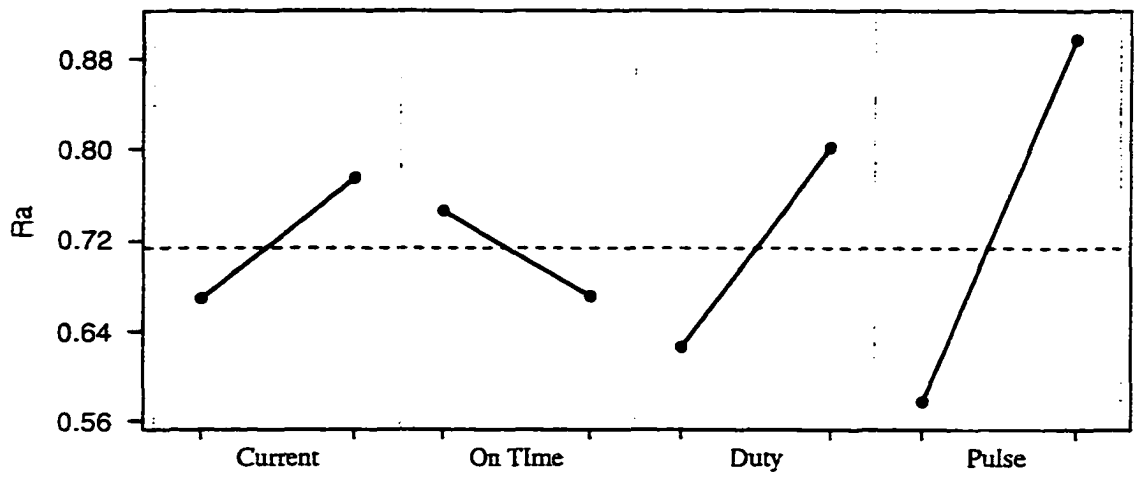


Figure 4.11: Main effects plot for  $R_a$

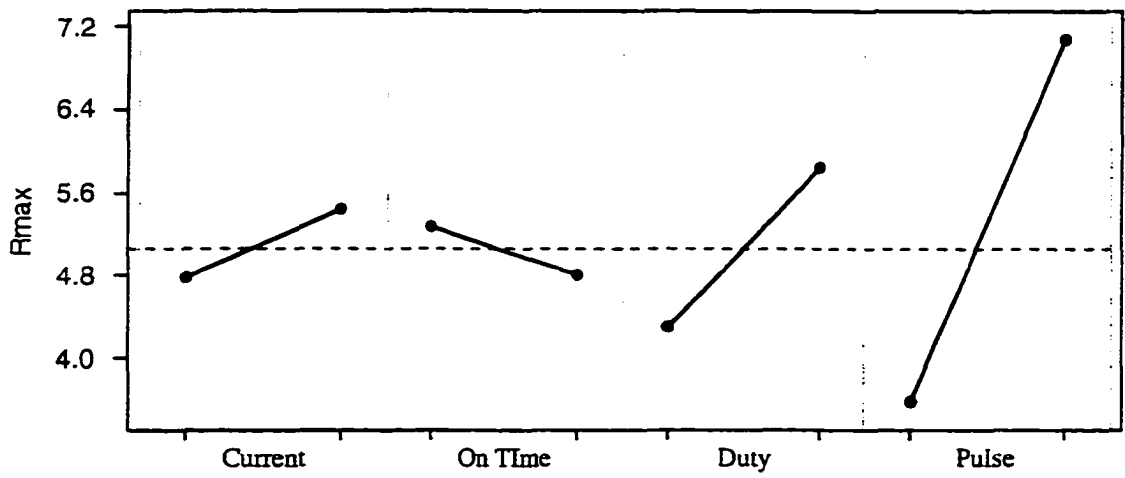


Figure 4.12: Main effects plot for  $R_{max}$

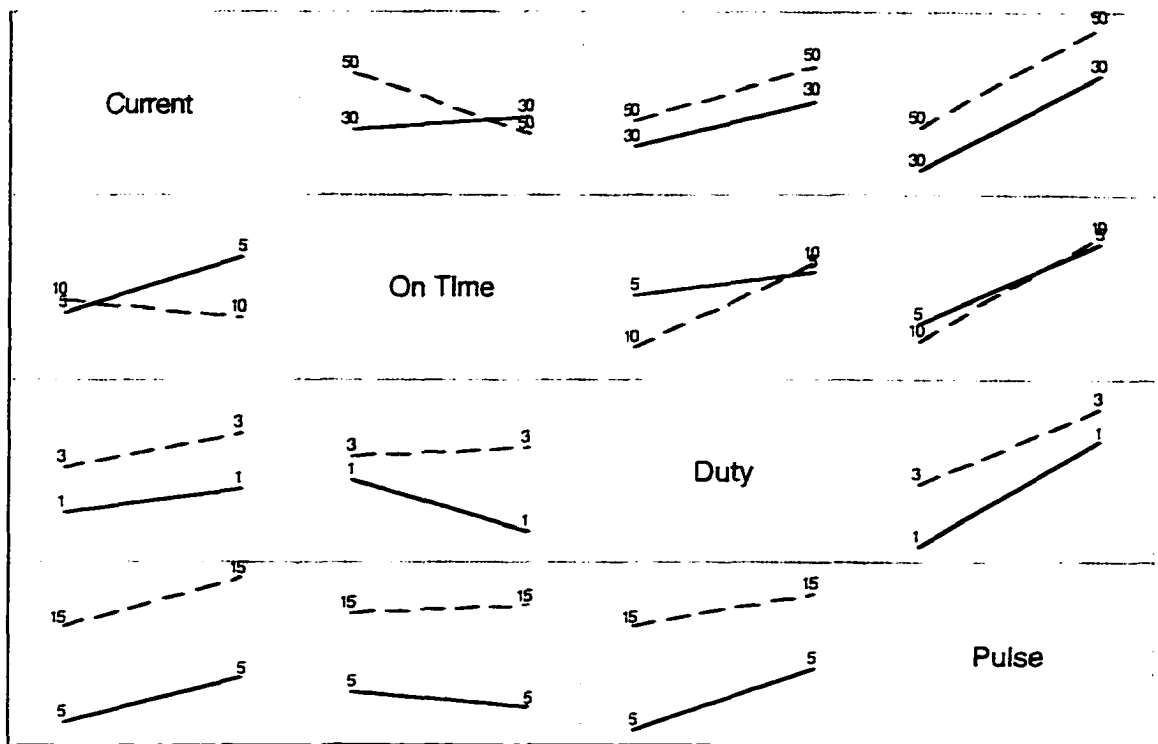


Figure 4.13: Composite interaction effects for  $R_a$

amount between pulse on-time and the number of pulses in a group. No significant amount of interaction is seen between any of the other factors, as evidenced by the fact that the lines connecting the means are roughly parallel for all other pairs of factors.

Figure 4.14 shows the interaction between pulse on-time and current level in more detail. From this graph it is clear that a higher current density results in a better surface finish, reflecting what was seen in the main effect chart for current density. However, it also seems clear that at the higher current density, the pulse on-time has a significant effect on the value of  $R_a$ , to judge from the chart.

At this point it's important to keep in mind that the actual difference in  $R_a$  shown on this chart is in reality not great at all. The total spread is only 0.2  $\mu\text{m}$ , which is well within the variation in  $R_a$  that can be detected by the profilometer. However, the same effect is noted in the interaction chart for pulse on-time and current density using  $R_{\text{max}}$  as a metric, as shown in Figure 4.15. Here the spread in the means at 30 A/cm<sup>2</sup> is only 1  $\mu\text{m}$ , while the spread at 50 A/cm<sup>2</sup> is 4  $\mu\text{m}$ . By way of comparison, the mean standard deviation for the original surface measurements from which this data is derived was 0.106 for  $R_a$  and 0.969 for  $R_{\text{max}}$ .

Based on the development of Datta and Landolt presented in Chapter Two, this coupling of on-time and current density is what one would expect

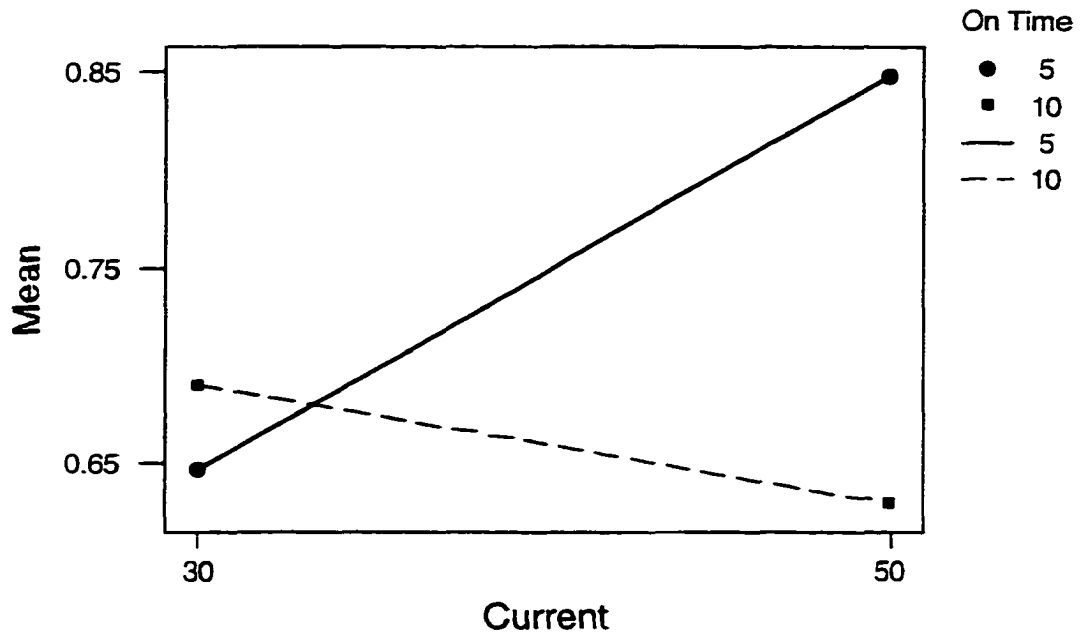


Figure 4.14: Interaction between pulse on-time and current density,  $R_a$

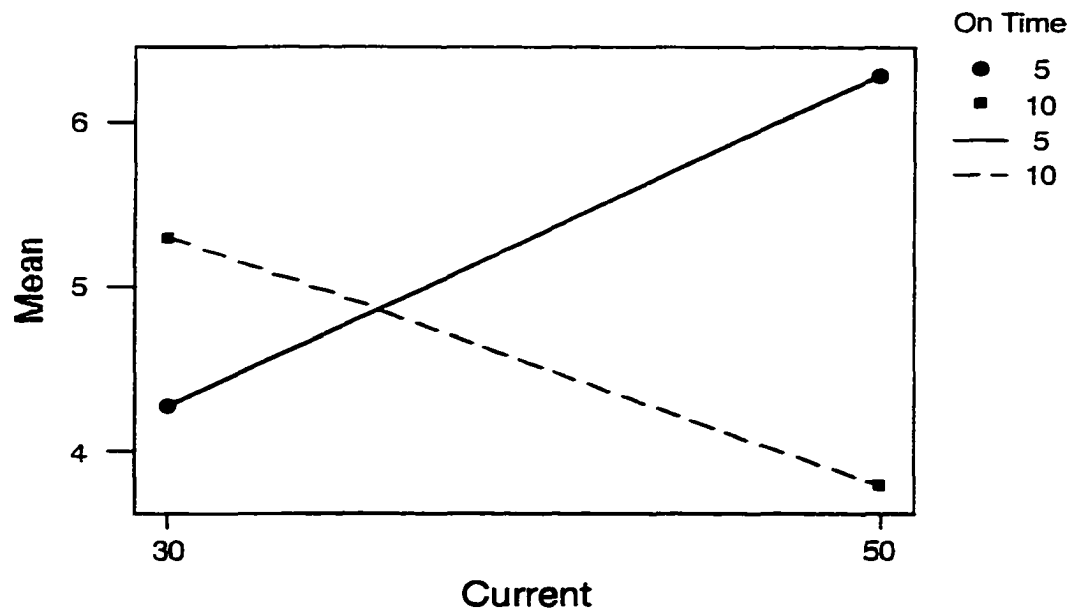


Figure 4.15: Interaction between on-time and current density,  $R_{max}$

to see. From equation 2.34 we know that for a given current density, the pulse on-time and duty factor will determine whether or not passivation, and hence polishing, will occur. In addition, one would also expect to see some interaction between the pulse time and duty factor, again due to the fact that a period of time is needed between each pulse to allow the heat and debris generated during the pulse to dissipate. While the actual extent of these interaction effects on the surface finish is difficult to determine, due to the limitations of the techniques available to measure the surface, the results of these experiments appear to bear out the theory.

In any event, the primary purpose of this first series of tests was to determine which set of parameters was most likely to affect the quality of the PECM'd surface, in order that a second experimental design, more closely focussed around the optimal point, could be investigated. The fact that both charts seem to show the same effect would indicate that some interaction effect exists.

Following Box, a series of three-dimensional, "first order" plots of  $R_a$  as a function of pulse time, current density, and duty factor were prepared. Two of these plots are shown in Figure 4.16, which shows the effect of pulse on-time and current density, and Figure 4.17, which does the same for duty factor and pulse on-time. Similar plots were created for the other possible combinations of factors. In all cases, the surfaces slope sharply downward in

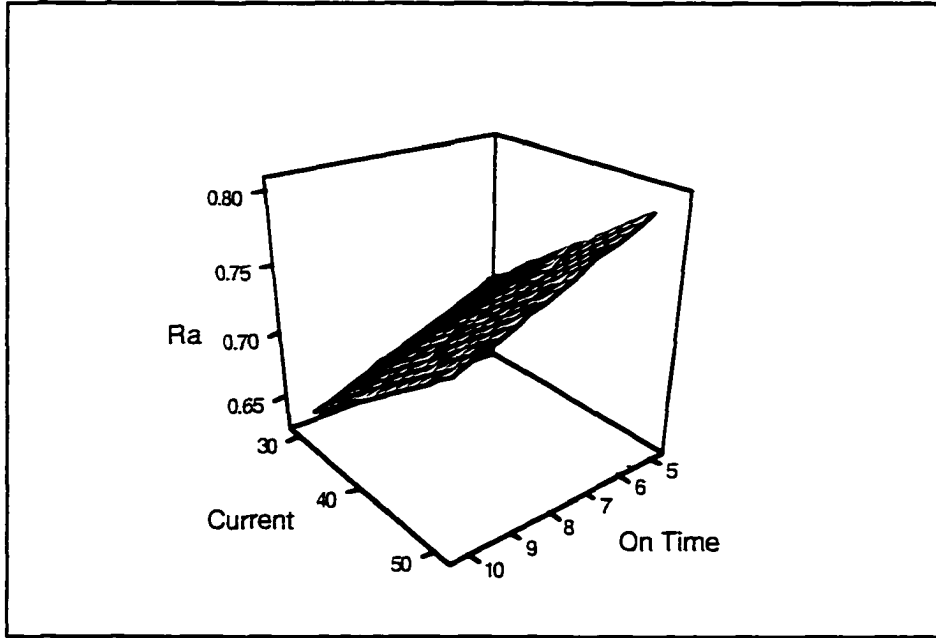


Figure 4.16: First order plot,  $R_a$  vs. current and pulse time

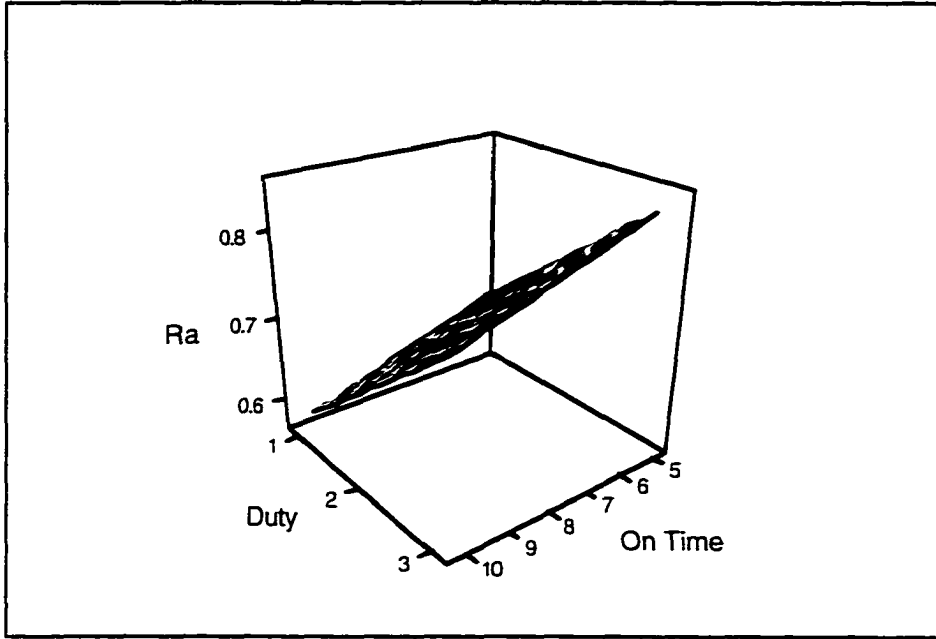


Figure 4.17: First order plot,  $R_a$  vs. duty factor and pulse time

the direction of lower current density, longer pulse times, and shorter duty cycles.

The results from this set of experiments led to two decisions. First, that a second set of sixteen experiments was probably unnecessary, since the only parameter that would change levels would be the initial gap dimension, which changes over the course of the erosion cycle in any event. In effect, a half factorial experiment in five variables became a full factorial experiment in four.

The second decision taken was to conduct a set of experiments much closer to the default setting used by the COTAC controller. Because it was unclear how strong the interaction effects among current density, pulse on-time, and pulse duty factor actually are, it was decided to hold the current density at a constant level while varying both on-time and duty factor in the immediate neighborhood of the default operating point.

#### **4.3.3 Design of the “second order” experiments**

The parameter levels used for this set of experiments is given in Table 4.7, with the default values from the COTAC controller shown in boldface type. These particular values were arrived at by creating a pattern in the two-dimensional on-time/duty factor parameter space, symmetric around the center point represented by the default value, as shown in Figure 4. 18.

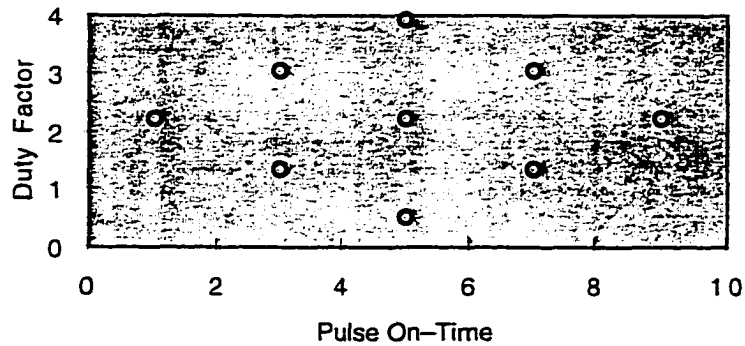


Figure 4.18: Experimental design for second experimental run

Based on the results of the first series of experiments, it was decided to hold current density constant at  $40 \text{ A/cm}^2$ , midway between the levels for this factor used earlier. The original idea was then to duplicate these tests at 60 and  $80 \text{ A/cm}^2$ , with the idea of generating a set of response surfaces in the parameter space. Due to time constraints, however, the tests at higher current density levels were not performed. However, the optimum settings found by these tests were used in combination with higher current densities to polish the final set of fatigue samples reported on in the next chapter.

For this series of tests the total charge passed to the workpiece was  $300 \text{ C/cm}^2$ . The total number of pulses employed was again varied, but for these experiments only pulse groups of five were used. The first set of experiments had shown that groups of fifteen pulses led to very heavy oxidation of the

surfaces, making accurate determination of surface finish and material removal difficult. In addition, the initial gap was set to 60  $\mu\text{m}$ , and the current density held at 60 A/cm<sup>2</sup>.

Specimen No.	Ton (msec)	Toff (msec)	Duty Factor (%)
F-1	5	255	2.2
F-2	1	46	2.2
F-3	3	219	1.35
F-4	5	990	0.5
F-5	7	512	1.35
F-6	3	98	3.05
F-7	5	123	3.9
F-8	7	223	3.05
F-9	9	400	2.2

Table 4.7: Parameter settings for second experimental run

The results of this set of experiments is shown in tabular form in Table 4.8. For these samples, not only were the three surface parameters  $R_a$ ,  $R_{max}$ , and  $R_z$  measured and recorded, but also the waviness parameter,  $W_v$ , was again used to check removal depth, and the sample weights were recorded before and after polishing. In order to ensure that resolution of the computer program used with the profilometer did not become an issue as it had in the earlier tests, in this experimental run the surface measurements were recorded in microinches, rather than in microns.

Sample No.	$R_a$ ( $\mu\text{in}$ )	$R_{\text{max}}$ ( $\mu\text{in}$ )	$R_z$ ( $\mu\text{in}$ )	$W_t$ ( $\mu\text{in}$ )	$\Delta$ mass (g)
F-1	19.3	135	109	84.4	0.64
F-2	38.3	319	211	24.9	0.53
F-3	13	100	68	95.1	1.03
F-4	23.6	167	120	92.4	1.42
F-5	24	172	127	55.5	—
F-6	27.3	230	142	98.6	1.5
F-7	13	94	73	74.8	1.21
F-8	31.6	230	171	70.2	1.04
F-9	23.6	154	128	74.8	1.13

Table 4.8: Results of the second experimental series

This data was used to generate a series of second order response surfaces for the three surface parameters as well as for the estimated mass removed. The response surfaces for  $R_a$  and  $W_t$  are shown in Figures 4.19 and 4.20. The response surfaces for  $R_{\text{max}}$  and  $R_z$  are very similar to that shown for  $R_a$ , so they are not included here.

The response surface for  $R_a$  shows what appears to be a minimax surface. Defining  $T_{\text{on}}$  as  $x_1$ , duty factor as  $x_2$ , and  $R_a$  as  $y$ , the equation that describes the surface is

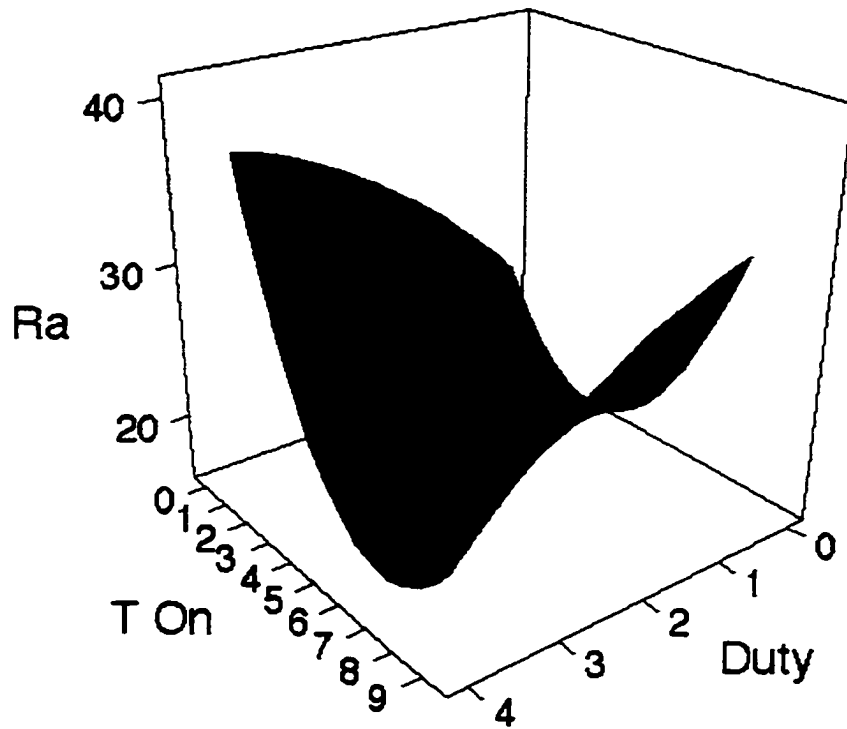


Figure 4.19: Response surface for  $R_a$

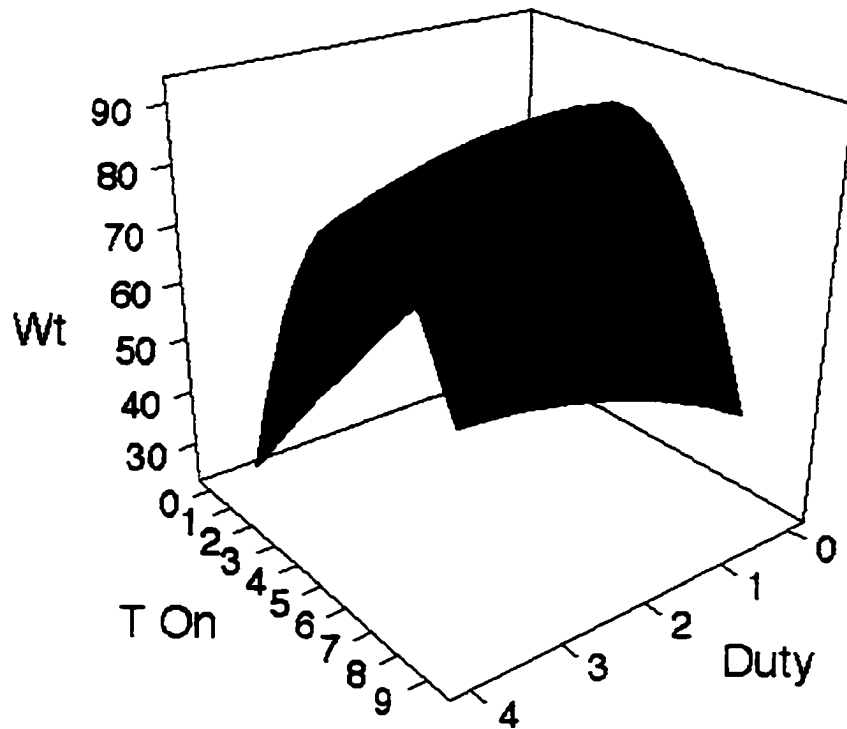


Figure 4.20: Response surface for  $W_t$

$$y = 26.8 - 5.061x_1 + 7.381x_2 + 0.647x_1^2 - 0.675x_2^2 - 0.882x_1x_2$$

which is in fact the equation of a minimax surface. The defining equation for the  $W_1$  response surface is given by:

$$y = 38.8 + 21.08x_1 - 4.332x_2 - 2.338x_1^2 - 1.226x_2^2 + 1.647x_1x_2$$

which again is the equation of a minimax surface.

Based on the limited amount of data points available, it is not possible to state categorically that the true response surfaces for the process are in fact minimax surfaces. As Box notes, true minimax surfaces are rare, though it is common for a surface to be approximated by one.

Much more common are stationary ridge systems, which may actually be the case here. Stationary ridge response surfaces are often evidence that the response being measured is actually a response to a fundamental variable that can only be measured as a combination of the parameters shown here. Box makes the point that very often we select quantities to measure not because they are fundamental to a phenomenon of interest, but rather because they are easily measured.

In this case, it is fairly clear that the process occurring in the gap during PECM is a complex phenomenon involving at a minimum local field strength, local pH, the amount of ionization and passivation at every location on the surface, and so on. However, the only means of controlling this complex process is through the parameters we have available to us on the control panel.

Nevertheless, if we assume that the response surfaces for this process are at least approximated by some form of a ridge, then that information by itself is quite valuable, because it implies that many combinations of the variables will result in acceptable finishes for the die or mold surface. This type of system behavior will allow the user to vary the current density as necessary to achieve better material removal rates, while still attaining an acceptable surface finish.

While the work performed here has not resulted in a truly optimal set of machining parameters for the process, it has at least pointed the way to further work along these lines. Further sets of experiments need to be performed to determine if the surfaces shown here will be duplicated at varying levels of current density, or if they will be shifted along either or both axis.

#### **4.3.4 Determination of the smoothing rate**

Having determined that a good surface does not depend on a unique set of parameter values, and having also determined that a charge density of  $300 \text{ C/cm}^2$  will result in the total removal of EDM damage from H-13 eroded to a level of  $4.0 R_a$ , the remaining step in the optimization process is to determine the rate at which the surface polishes, to ensure that both the damaged layer is removed and the resulting surface finish is acceptable.

During the course of these experiments, samples of widely varying initial surface conditions were polished with PECM. The  $R_a$  values of the specimens ranged from approximately 12 for those EDM'd at very high energy levels, to 0.2 for specimens receiving a lengthy, multi-energy level erosion cycle with EDM.

Figure 4. 21 shows the improvement in the  $R_a$  value with increasing charge. Each of the samples shown was polished using identical parameters: a pulse on-time of 5 ms, a peak current density of 40 A/cm<sup>2</sup>, and a duty factor of 2%. The only essential difference in the surfaces was the initial roughness.

This data essentially duplicates the findings of Rosset *et al.*, and also the data supplied by Shizuoka Seiki, the manufacturers of the COTAC machine. Two facts are worth noting here. First, the rate at which smoothing occurs drops off rapidly as the polishing process progresses. This is to be expected, given the nature of the PECM process.

At the onset of polishing, the initial gap is set by bringing the anode and cathode into contact, and then manually separating them the desired amount. For the experiments reported here, the initial gap width was 80  $\mu\text{m}$ . The profilometer traces taken on the unpolished 12  $\mu\text{m}$   $R_a$  surface show that the  $R_{\text{max}}$  value of this surface was 68.5  $\mu\text{m}$ . This means that the largest peak-to-valley distance on the surface was on the order of the initial dimension of the machining gap. Thus the peaks of the surface are not only exposed to the electrolyte to a greater degree than any other part of the surface, they are also

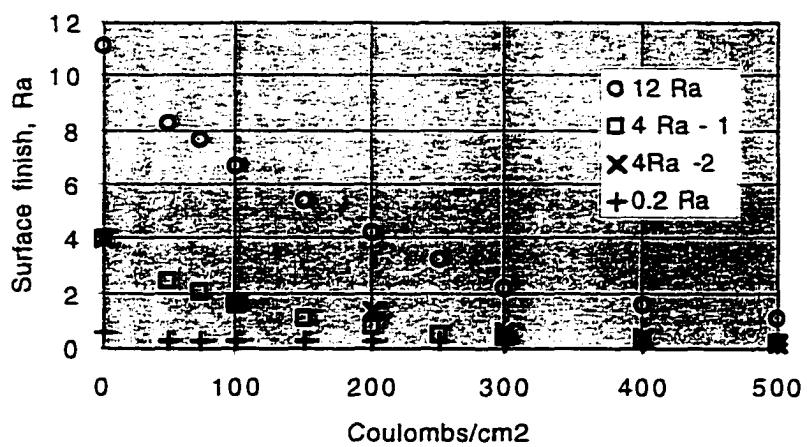


Figure 4.21: Smoothing rate – three initial surface roughness values

exposed to a much higher current density. This analysis neglects the fact that the local field will also be concentrated at the peaks, leading to even higher current densities at these locations.

The second significant fact is that after approximately  $300 \text{ C/cm}^2$  have passed across the gap, the surface of the specimens that was initially at a value of  $4.0 R_a$  is almost as smooth as the specimen whose initial surface roughness was only  $0.2 R_a$ . At this point, the surface that was originally at  $12.0 R_a$  has been smoothed out to approximately  $2.0 R_a$ .

A  $12 \mu\text{m } R_a$  EDM'd surface is actually quite rough. It is quite unlikely that any machinist or diemaker would consider such a surface acceptable for a die cavity or section leaving the EDM process. An  $R_a$  value of  $4 \mu\text{m}$  is much smoother, and quite typical of current die making practice [81]. Based on the data presented here, it seems likely that a charge density of  $300 \text{ C/cm}^2$  would be adequate both to remove the recast layer for a die section eroded to  $4.0 \mu\text{m } R_a$ , and also to bring it to an acceptable level of surface finish.

#### **4.4 Concluding remarks**

The experiments described in this chapter were designed and performed to develop the data necessary for integrating the PECM process into the die making cycle. In this research project, it is assumed that PECM will only be used in conjunction with a previous EDM operation in which

the die or mold surface is brought to within a few hundredths of a millimeter of the final surface.

The starting point for the PECM operation is thus the end product of the EDM cycle. It was assumed in this case that the die surface would be eroded by EDM to a condition of approximately  $4.0 R_a$ . From this condition, it was determined that a charge density of roughly  $300 \text{ C/cm}^2$  would completely remove the damaged layer created by the EDM process. Further, it was determined that the same level of charge density would polish an H-13 steel surface from a  $4.0 R_a$  condition to approximately a  $0.2 R_a$  state.

Finally, a response surface was developed for a moderate current density which shows that the process performs relatively well over a range of pulse times and duty factors. While a true optimum operating point for the process has not yet been determined, it is clear that the methods used here work well. Further experimentation should allow us to refine the model both for minimum operating time and a more optimal surface finish.

## CHAPTER 5

### VALIDATION OF PECM AS A DIE FINISHING METHOD

#### 5.1 Objectives

In order for the PECM process to have a real impact in the die and mold making industry, it must be able to provide the industry with a clear advantage over current practice. The die making industry in the United States is very conservative in general, and will only adopt a new technology when it is clear that it offers real gains in productivity.

The primary reason for developing this technology is to offer a reliable means of completely removing the EDM recast layer from the die surface. The problem with this idea is that it's not clear what advantages this entails. We can assume that it would lead to increased die life, but to what degree? Would it double or even triple die life? How would these gains in productivity be measured?

For the purposes of this dissertation, I have elected to use mechanical fatigue failure as the metric for gauging die life. With the exception of extrusion and drawing dies, practically every other type of die is exposed to

constant cyclic loading. Very often this loading is accompanied by thermal cycling, as is the case in injection molding, hot forging, and especially die casting. But in almost every case, dies are exposed to environments that are conducive to mechanical fatigue failure.

It is well established that machining methods and the resulting surface integrity play a very large role in determining the resistance of a machine component to mechanical fatigue. This is of course the primary reason why the EDM surface finish has to be removed before the dies and molds are put into service. If PECM has any future in the die making trade, then it obviously must be shown to be effective in improving the resistance of the die to both mechanical and thermal fatigue.

The purpose of this chapter is to present the results of a two-year program designed to measure and document the effect of various surface treatments on the mechanical fatigue life of H-13 steel. The treatments described here include high and low power EDM, residual stress relief following both EDM treatments, surface grinding, and finally, the effectiveness of PECM at removing the negative after-effects of EDM.

## **5.2 Experimental procedure**

### **5.2.1 Testing equipment**

The experiments described in this chapter were performed on a Krouse 5000 lbf. axial fatigue tester. The machine uses a variable cam and cantilever

beam to exert a purely axial force on the specimen. Due to the design, the Krouse is essentially a constant-displacement machine. When the sample begins to crack, the force will decrease to some extent. The machine can be set up to automatically shut down, however, if the displacement becomes excessive.

The particular cantilever beam used for these experiments was calibrated using a Sensotec 51/1073, 0–10,000 lbf. load cell. The calibration values agreed very closely with previous calibrations performed on this machine at Battelle Memorial Institute, further confirmation that the load values recorded in this experimental run were accurate.

The procedure for using the machine is as follows. The specimen is placed into the machine with the upper part of the specimen secured to the machine frame. The lower section of the specimen is connected through a coupling to the cantilever beam, the other end of which connects to the variable cam. With the cam set at zero eccentricity, the specimen is preloaded. A dial indicator placed on the beam measures the amount of load.

The variable cam is then adjusted to apply a previously determined cyclic load to the specimen, and locked into place. A tensile load cycle was used in these tests, with the load varying between the maximum load, which is indicated on the fatigue diagrams, and a minimum load equal to two-tenths of the maximum. The loads were adjusted by a dynamic factor to account for the the inertia of the coupling and beam.

The largest source of error in these experiments was no doubt due to the use of the dial indicator to measure the beam deflection. Each division on the indicator was equal to approximately 56.5 lbf. Using the rule of thumb that the maximum precision possible is half the smallest increment, the measurements recorded for these experiments were precise to within  $\pm 28.3$  lbf. For the worst case, when the load was approximately 1000 lbf., the error was  $\pm 3\%$ .

### **5.2.2 Selection of steel and heat treatment**

As mentioned previously, the steel used in all of these experiments, both for the PECM testing and for the mechanical fatigue tests, was Crucible NuDie<sup>®</sup> premium grade H-13 hot work die steel. This steel was developed in conjunction with the North American Die Casting Association, and is believed to be the best available steel for die casting applications.

The steel was heat treated by Certified Heat Treating of Dayton, Ohio. The steel was vacuum hardened, rapid quenched, and then double tempered at a minimum of 1000° F to a final Rockwell "C" hardness of 45.

A total of 200 fatigue specimens were cut from eight blocks of steel using the Sodick Wire EDM machine at The Ohio State University. The specimens were prepared from steel from two different melts. The first four blocks were prepared in 1995, and were used in the initial series of tests reported on below.

The second set of specimens was prepared in 1996–97, the only difference between the two sets being the shape of the fatigue specimen, which is described in the following section. In both cases, the remainder of the blocks was then machined into small samples, on which all of the PECM tests reported on in Chapter Four were performed. This was done deliberately so that the PECM data could be applied to these samples without question.

### 5.2.3 Initial fatigue specimen design

The design of the first fatigue specimens was intended to follow the guidelines given in ASTM specification E466–82, *Standard Practice for Conducting Constant Amplitude Axial Fatigue Tests of Metallic Materials*. In preparing the original samples, however, two crucial points of the standard were not followed.

First, and most importantly, the devices used for clamping the specimens were poorly designed. Rather than use one of the specimen designs shown in the section, “Fatigue Testing” of the ASM Metals Handbook[82] which result in non–stress–rising clamping arrangements, it was decided to hold the specimens with one–half inch pins inserted through holes cut in each end of the specimen. The design of the original specimen is shown in Figure 5.1.

Although this problem was not apparent at first, due to the fact that the specimens generally failed at the location of the second stress riser described

below, over time this design flaw proved to be a very costly error. This problem will be dealt with more fully in the following section on the second fatigue specimen design.

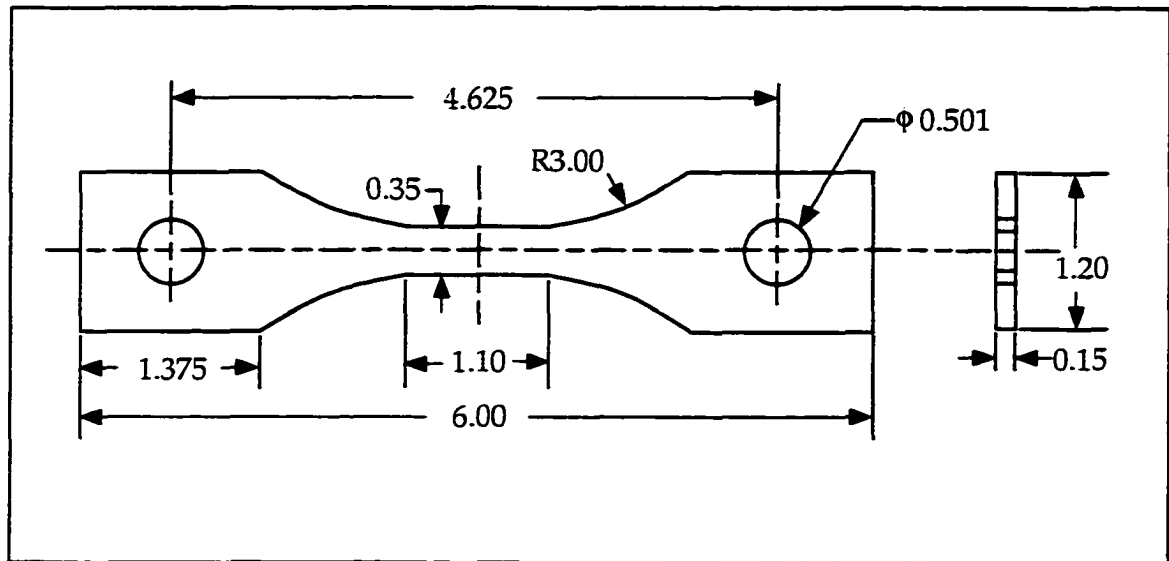


Figure 5.1: Design of the original fatigue specimen, from [83]

The second problem with this first design is less obvious, but was immediately a cause for concern. Close inspection of Figure 5.1 shows that at the point where the three inch radius blends with the specimen neck, a slight discontinuity exists. This is due to the manner in which the specimen was programmed to be cut on the wire EDM machine, and resulted in a point of non-tangency in the specimen profile.

The end result of this error was that almost all of the specimens from the entire first series of fatigue tests failed in exactly the same location,

namely the point of non-tangency. Because the loading of the fatigue tester was calculated based on the cross-sectional area of the neck, and assumed no stress concentration factors, the repeated failure of the specimens at the same location obviously indicated that a stress-riser was present. The question then became, to what extent was the true failure stress underestimated?

To determine the magnitude of the problem, a finite element program was run for this specimen design using the ANSYS FEM code. The specimen design itself is quite simple, and the loading was programmed to occur radially on the outside half of each hole, in order to accurately simulate the true loading condition.

The results are shown in Figure 5.2, and they clearly show a stress concentration at the non-tangent point. The stress concentration factor was determined from this analysis to be approximately 1.3 times the calculated stress applied to the neck of the specimen.

Because this problem was not uncovered until the original blocks were machined, the fatigue tests were conducted as planned. The results are discussed in Section 5.3.1, and formed part of the M.S. Thesis work of Kevin Chen.

#### **5.2.4 Second fatigue specimen design**

After the initial fatigue tests were performed using the first design, it was decided to machine a second set of specimens from a second billet of

Crucible H-13, in order to be able to gauge the effect of the stress riser on the first results. Accordingly, the steel was purchased, heat treated by Certified Heat Treating of Dayton again in accordance with NADCA specifications, and machined on the Sodick wire EDM machine.

The second set of specimens used the design shown in Figure 5.3. Great care was taken in the design of this specimen, so that no stress risers were machined into the profile. To confirm that this was actually the case, an analysis was performed using the FEM program, Abaqus. The results of this analysis are shown in Figure 5.4, and indicate that while the stress riser at the junction of the neck and the clamping area had been greatly reduced, the stress at the edge of the one-half inch hole was roughly equal to the stress at the neck.

At this point a decision was made to proceed with the experiments as planned, although the clamping design using the pin through hole arrangement was quite obviously not desirable. Due to the stringent time constraints on finishing this research, it was thought that redesigning and fabricating a new clamping device for the fatigue tester would lead to delays in finishing the research on time.

A second reason for not redesigning the clamping arrangement was the idea that because the specimens would be undergoing an EDM treatment at the neck area, the effect of EDM on the steel was quite likely to override the

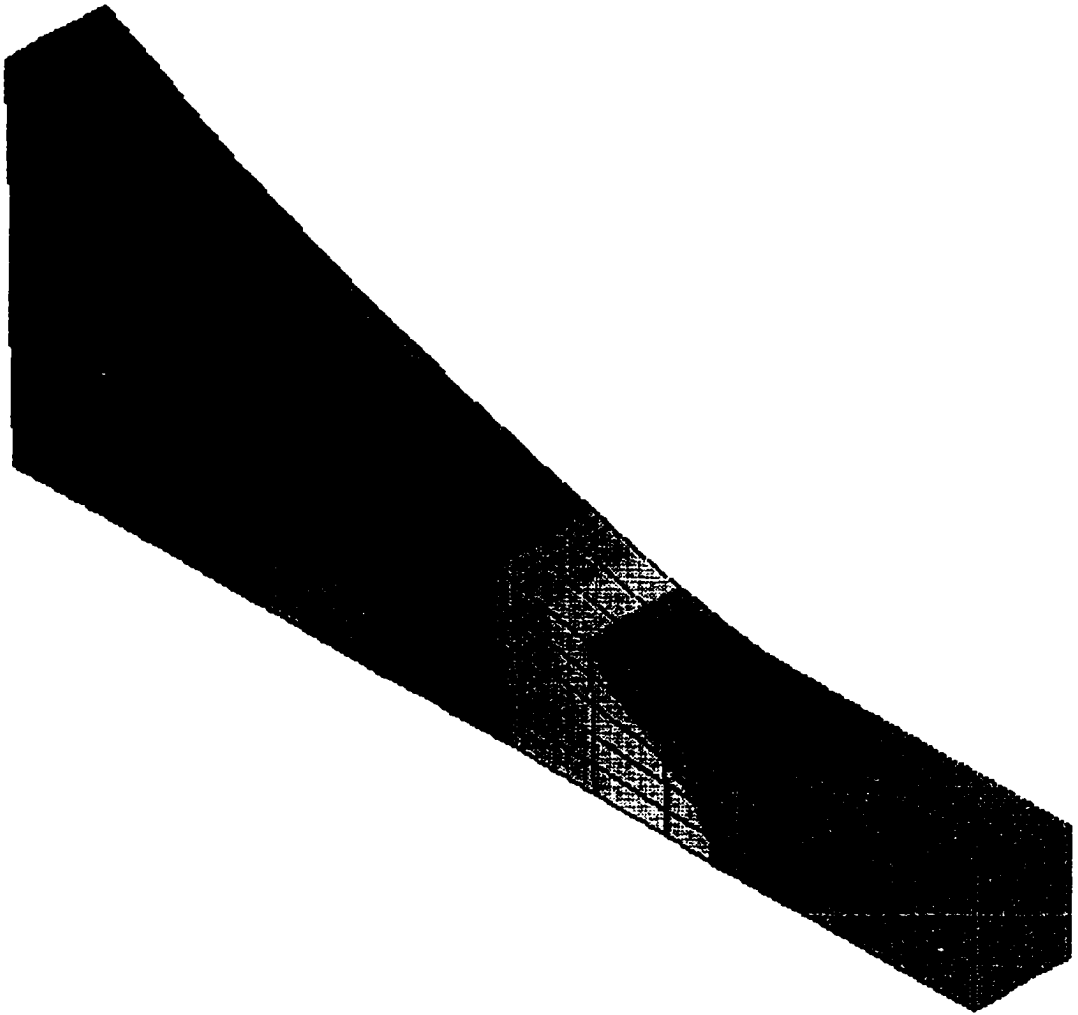


Figure 5.2: FEM analysis of the first specimen design

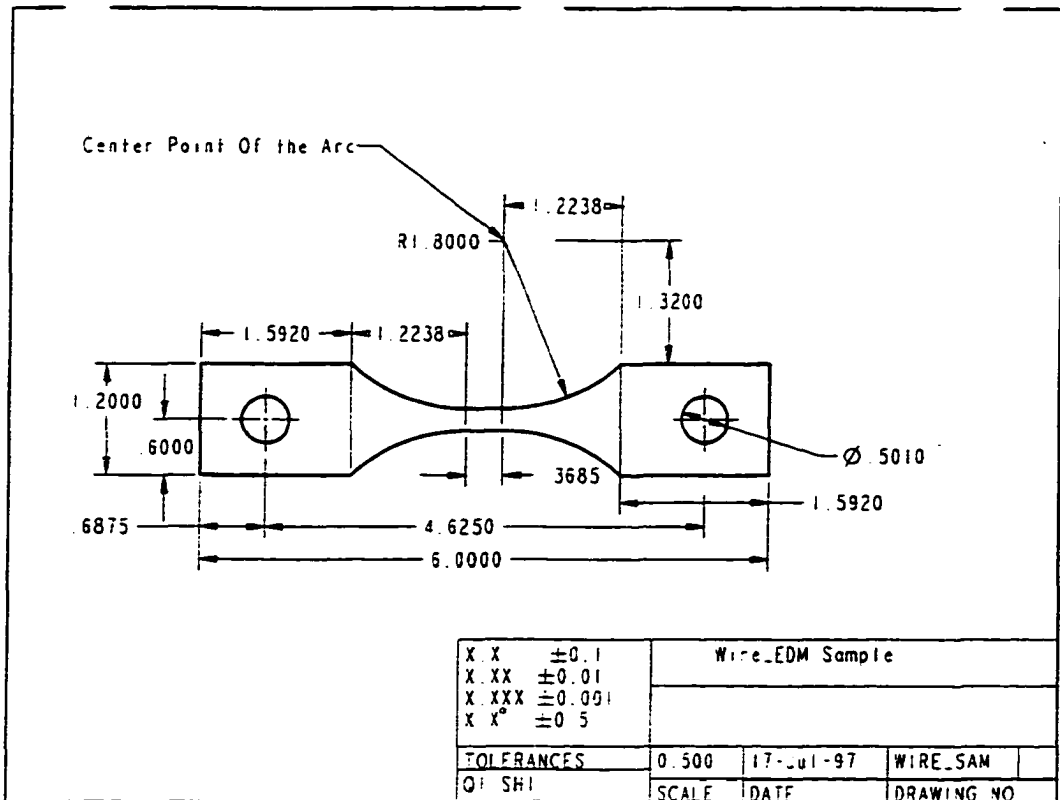


Figure 5.3: Design of the improved fatigue specimen

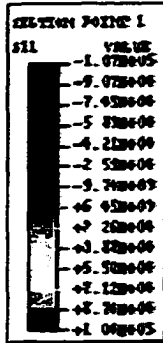


Figure 5.4: FEM analysis of second fatigue specimen

stress factor at the holes. This in fact turned out to be the case in most instances, but as we will see, not in all cases.

In retrospect it would have been better to completely redesign the specimen holder and specimens, and this project will be completed before any further fatigue tests are performed.

### **5.3 Results of the mechanical fatigue experiments**

#### **5.3.1 High-energy EDM treatment**

The results reported on here span a period of time of approximately two years and involving four students. The first results on specimens eroded by EDM using relatively high-energy pulses was performed by Kevin Chen as a part of his M.S. thesis [83]. This work was followed by Andrew Kaley, who used the same set of specimens to look at the effect of very low energy EDM on mechanical fatigue for his Senior Honors Thesis [84]. The set of tests reported on here using the second specimen design, and investigating the effects of both EDM and PECM on fatigue life were performed by Mr. Qi Shi, working with the author.

At the outset of this research project, the decision was made to try to determine a “worst case” machining method, against which every other method could be judged. Several of the references noted in Chapter Two were concerned with the effect of EDM on mechanical fatigue life of steel, but none of them were specifically concerned with tool steel, let alone H-13 steel.

Further investigation turned up almost no data on the fatigue life of H-13 after undergoing various surface treatments.

For this reason, this test series began by eroding a set of thirty-two specimens at very high EDM pulse energies. The electrodes used were graphite, the dielectric fluid was a hydrocarbon, and the pulse parameters used are shown in Table 5.1. It was felt that such a harsh machining regimen would result in a very rough surface finish and brief fatigue life, and these suppositions turned out to be correct.

Voltage (Volts)	Current (Amperes)	Pulse On/Off Time (Secs)	Average Gap ( $\mu\text{m}$ )
100	37	320/320	80

Table 5.1: EDM pulse parameters for initial experiments, from [83]

After the initial EDM treatment, sixteen of the samples were then polished with the COTAC PECM machine to an average surface finish of  $2.7 \mu\text{m} R_a$ . These samples received a total of  $1475 \text{ C/cm}^2$ , using the parameters shown in Table 5.2. Note that all of the pulses were single, 40 ms pulses, and that the current density was at a very high level,  $100 \text{ A/cm}^2$ . Chen measured the removed depth at approximately  $125 \mu\text{m}$ , which is extremely low, considering the amount of charge that was passed.

The results of the initial tests are shown in Figure 5.5, taken from the M.S. Thesis of Chen. These experiments showed that the fatigue limit of H-13

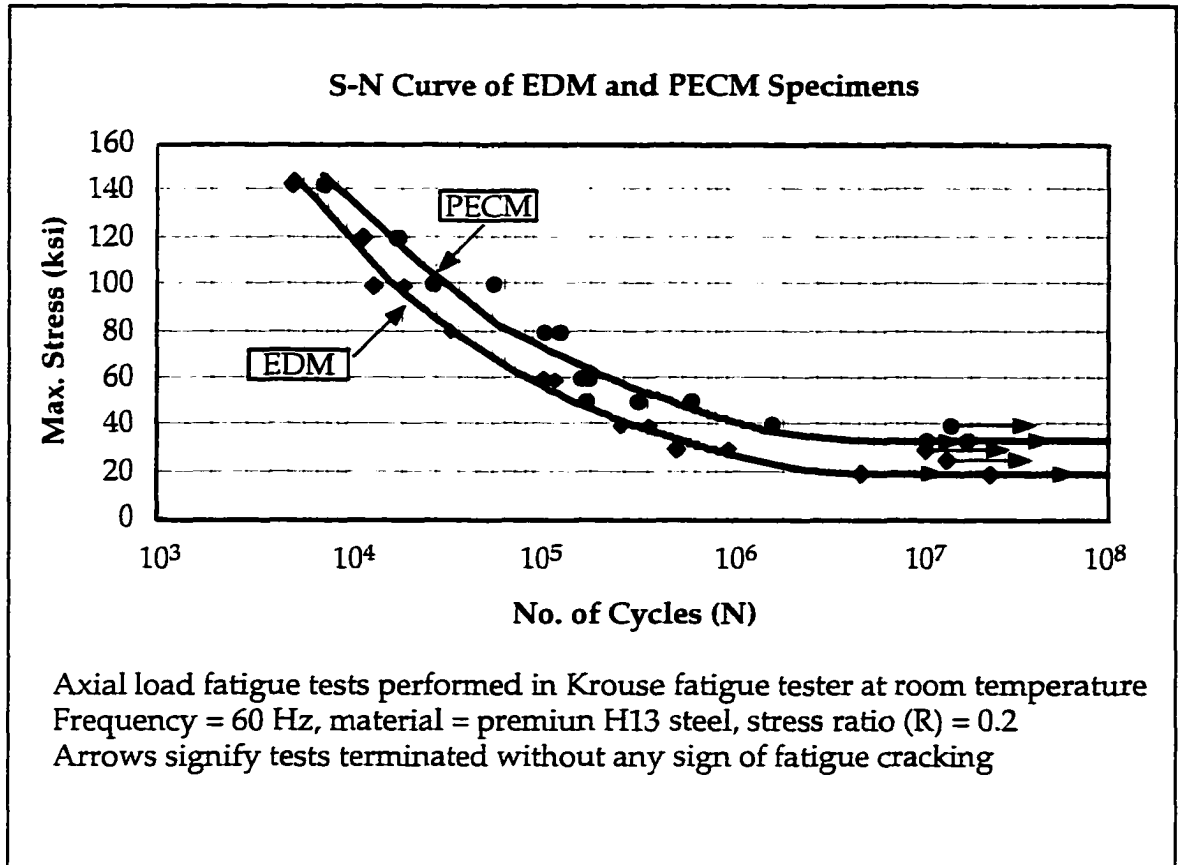


Figure 5.5: Results of initial fatigue tests, from [83]

with the harsh EDM surface treatment was in the region of 20–30,000 psi. Three samples did not fail at  $10^7$  cycles when stressed at 20,000psi, and one sample did not fail at 30,000 psi. The surface finish of these specimens was approximately  $10.5 \mu\text{m}$ ,  $R_a$ .

The results for the specimens receiving the PECM surface treatment were slightly better, showing an improvement in the fatigue limit to approximately 35–40,000 psi, with the polished specimens consistently showing superior fatigue life over the unpolished samples.

While this research showed some promise for PECM, several questions remained unanswered. The most important question was, did the improvement in fatigue life shown by the PECM samples result from the improved surface finish, or from the removal of at least part of the recast layer? Secondly, while the PECM samples showed that the process could result in increased fatigue life, the difference shown by these experiments was not significant enough to justify adding an entirely new process to the die making cycle.

Finally, how would these results compare to a less harsh EDM treatment? Even though these first tests were designed to establish a “worst case” scenario, they were criticized on the grounds that no one in industry would ever think of using such high power pulse levels on a die or mold component.

### 5.3.2 Multiple -level EDM treatment

Accordingly, a second set of experiments was conducted by Kaley for his Senior Honors Thesis. Where Chen's primary task was to produce a "worst case" analysis of an EDM surface in mechanical fatigue, Kaley's goal was to produce "best case" surfaces—one series using multiple-step EDM, the second using surface grinding. Kaley also looked at the effect of stress relieving the EDM'd specimens to try to gauge the effect of the residual stresses created by EDM on fatigue life.

Because of the cost and time involved in preparing the specimens, Kaley also used the original specimen design in his work. The EDM cycle used for the first group of specimens applied gradually decreasing energy cycles to the workpiece. The net effect was to gradually remove the recast layer, with each step of the cycle eroding the recast left by the previous cycle. At the end of the program, the energy level of each pulse was only 0.26 millijoules, and the roughness of the surface was approximately 0.2  $\mu\text{m}$ , Ra. The energy levels used to prepare the specimens are given in Table 5.2.

Twelve of these specimens were then tested to failure on the Krouse fatigue tester. The data for each specimen is presented in Table 5.3, and the data is shown on the S-N diagram of Figure 5.6. Although the data from Chen's earlier tests was not shown, the fatigue life of Kaley's samples

Level	Voltage (Volts)	Current (amp)	On Time (microseconds)	Off Time (microsecond s)	Discharge Energy (millijoules)
1	100	24.8	75	5.6	186.00
2	100	18.3	75	5.6	137.25
3	100	14.8	56	4.2	82.88
4	100	10.8	32	4.2	34.56
5	100	8.3	32	3.2	26.56
6	100	5.6	18	2.4	10.08
7	100	4.0	18	2.4	7.20
8	100	4.0	10	1.8	4.00
9	100	3.2	7.5	1.8	2.40
10	100	1.8	5.6	1.8	1.01
11	100	1.4	4.2	1.8	0.59
12	100	0.8	3.2	1.8	0.26

Table 5.2: EDM parameters for multiple energy level specimens, from [84]

Test	Specimen	Maximum	Fatigue Life	Remarks
Sequence	Number	Stress (ksi)	(# of cycles)	(Fail/NF)
1	B2	140	30,200	F
2	B7	100	87,000	F
3	B9	80	702,500	F
4	B4	120	54,300	F
5	B11	60	6,931,400	NF
6	B6	100	71,400	F
7	B8	80	87,600	F
8	B12	80	359,600	F
9	B5	120	40,000	F
10	B3	140	8,500	F
11	B13	140	14,600	F
12	B10	60	7,287,000	NF

Table 5.3: Fatigue test data, multiple energy level specimens, from [84]

**S-N Curve for Multi Step EDMed Specimens**

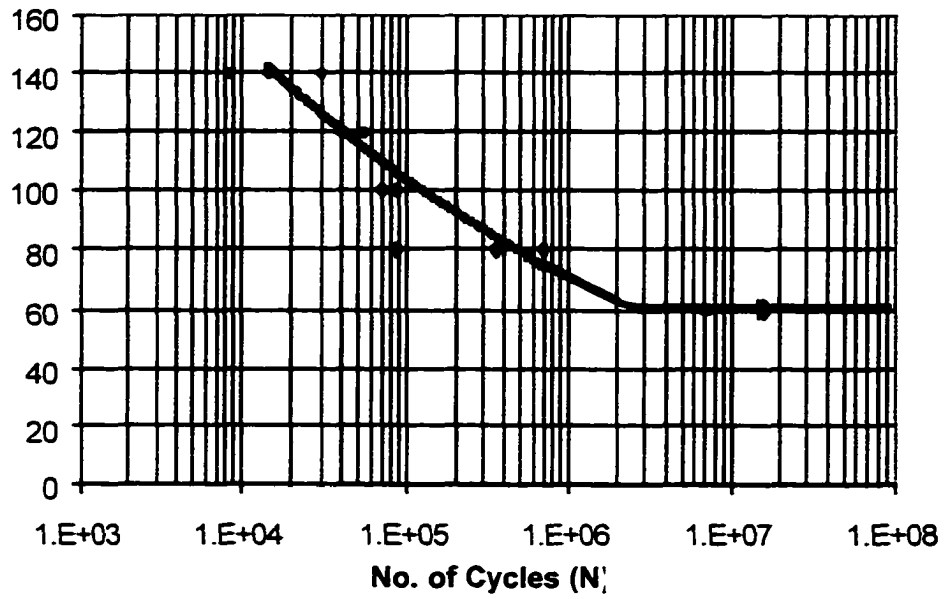


Figure 5.6: S-N Curve of multiple energy level EDMed specimens, from [84].

<b>Test Sequence</b>	<b>Specimen Number</b>	<b>Max Stress (ksi)</b>	<b>Fatigue Life (# of cycles)</b>	<b>(Fail/NF)</b>
1	B24	140	22,400	F
2	B18	80	223,400	F
3	B21	100	70,200	F
4	B22	120	46,600	F
5	B25	140	21,000	F
6	B20	100	60,100	F
7	B23	120	38,000	F
8	B19	80	280,600	F
9	B16	60	6,076,300	NF
10	B15	70	2,506,800	F
11	B14	70	283,000	F
12	B17	70	7,579,100	NF

Table 5.4: Fatigue test data, stress-relieved specimens, from [84]

exceeded the life of both the high-energy EDM samples and the PECM samples from Chen's work.

The second twelve specimens that were prepared with the multiple energy level EDM treatment were first stress-relieved before undergoing fatigue testing. The stress relief heat treatment, which consisted of one hour in an air-atmosphere furnace preheated to 625°F, was deliberately designed to be rather mild. The idea was that such a low temperature heat treatment would be sufficient to relieve any stresses that might be left over from the EDM treatment, but would not be severe enough to lead to oxidation, decarburization of the surface layer, or changes in the hardness of the material, which would confound the fatigue results.

Table 5.4 shows the results of the fatigue tests performed on these specimens. Note that although one of the stress-relieved specimens showed a fatigue limit of 70,000 psi, as compared to 60,000 psi for the non-stress relieved tests, the two sets of specimens showed essentially no difference in fatigue behavior.

This finding is in keeping with the results of Barash, Aleksandrov, and Lloyd and Warren, all of whom found that residual stresses created by the EDM process had very little overall effect on fatigue life. The reason is clear: since the residual stresses only affect a layer a few microns thick at the very surface, they can only assist in crack growth for a very limited number of cycles. Once the crack has penetrated the heat-affected layer, the residual

stresses will have no affect. Much more likely is that the microcracks that result from EDM will play a much greater role as fatigue crack initiation sites.

Nevertheless, these tests were criticized on the grounds that the stresses created by such a "benign" surface treatment would not be large in any case. For this reason, the investigation of the residual stresses was repeated in a later series of tests, which are discussed in the following section.

The final series of tests performed by Kaley was on a series of specimens that were surface ground after being cut from the original block by wire EDM. Each specimen had at least 0.04 mm (0.008 in) removed from each side, to ensure that no recast layer from the wire EDM process remained. For this treatment, the fatigue limit of the specimens was considerably higher, with one sample showing over five million cycles without failure.

However, at this point the stress concentration factor in the specimen due to the one-half inch hole in the clamping surface became a problem. Due to the severity of the EDM treatment, the samples from the earlier runs had failed reliably in the EDM'd region. Because of this, very few of the specimens had shown breakage at the hole.

Under the surface grinding treatment, all but two of the specimens broke at this location, with the fatigue crack initiating at the inner surface of the hole. Although this behavior clearly shows the negative effect of EDM on fatigue life, it essentially rendered the data worthless. All that can be said of these tests is that they show that the ground surface is at least as good as

shown here, but is probably much better. The failure of the specimens to perform adequately meant that these experiments would have to be repeated at a later date, with an improved specimen geometry.

Finally, all of the results from these tests are shown plotted together in Figure 5.7. All three curves show a fatigue life that exceeds the values found by Chen by a considerable amount. As a result of this work, the ability of the PECM process to improve the performance of dies subjected to cyclic mechanical loading was called into question.

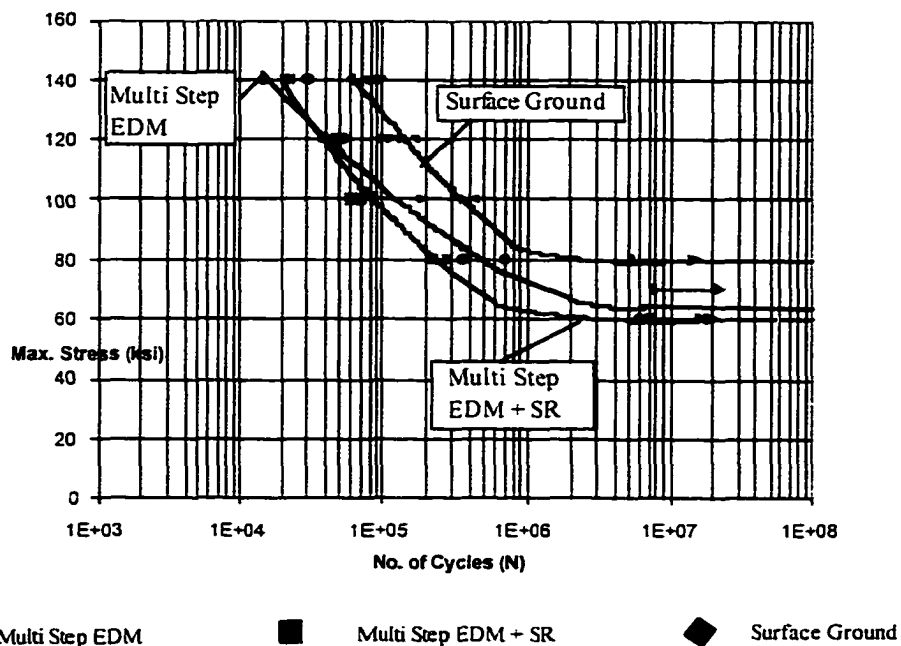


Figure 5.7: S-N curves for multiple-energy-level EDM and surface ground specimens. Axial loading,  $R = 0.2$ , room temperature in air. From [84].

### 5.3.3 PECM and surface grinding treatments

Based on the results of the work of Chen and Kaley, two decisions were made. First, it was decided to fabricate a new set of H-13 specimens with an improved geometry that would eliminate the stress riser at the junction of the neck and clamping area. As noted in section 5.2.3, every effort was made to ensure that the methods used to prepare these samples was identical to the methods used for the first set.

Secondly, at this point in the research the surface optimization experiments of Chapter Four were essentially complete. Thus it was decided to apply the optimized PECM process to an entire set of twenty-five specimens, to try to determine whether the process would actually add any real value to the die surface. If no dramatic improvement in the performance of the steel can be shown to result from the use of PECM, then the process is probably not viable as a die finishing method.

These experiments were carried out by Mr. Qi Shi and the author on samples machined according to the drawing of Figure 5.3. In an effort to gauge the effect of the stress riser at the neck, twenty-five of the specimens were eroded with high energy level EDM pulses, and fatigued to failure. The results showed very little difference in fatigue strength compared to the earlier data found by Chen for the original specimen design. Half of these specimens were again stress-relieved as before, at a temperature of 625°F for

one hour. As shown in Figure 5.8, no essential difference can be seen between the two treatments. The data for these tests are provided in Table 5.5.

A second set of twenty-five specimens was given a multiple-energy-level treatment identical to the erosion cycle used by Kaley on the original specimen design. Again, twelve of these specimens were fatigued to failure, and again, no difference was seen between the fatigue data of this test and the earlier test.

Following these tests, a total of 25 fatigue samples were eroded on the AGIE EDM machine at multiple power levels, to a final surface finish of 4.0  $\mu\text{m Ra}$ . The power levels used to prepare these samples are shown in Table 5.6. These samples were then polished in the COTAC PECM machine using the algorithm shown in Table 5.7. This polishing cycle was developed after the optimization tests described in Chapter Four.

Basically, the cycle applies a total charge density of 350 C/cm<sup>2</sup> to each surface of the fatigue specimen. Due to the structure of the COTAC control algorithm, described in Section 2.3.4, the total cycle is divided into groups of pulses, called "Conditions", in each of which the user can specify unique values for each of the primary parameters: peak current density, pulse on and off times, the number of pulses in a group, and the number of times the pulse group is repeated before the next condition is begun.

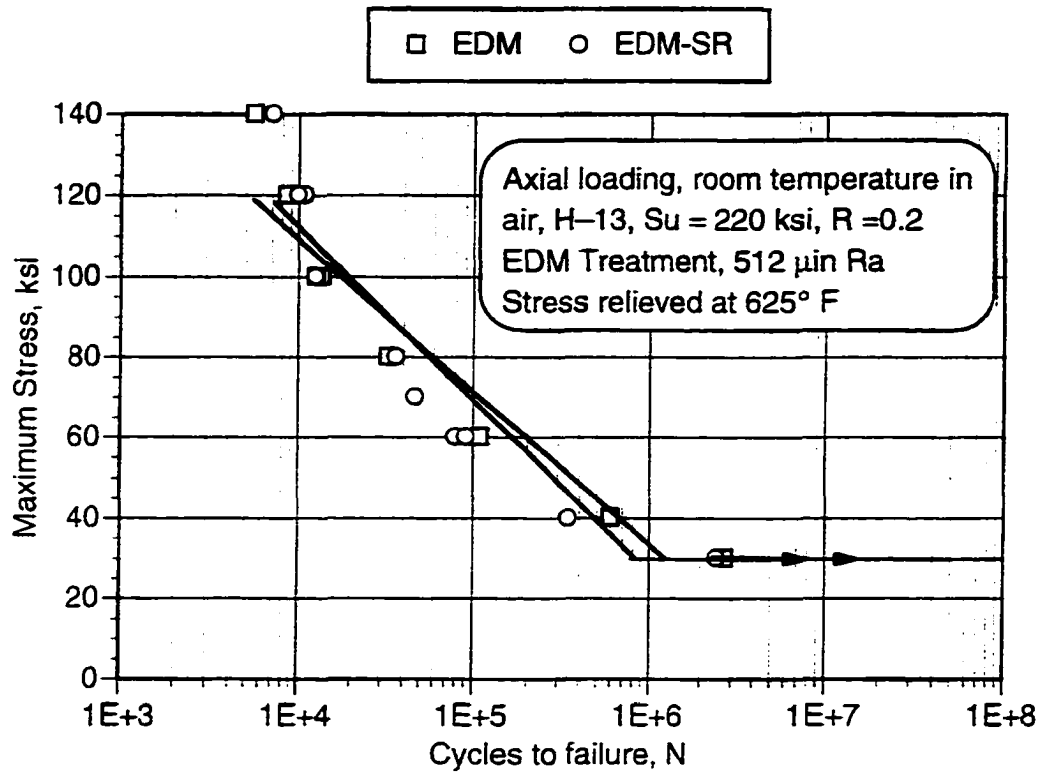


Figure 5.8: Comparison of stress relieved and non-stress-relieved specimens after high energy EDM treatment

<b>Stress Relieved</b>		<b>Non-Stress-Relieved</b>	
<b>Stress Level (ksi)</b>	<b>Cycles to Failure</b>	<b>Stress Level (ksi)</b>	<b>Cycles to Failure</b>
140	7000	140	7400
120	10800	140	5500
120	9900	120	8500
100	100000	100	13600
100	12500	100	12600
80	36200	80	32400
70	46600	80	32700
60	90900	60	109500
40	342500	40	597700
30	2478000	30	2760000

Table 5.5: Fatigue data, stress relieved and non-stress-relieved specimens after high energy EDM treatment

Level	Voltage (Volts)	Current (amp)	On Time (microseconds)	Off Time (microsecond s)	Discharge Energy (millijoules)
1	100	24.8	75	5.6	186.00
2	100	18.3	75	5.6	137.25
3	100	14.8	56	4.2	82.88
4	100	10.8	32	4.2	34.56
5	100	8.3	32	3.2	26.56
6	100	5.6	18	2.4	10.08
7	100	4.0	18	2.4	7.20
8	100	4.0	10	1.8	4.00

Table 5.6: EDM machining parameters for 4.0  $\mu\text{m}$   $R_a$  surface

Condition Number	Current Density (A/cm <sup>2</sup> )	Pulse On-time (ms)	Pulse Off-time (ms)	Pulses/ Group	Repetitions
0	80	20	—	1	25
1	80	5	123	5	50
2	80	20	—	1	50
3	80	5	123	5	25
4	100	20	—	1	25

Table 5.7: PECM machining parameters, 350 C/cm<sup>2</sup>

During the optimization experiments it became clear that the shorter (1–5ms) pulse times, used in groups of five, were the most effective method for removing material. However, the surface rather quickly became coated with a thick layer of metal salts, which led to a decrease in machining efficiency, and a roughening of the surface. It was learned that by inserting a series of single long (20 ms) pulses, repeated twenty–five to fifty times, would lead to a total disappearance of the salt film on the surface, and a much better surface finish and removal rate.

Accordingly, the polishing cycle shown in Table 5.7 was devised and used for the fatigue specimens. Condition 0 begins the cycle by cleaning the surface with a series of 25 20 ms single pulses, separated by flushing. The principal machining occurs during condition 1, in which groups of five 5 ms pulses occur. Between each group the tool retracts, and the workpiece is flushed with electrolyte. After a repetition of 50 pulse groups, the machine enters condition 2, during which fifty 20 ms pulses clean the surface completely. The controller cycles between these two conditions a user–specified number of times, then finishes with another group of short pulses (condition 3) and a final series of cleaning pulses (condition 4).

This cycle led to the best surface finish yet attained on this particular PECM machine. Surface finishes in the range of 0.2  $\mu\text{m}$  and less were achieved as a matter of routine. Figure 5.9 shows two fatigue specimens, one of which is heavily coated with the salt film after a series of fifty 5x 5ms

pulses. The specimen beside it to the left was subjected to the same cycle, followed by a set of fifty 20 ms single pulses. The difference in the two specimens is clear from the photograph. The surface shown on the polished specimen is typical of the surfaces of the final set of PECM'd fatigue specimens.

After polishing with this cycle, the specimens were fatigued to failure. The results of this series of tests are shown in Figure 5.10. The difference in the results compared to the initial specimens polished and tested by Chen was striking. The polished samples now showed a fatigue limit in the range between 100,000 psi and 120,000 psi, a three-fold improvement from the earlier tests. One polished sample remained unbroken after 10,000,000 cycles at 130,000 psi, by far the best performance of any specimen that had been previously subjected to EDM.

Only the surface ground specimens showed a better fatigue life than the PECM'd samples, as shown in Figure 5.11. One interesting issue that came to light when conducting these tests was the continuing failure of the samples at the clamping hole. After careful examination of the interior surface of the hole, it was determined that the very thin recast layer left from the wire EDM operation was responsible for this failure. After the holes were manually honed to remove this layer, the problem of breakage at the hole disappeared. This incident shows what a deleterious effect even a small amount of EDM recast can have on a machine part subjected to cyclic loading.

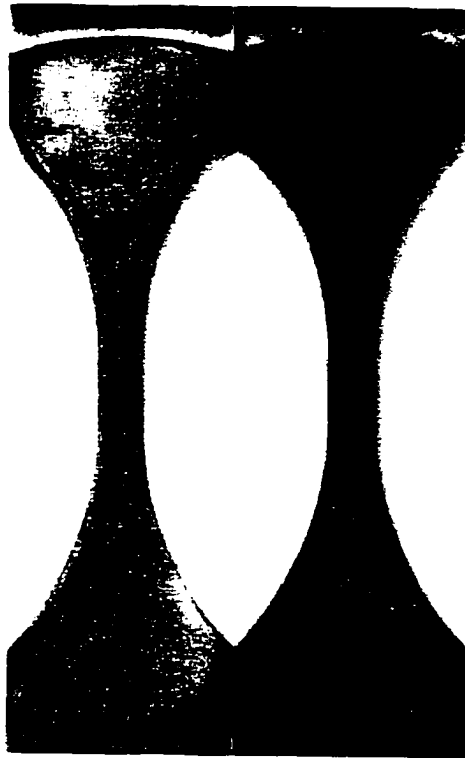


Figure 5.9: Two fatigue specimens showing cleaning effect of long pulses

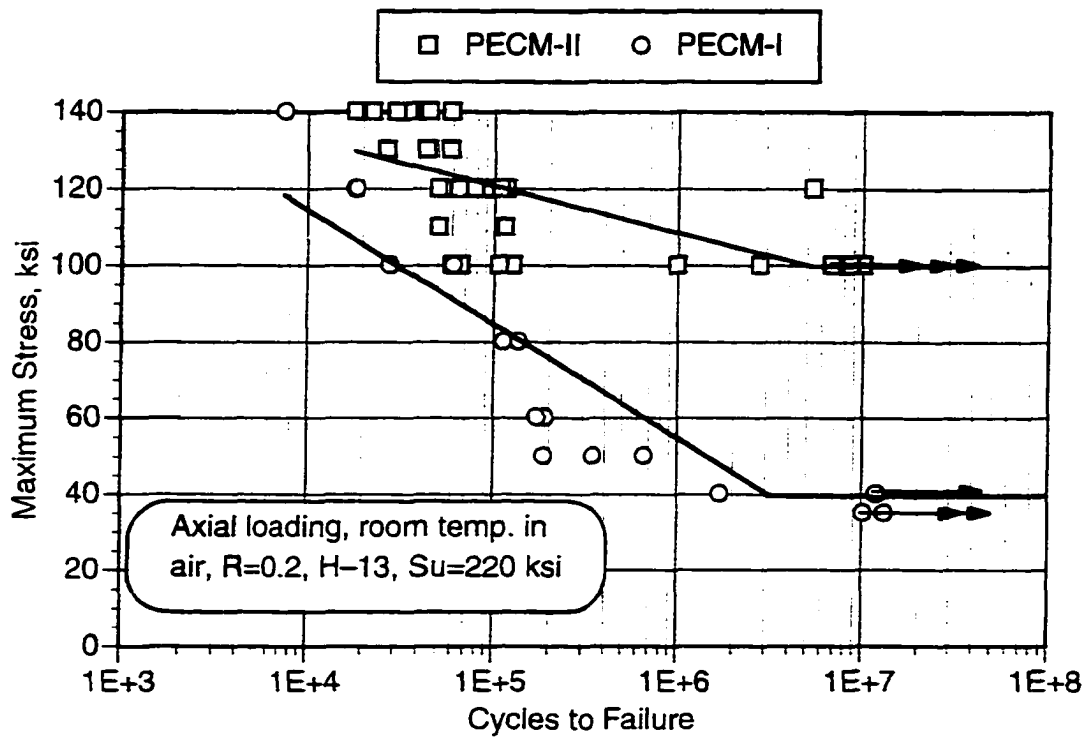


Figure 5.10: S-N diagrams of specimens polished using non-optimal (PECM-I) and optimal (PECM-II) machining parameters

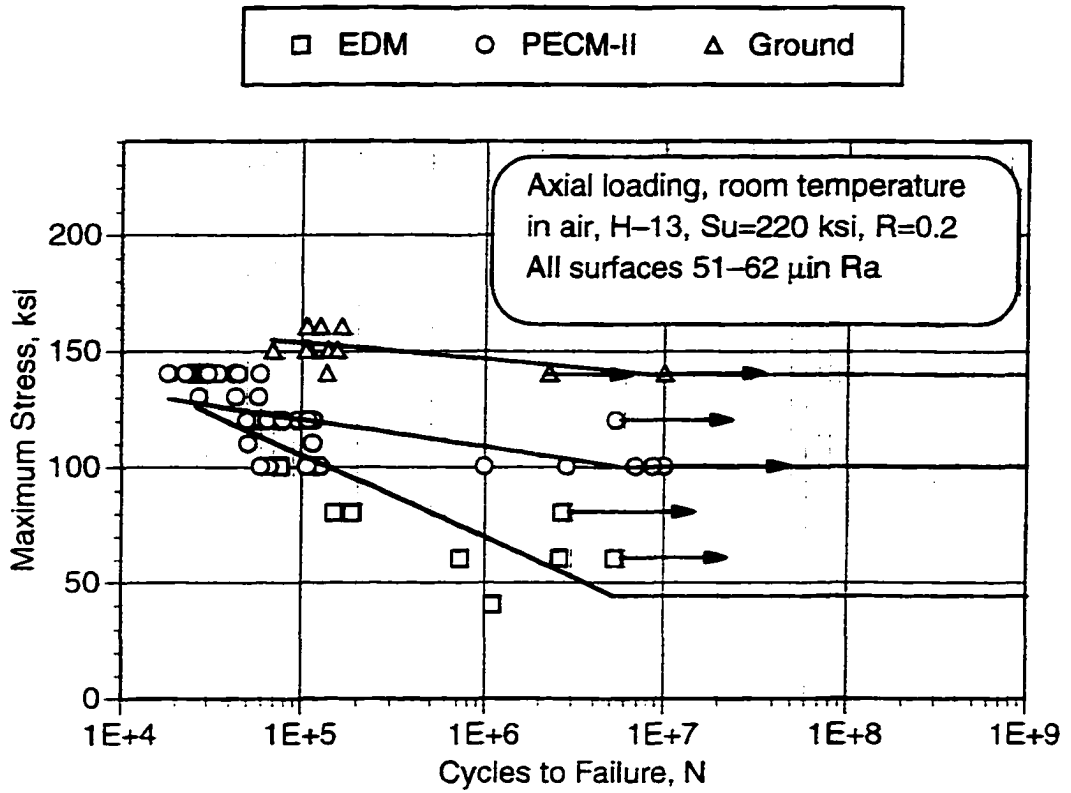


Figure 5.11: S-N diagrams of EDM'd, PECM'd and surface ground specimens

Finally, the question remains, why do the samples subjected to PECM fail before the surface ground specimens? Careful examination of several PECM fatigue specimens showed that quite often, the initiation site for the crack was either at the corner of the specimen, or at a pit on the surface. Figure 5.12 shows a fatigue crack that started at the corner of the neck cross section, while in Figure 5.13 the crack obviously began at the midpoint of the longer side of the cross section.

At other times, no obvious crack initiator could be seen with the naked eye. This led to a series of microphotographs of the PECM'd surfaces with both optical and scanning electron microscopes. Figures 5.14, 5.15, and 5.16 show three different views of the same PECM'd surface. This surface was polished to approximately a  $0.2 \mu\text{m } R_a$  finish.

In Figure 5.14, the surface appears rather like a heavily eroded floodplain. It is similar to an EDM surface in that no pattern or lay to the surface is discernable, but there is also no trace of any EDM recast layer to be seen.

In Figure 5.15, the magnification is five times higher. At this magnification level, it appears that some preferential erosion has occurred at the grain boundaries. Further, the surface now appears to have an etched appearance, with martensitic formations easily visible.



Figure 5.12: Fractured surface showing crack initiation at corner



Figure 5.13: Fractured surface showing crack initiation at specimen surface

Finally, in Figure 5.16, although the image is rather fuzzy, we can see that the grain boundaries are indeed more eroded than the grains themselves. Although it is not visible in this photograph, it is quite possible that the metal salt and oxides that occur during the polishing cycle have worked themselves down into the crevices between the grain boundaries during the repeated mechanical cycling, and can lead to crack initiation and growth. In any case, it would appear that the differential dissolution at the grain boundaries provides an ideal site for crack initiation.

It seems likely, therefore, that even though the PECM process is capable of removing all of the EDM recast layer, and although it can create a theoretically stress free surface, the issue of differential erosion at the grain boundaries might still lead to mechanical fatigue performance inferior to ground or hand polished surfaces. However, on the basis of the limited amount of data presented here, it is no doubt premature to write off the PECM process for that reason. It clearly shows promise as a die finishing process, at least in terms of mechanical fatigue behavior.

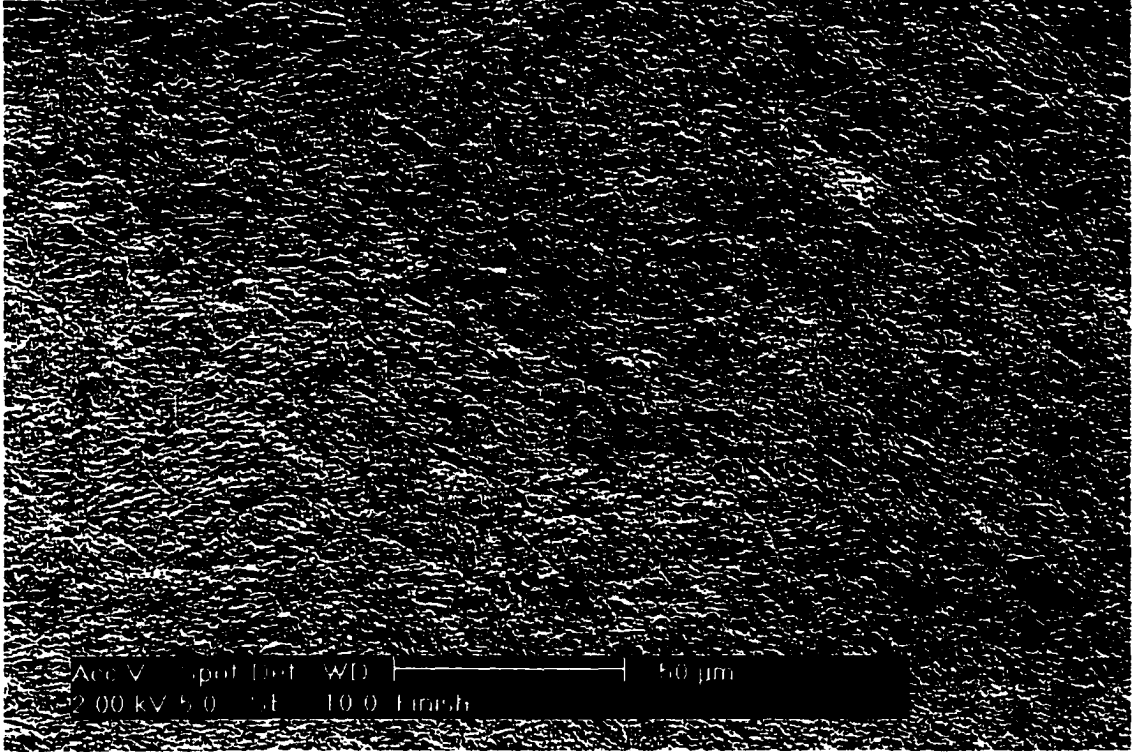


Figure 5.14: H-13 polished by PECM to 0.2  $\mu\text{m}$   $R_a$  finish

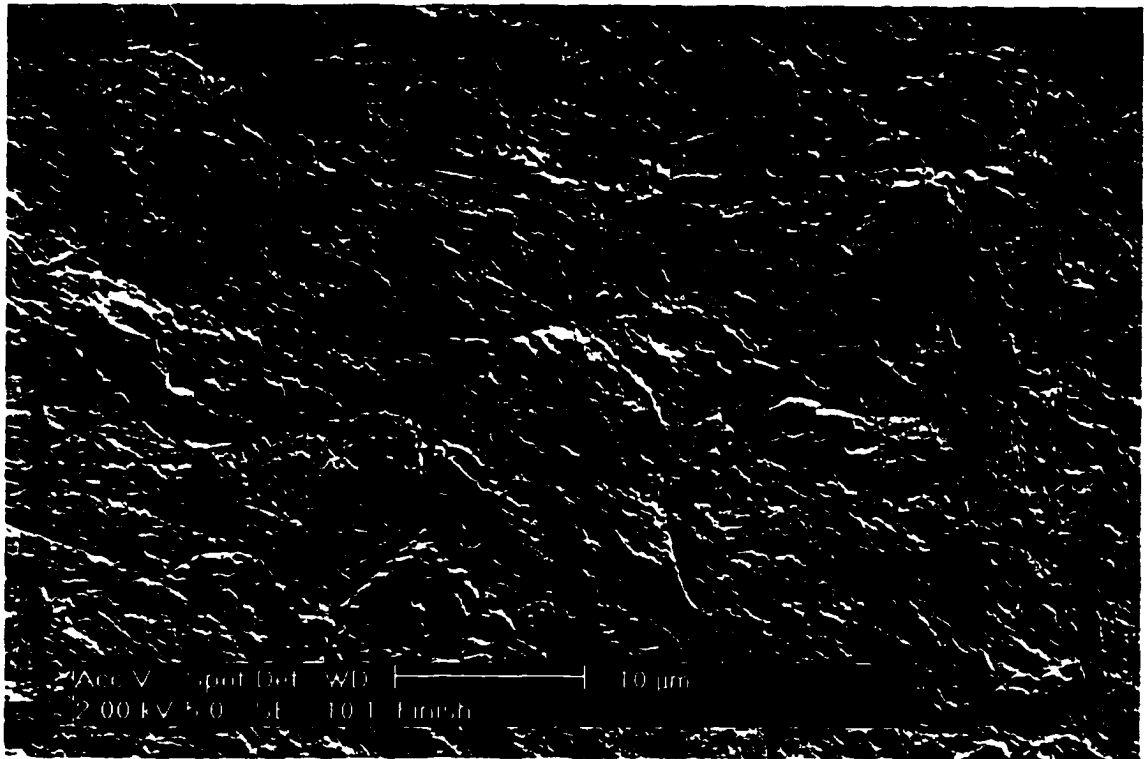


Figure 5.15: View of the H-13 surface showing grain boundary erosion

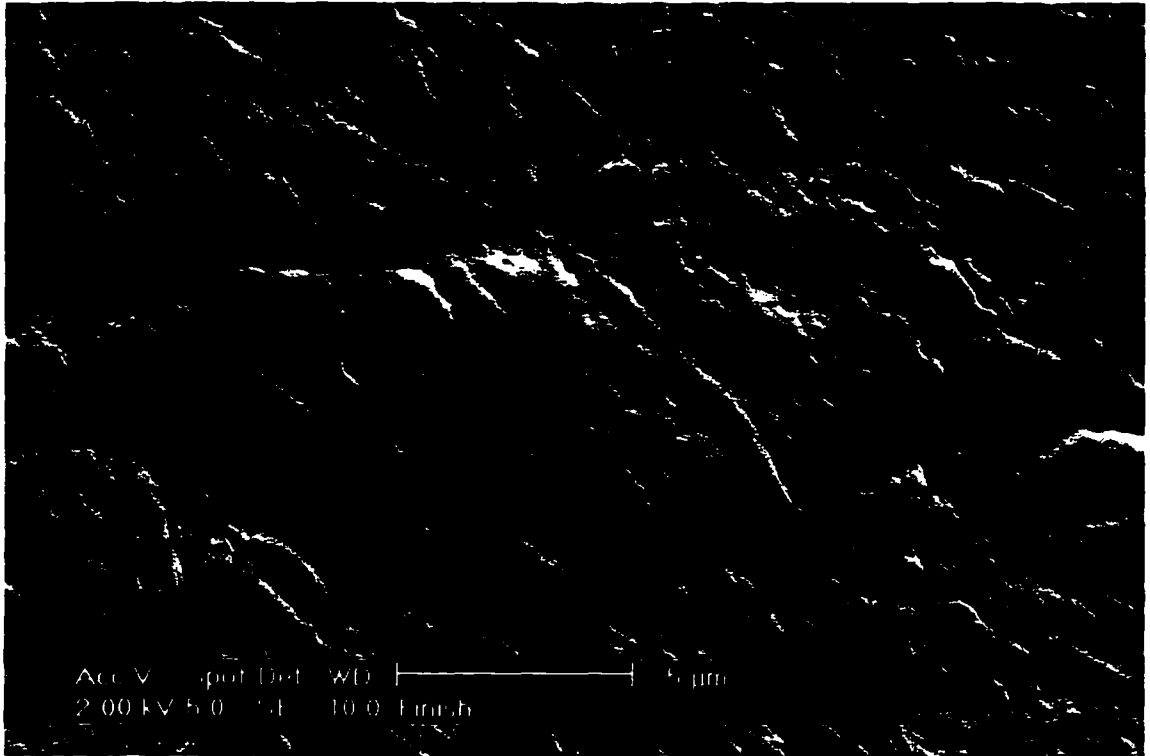


Figure 5.16: Close-up view of grain boundary erosion

## CHAPTER 6

### CONCLUSIONS AND FUTURE WORK

#### 6.1 Conclusions

From the work reported on here, several conclusions regarding the appropriateness of pulsed electrochemical machining as a die finishing process can be drawn.

First, an optimization model for the entire die and mold making process was developed, which takes the total time for each individual machining process as the objective function. Those aspects of the process that directly impact the quality of the die or mold component are then treated as constraints in the optimization.

Secondly, this model was applied to the PECM process to determine its potential as a die finishing method. Because the objective function for the process is the total time needed to bring the die or mold to the desired state, the material removal rate, embodied in the Faraday Law, was investigated to

determine what effect, if any, the processing parameters had on the removal rate.

The conclusion was that the removal rate was affected only slightly by variations in the parameters. The effective valence of the H-13 steel was found to vary between approximately 7 at a current density of 60 A/cm<sup>2</sup> and 5 at 100 A/cm<sup>2</sup>. However, there are indications that groups of short pulses are more effective at removing metal than single long pulses. This is an area that requires further and more systematic research.

The primary constraint on the finishing process is the roughness of the finished surface. The surface roughness is known to be affected by peak current density, pulse on-time, and pulse duty factor, as well as by the number of pulses occurring in a group. A response surface methodology was applied to this problem, and response surfaces were developed for surface roughness as a function of these variables.

Time constraints permitted only the development of response surfaces at a single current density. Further research is needed to develop more precise response surfaces for several current densities within the operating range of the process. From these surfaces, a better theoretical basis for understanding the process should emerge.

Following the development and application of the optimization model, parameter levels derived from the model were applied to a series of mechanical fatigue specimens. Using these levels, the specimens were

polished to approximately a  $0.5 \mu\text{m } R_a$  surface finish, and were then cycled to failure on a Krouse axial fatigue tester.

The results of the fatigue tests were quite impressive. The samples that received the PECM treatment showed significant improvement in fatigue life over specimens that were given EDM treatment at several different levels. The PECM samples were exceeded in fatigue life only by specimens prepared by abrasive surface grinding. This work clearly shows that PECM can have a strong positive effect on fatigue life, and hence, on die and mold life.

## **6.2 Future Work**

This dissertation was intended to provide the background for further work in the general area of die finishing and especially pulsed electrochemical machining. In that respect, it has been very successful, because a wealth of new ideas have come out of this research. Several of these ideas are listed below.

First, further work is clearly needed to refine the model presented here. As noted above, more work needs to be done to develop more precise and more extensive response surfaces for the process. A major stumbling block in the research reported on here was a lack of funding to acquire an adequate data acquisition system. For all of the important system parameters, it was necessary to rely solely on the control screen of the COTAC-51; it was not possible to independently verify these levels, whether pulse time or peak

current density. Thus the first order of business is to obtain and implement a state-of-the-art data acquisition system, and use it to obtain a more accurate picture of what is actually occurring in the machining gap during PECM.

Secondly, the work presented here deals only with one specific steel, premium grade H-13. It is known that the alloying elements, particularly chromium, play a strong role in the electrolytic dissolution of the metal. It is also reported anecdotally that certain tool steels, in particular AISI P-20, react poorly to the PECM process, but the reasons are not known.

Clearly, a fruitful avenue for research is to pursue the use of PECM with other tool steels. The end result of this work would be a model of the process that would be able to predict the results of the process based on the principal alloying elements of the steel. This line of research would obviously require a stronger emphasis on the metallurgy of the tool steels than was present here.

Another necessary step in proving this process to be valuable to industry is determining if and to what degree the thermal fatigue performance of the tool steels, in particular premium grade H-13, would be enhanced by the use of PECM. The argument is often made that better performance in mechanical fatigue indicates better performance in thermal fatigue, especially in regard to the role of surface treatments: certainly fewer microcracks and other flaws should result in the delayed onset of both failure modes, at least.

The greatly improved mechanical fatigue life of the specimens reported on here would lead one to the conclusion that the thermal fatigue life would also show significant improvement. In fact, one thermal fatigue study was performed on a PECM sample at Case Western University in the early stages of this study. Unfortunately the results were inconclusive, due to the nature of the study and the limited knowledge of the PECM process at the time.

Discussions are ongoing with a group of researchers at CSIRO in Australia to conduct thermal fatigue tests on PECM'd samples. The test used by the Australian group does not require immersing the sample in liquid aluminum, the process used in the Case Western test. The effect of the liquid aluminum proved to be so harsh on the samples that no real conclusions could be drawn about the surface. It is hoped that the Australian method, which uses inductive heating to thermally cycle the sample, will prove to be a better method for this application.

Another possible application for this process lies in the area of porous metals for use in injection molding and die casting. These metals are specifically designed so that air will flow through the metal itself, for use in situations in which a vacuum is desirable in the mold or die cavity. The problem in applying these metals in practice is machining them without blocking a large proportion of the pores.

Almost any machining process that one can think of would result in closing the pores with molten or deformed metal. However, an electrolytic

process such as PECM should be able to form the surface without sealing off the pores, which should give the optimum performance for these metals. The question with PECM is, will the oxides and metal salts that form in the gap have the same effect? Because these materials open up new areas in the process technologies, this line of research may prove fruitful.

Finally, another possible area in which PECM may find an application is in preparing metal surfaces for coatings. Coating technology has grown rapidly in the past decade or two, both for cutting tools and for dies and molds. The surfaces shown in Figure 5. 14 at least appears to be an excellent surface for a coating to adhere to. The question again is whether or not it is possible to create an absolutely clean, polished surface with PECM. Again, only further research will tell.

## BIBLIOGRAPHY

- [1] J. P. Womack and D. T. Jones, *The Machine That Changed the World*. New York: Rawson Associates, 1990.
- [2] J. P. Womack and D. T. Jones, *Lean Thinking*. New York: Simon & Schuster, 1996.
- [3] K. Suzaki, *The New Manufacturing Challenge*. New York: The Free Press, 1987.
- [4] B. Lilly, "Preliminary Studies in Automated Finishing of Dies and Molds," ERC for Net Shape Manufacturing ERC/NSM-87-10, 1987 1987.
- [5] T. Altan, B. Lilly, J. P. Kruth, W. König, H. K. Tönshoff, and C. A. van Luttervelt, "Advanced Techniques for Die and Mold Manufacturing," *Annals of the CIRP*, vol. 42, 1993.
- [6] P. Fallböhmer, N. Akgerman, and N. Altan, "Survey of the U.S. Die and Mold Manufacturing Industry," ERC for Net Shape Manufacturing ERC/NSM-D-95-41, July, 1995 1995.
- [7] M. Papoy, "Personal communication," , 1997.
- [8] W. Smith, "Personal communication," , 1997.
- [9] T. Masuzawa and S. Sakai, "Quick Finishing of WEDM Products by ECM Using a Mate-Electrode," *Annals of the CIRP*, vol. 36, pp. 123-126, 1987.
- [10] K. P. Rajurkar and R. F. Ross, "State-of-the-Art Assessment of the Pulsed Electrochemical Machining Process," National Center for Manufacturing Sciences, State of the Art NCMS No. 14-13-9018, November 1991 1991.
- [11] B. R. Lazarenko, "Electrospark Machining of Metals," , vol. 2. New York: Consultants Bureau, 1964.

- [12] B. A. Krasnyuk, "Electrospark Machining of Metals," , vol. 3. New York: Consultants Bureau, 1965.
- [13] F. Llewellyn Jones, "Electrode Erosion by Spark Discharges," *British Journal of Applied Physics*, pp. 60–65, 1950.
- [14] E. M. Williams, "Theory of Electric Spark Machining," *Transactions of the ASME*, pp. 105–107., 1952.
- [15] E. M. Williams, J. B. Woodford, and R. E. Smith, "Recent Developments in the Theory and Design of Electric Spark Machine Tools," *AIEE Transactions*, vol. 73, pp. 83–88, 1954.
- [16] E. M. Williams and R. E. Smith, "Phenomena Accompanying Transient Low-Voltage Discharges in Liquid Dielectrics, I: Anode Phenomena at Low Currents," *AIEE Transactions*, vol. 74, pp. 164–169, 1955.
- [17] E. M. Williams and R. E. Smith, "Phenomena Accompanying Transient Low-Voltage Discharges in Liquid Dielectrics, II: Cathodic Phenomena at Low Currents," *AIEE Transactions*, vol. 76, pp. 97, 1957.
- [18] L. Solymar and D. Walsh, *Lectures on the Electrical Properties of Materials*, 4th ed. Oxford: Oxford University Press, 1988.
- [19] J. R. Crookall, "A Basic Analysis of Pulse Trains in Electro-Discharge Machining," *Int. J. Machine Tool Design & Research*, vol. 13, pp. 199–213, 1973.
- [20] Y. S. Tarng, C. M. Tseng, and L. K. Chung, "A Fuzzy Pulse Discriminating System for Electrical Discharge Machining," *International Journal of Machine Tools & Manufacture*, vol. 37, pp. 511–522, 1997.
- [21] M. Boccadoro and D. F. Dauw, "About the Application of Fuzzy Controllers in High-Performance Die-Sinking EDM Machines," *Annals of the CIRP*, vol. 44, pp. 147–150, 1995.
- [22] B. N. Zolotykh, "The Mechanism of Electrical Erosion of Metals in Liquid Dielectric Media," *Soviet Physics – Technical Physics*, vol. 4, pp. 1370–1373, 1960.
- [23] T. Hockenberry and E. M. Williams, "Dynamic Evolution of Events Accompanying the Low-Voltage Discharges Employed in EDM," *IEEE Trans. on Industry and General Applications*, vol. 3, pp. 302–309, 1967.

- [24] L. S. Palatnik and A. N. Liulichiev, "Investigation of the Temperature in the Vapor Phase Occurring during the Electrical Spark Treatment of Metals," *Soviet Physics – Technical Physics*, vol. 1, pp. 818–824, 1957.
- [25] M. Toren, Y. Zvirin, and Y. Winograd, "Melting and Evaporation Phenomena During Electrical Erosion," *ASME J. of Heat Transfer*, pp. 576–581, 1974.
- [26] J. R. Crookall and C. J. Heuvelman, "Electro-Discharge Machining — the State of the Art," *Annals of the CIRP*, vol. 20, pp. 113–120, 1971.
- [27] AGIE, "Understanding EDM Surface Integrity," AGIE, Ltd.
- [28] L. C. Lee, L. C. Lim, and Y. S. Wong, "Crack susceptibility of electro-discharge machined surfaces," *J. of Materials Processing Technology*, vol. 29, pp. 213–221, 1992.
- [29] H. Kojima and M. Kunieda, "Investigations on Distribution of Spark Locations in EDM Process," *Japanese Society of Precision Engineering*, vol. 57, pp. 83–88, 1991.
- [30] M. Kunieda, H. Xia, and N. Nishiwaki, "Observation of Arc Column Movement during Monopulse Discharge in EDM," *Annals of the CIRP*, vol. 41, pp. 227–230, 1992.
- [31] B. M. Schumacher, "Electrodischarge Machining," AGIE, Lecture Notes August 15–16, 1991 1991.
- [32] K. J. Stout, E. J. Davis, and P. J. Sullivan, *Atlas of Machined Surfaces*. London: Chapman and Hall, 1990.
- [33] L. C. Lee, L. C. Lim, and Y. S. Wong, "Towards crack minimisation of EDMed Surfaces," *J. of Materials Processing Technology*, vol. 32, pp. 45–54, 1992.
- [34] H. K. Lloyd and R. H. Warren, "Metallurgy of Spark Machined Surfaces," *J. of the Iron and Steel Institute*, pp. 238–247, 1965.
- [35] J. E. Greene and Guerrero-Alvarez, "Electro-Erosion of Metal Surfaces," *Metallurgical Transactions*, vol. 5, pp. 695–706, 1974.

- [36] J. Longfellow, J. D. Wood, and R. B. Palme, "The Effects of Electrode Material Properties on the Wear Ratio in Spark-Machining," *J. of the Institute of Metals*, vol. 96, pp. 43–48, 1968.
- [37] L. C. Lee, L. C. Lim, Y. S. Wong, and H. H. Lu, "Solidification Microstructure of electrodischarge machined surfaces of tool steels," *Materials Science and Technology*, vol. 7, pp. 239–248, 1991.
- [38] R. Ziehm, B. Lilly, and J. Brevick, "Removal of EDM Induced Surface Damage of Tool Steels by Subsequent Electro-Chemical Polishing," Engineering Research Center for Net Shape Manufacturing ERC/NSM-D-93-30, 1993 1993.
- [39] J. P. Kruth, L. Stevens, L. Froyen, and B. Lauwers, "Study of the White Layer of a Surface Machined by Die-Sinking Electro-Discharge Machining," *Annals of the CIRP*, vol. 44, 1995.
- [40] F. Roethel, L. Kosec, and V. Garbajs, "Contribution to the Micro-Analysis of Spark Eroded Surfaces," *Annals of the CIRP*, vol. 25, pp. 135–140, 1976.
- [41] L. Centa, "The Effect of Electro-Discharge Machining on the Thermal Fatigue Resistance of H-13 Die Steel for Aluminum Die Casting Dies," : Case Western Reserve University, 1989.
- [42] L. C. Lim, Y. S. Wong, and L. C. Lee, "Effects of Reagents on Electrodischarge Machined Surfaces and Globule Appendages," *Surface Engineering*, vol. 6, pp. 206–208, 1990.
- [43] N. I. Lazarenko, "Electrospark-Induced Changes in the Properties of Metal Surfaces," in *Electrospark Machining of Metals*, vol. 2, B. R. Lazarenko, Ed. New York: Consultants Bureau, 1965, pp. 20–42.
- [44] M. M. Barash, "Effect of EDM on the Surface Properties of Tool and Die Steels," *Metals Engineering Quarterly*, pp. 48–51, 1965.
- [45] P. F. Thomson, "Surface damage in electrodischarge machining," *Materials Science and Technology*, vol. 5, pp. 1153–57, 1989.
- [46] L. C. Lee, L. C. Lim, V. Narayanan, and V. C. Venkatesh, "Quantification of Surface Damage of Tool Steels after EDM," *Int. J. Mach. Tools Manufact.*, vol. 28, pp. 359–372, 1988.

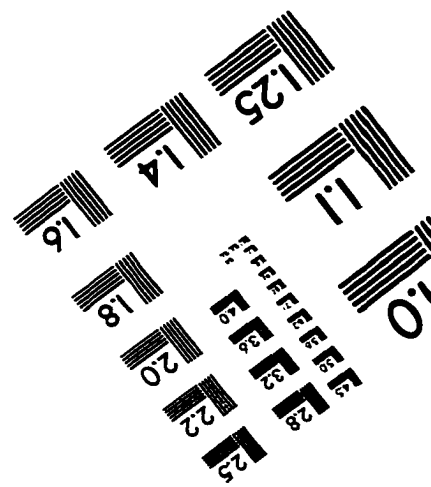
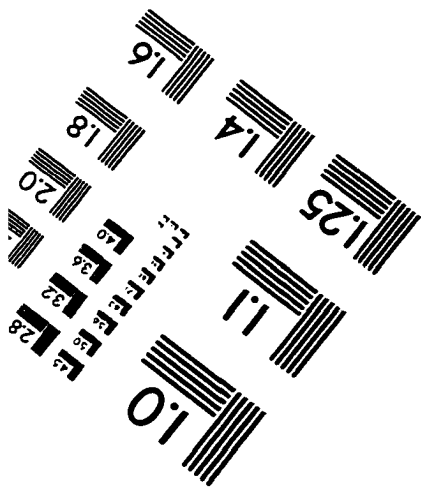
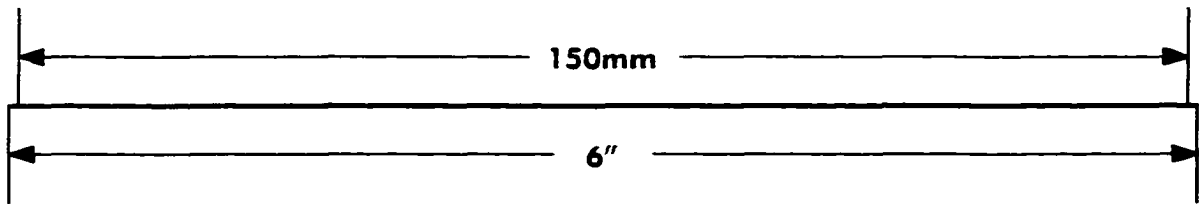
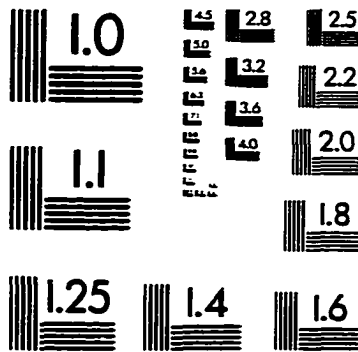
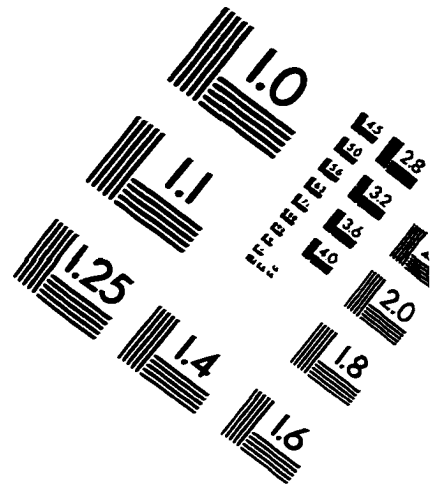
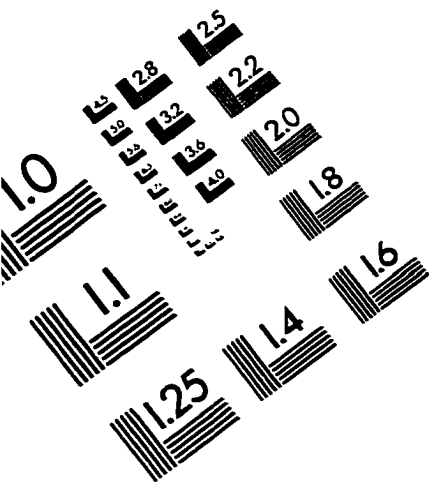
- [47] L. C. Lee, L. C. Lim, Y. S. Wong, and H. H. Lu, "Towards a Better Understanding of the Surface Features of Electro-Discharge Machined Tool Steels," *Journal of Materials Processing Technology*, vol. 24, pp. 513–523, 1990.
- [48] L. Centa and J. F. Wallace, "Effect of Electro-Discharge Machining on the Surface and Sub-Surface Micro Structure of H-13 Steel," presented at 15th International Die Casting Congress and Exposition, St. Louis, 1989.
- [49] V. P. Aleksandrov, "Residual Stresses and the Long-Term and Fatigue Strengths of Heat-Resistant Materials after Electrospark Machining," in *Electrospark Machining of Metals*, vol. 3, B. A. Krasnyuk, Ed. New York: Consultants Bureau, 1965, pp. 98–102.
- [50] V. P. Aleksandrov and B. N. Zolotykh, "On the selection of the optimum conditions in machining nickel-based heat-resistant alloys by the electrospark method," *Izv. Akad. Nauk SSSR, Otd. Tekhn. Nauk.*, vol. 6, 1958.
- [51] J. R. Crookall and B. C. Khor, "Residual Stresses and Surface Effects in Electro-Discharge Machining," presented at 13th Machine Tool Design and Research Conference, Birmingham, 1972.
- [52] M. A. E. R. Merdan and R. D. Arnell, "The Surface Integrity of a Die Steel after Electrodischarge Machining: 2 Residual Stress Distribution," *Surface Engineering*, vol. 7, pp. 154–158, 1991.
- [53] J. F. Wilson, *Practice and Theory of Electrochemical Machining*, 1 ed. New York: Wiley Interscience, 1971.
- [54] J. A. McGeough, *Principles of Electrochemical Machining*. London: Chapman and Hall, 1974.
- [55] K. P. Rajurkar, B. Wei, and C. L. Schnacker, "Monitoring and Control of Electrochemical Machining (ECM)," presented at ASME Symposium on Monitoring and Control of ECM, 1990.
- [56] B. Wei, "Modeling and Analysis of Pulse Electrochemical Machining," : University of Nebraska, 1994.
- [57] R. P. Frankenthal and J. Kruger, *Passivity of Metals*: Electrochemical Society, 1978.
- [58] R. W. Staehle and H. Okada, *Passivity and its Breakdown on Iron and Iron Base Alloys*. Houston: National Association of Corrosion Engineers, 1976.

- [59] M. Datta, "Anodic Dissolution of Metals at High Rates," *IBM J. of Research and Development*, vol. 37, pp. 207–226, 1993.
- [60] W. König and P. Lindenlauf, "Surface Generation in Electrochemical Machining," *Annals of the CIRP*, vol. 27, 1978.
- [61] M. Datta and D. Landolt, "Film Breakdown on Nickel under Transpassive Dissolution Conditions in Sodium Nitrate Solutions," *J. of the Electrochemical Society*, vol. 124, pp. 483–489, 1977.
- [62] M. Datta and D. Landolt, "Electrochemical Machining under Pulsed Current Conditions," *Electrochimica Acta*, vol. 26, pp. 899–907, 1981.
- [63] Y. Kuwabara, T. Asaoka, and Y. Iwasaki, "Electro-Chemical Machine," in *United States Patent Office*. United States: Shizuoka Seiki, Ltd., 1989.
- [64] Y. Kuwabara, T. Asaoka, S. Yoshioka, and H. Sugiyama, "Finishing Method Employing Electro-Chemical Machining and an Electro-Chemical Finishing Machine," in *United States Patent Office*. United States: Shizuoka Seiki, Ltd., 1990.
- [65] M. Datta and D. Landolt, "Surface Brightening during High Rate Nickel Dissolution in Nitrate Electrolytes," *J. Electrochemical Society*, vol. 122, pp. 1466–1472, 1975.
- [66] M. Datta and D. Landolt, "Electrochemical Machining under Steady State and Pulsed Current Conditions," presented at ISEM-6, Moscow, 1980.
- [67] N. Ibl, "Some Theoretical Aspects of Pulse Electrolysis," *Surface Technology*, vol. 10, pp. 81–104, 1980.
- [68] O. A. Abu-Zeid, "On the effect of electrodischarge machining parameters on the fatigue life of AISI D6 tool steel," *J. of Materials Processing Technology*, vol. 68, pp. 27–32, 1997.
- [69] M. A. Béjar, W. Schnake, and J. Gallardo, "Oxidation and fatigue life of an AISI-D3 steel machined by electrodischarge," *J. of Materials Processing Technology*, vol. 65, pp. 179–182, 1997.
- [70] B. Cina, "The Effect of Surface Finishing on Fatigue," *Metallurgia*, pp. 11–19, 1957.

- [71] G. Rowden, "Effects of Non-Conventional Machining Processes on the Mechanical Properties of Metals," *Metallurgia*, pp. 189–193, 1968.
- [72] N. A. Morozov and A. I. Maksimov, "Effects of Electrochemical Machining on Turbine Blades," *Russian Engineering Journal*, vol. 67, pp. 55–58, 1967.
- [73] E. Rummyantsev and A. Davydov, *Electrochemical Machining of Metals*. Moscow: MIR Publishers, 1989.
- [74] W. F. Stoecker, *Design of Thermal Systems*. New York: McGraw-Hill, 1971.
- [75] C. A. Rodríguez, "Ball-nose End Milling – Development of Criteria for Automatic Selection of Spindle Speed and Feed Rate," : The Ohio State University, 1997.
- [76] M. Datta, R. V. Shenoy, and L. T. Romankiw, "Recent Advances in the Study of Electrochemical Micromachining," *J. of Eng. for Industry*, vol. 118, pp. 29–36, 1996.
- [77] E. Rosset, M. Datta, and D. Landolt, "Pulse Polishing of Die Steels in Neutral Solutions," *Plating and Surface Finishing*, vol. 72, pp. 60–64, 1985.
- [78] G. E. P. Box, W. G. Hunter, and J. S. Hunter, *Statistics for Experimenters: An Introduction to Design, Data Analysis, and Model Building*. New York: J. Wiley & Sons, 1978.
- [79] H. J. Kim and J. F. Wallace, "Effects of EDM and its Mitigation by Surface Modification on Thermal Fatigue Properties," *Surface Engineering*, vol. 10, pp. 56–64, 1994.
- [80] M. Sander, *A Practical Guide to the Assessment of Surface Texture*. Göttingen: Feinprüf GmbH, 1991.
- [81] V. J. Vohnout, "Personal communication," , 1997.
- [82] E. J. Czyryca, "Fatigue Crack Initiation," in *ASM Metals Handbook*, vol. 8, 9 ed, pp. 366–375.
- [83] C. S. Chen, "The Effect of Pulsed Electrochemical Machining on the Fatigue Life of H-13 Steel," : The Ohio State University, 1996.

[84] A. S. Kaley, "The Effect of Surface Grinding and EDM Finishing on the Fatigue Life of H-13 Steel," : The Ohio State University, 1997.

# IMAGE EVALUATION TEST TARGET (QA-3)



**APPLIED IMAGE, Inc**  
1653 East Main Street  
Rochester, NY 14609 USA  
Phone: 716/482-0300  
Fax: 716/288-5989

© 1993, Applied Image, Inc., All Rights Reserved